Universitetet i Stavanger
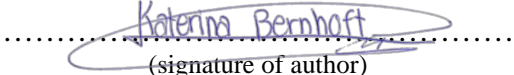
FACULTY OF SCIENCE AND TECHNOLOGY

MASTER'S THESIS

Study programme/specialisation: Mechanical and Structural Engineeering and Materials Science	Spring / Autumn semester, 20.1.7.. Open/Confidential
Author: Katerina Bernhoft	………… *Katerina Bernhoft* ………… (signature of author)

Programme coordinator: Supervisor(s):   Samindi Samarakon, Luis Evangelista

Title of master's thesis: Numerical modeling of recycled fibre reinforced concrete beams and comparison with experimental findings

Credits: 30

Keywords: Nonlinear analysis Fibre reinforced concrete Recycled fibre made from tyre waste Steel fibre Finite element method	Number of pages: …………115………… + supplemental material/other: ……14…… Stavanger,……15.06.2017……… date/year

Title page for Master's Thesis
Faculty of Science and Technology

Abstract

The presented work has the main focus on fibre reinforced concrete (FRC). FRC is examined in ATENA, and the numerical results are compared to the experimental.

The first part of this report treats the concept of nonlinear finite element method to get a better understanding of the analysis. A literature study based on previous research and published material of fibres and fibre reinforced concrete is also given within this report. Important mechanical properties of FRC are presented, such as tensile strength and fracture behavior.

The procedure of testing FRC at the laboratory is included within this report.

Modeling and analysis is performed with the FEM-software ATENA-GiD interface. The beams are modeled with respect to recreate a four-point bending situation. By advantage of symmetry, half the beam is constructed and analysed in ATENA. Computed load-displacement diagrams are compared to experimental results, and the behaviour is compared. Crack pattern and crack widths are studied with the use of a full-field measuring technique, using Digital Image Correlation (DIC) system to monitor the cracking on the beam surfaces.

In total, five beams were tested at the laboratory and recreated in ATENA. One of the beams served as a reference beam containing plain concrete and conventional steel bars, while the other beams additionally contained steel fibres of different type and amount.

This thesis shows through nonlinear FEM-analysis that it is possible to make somewhat good approximations to experimental fibre reinforced concrete. However, further research must be provided to determine the tensile and fracture behaviour of FRC.
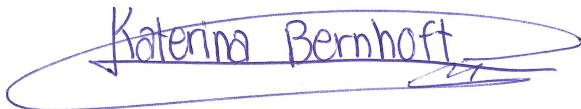
Preface

This master thesis is carried out as a final result of the two-year Master´s degree programme in Mechanical and Structural Engineering and Material Science at the University of Stavanger (UiS). The report exhibits the work performed through the spring of 2017.

It has been both exciting and challenging to model the behavior of fibre reinforced concrete using ATENA. Also, it has been inspiring to see how well the simulated results were in comparison to those obtained through experimental results. Besides from using knowledge acquired from previous studies, the project has also provided me with new knowledge.

I would like to thank my supervisors, Samindi Samarakon and Luis Evangelista, for all help and support throughout the project period. The author would also like to express sincere gratitude to the bachelor students Pål Ruben Hovind, Bjarne Mikalsen and Jørgen Wie Pedersen for excellent cooperation and execution of the laboratory work. Last, but not least I want to thank the staff at the laboratory of the department for technical help and assistance.

University of Stavanger, June 15th, 2017

Katerina Bernhoft

Contents

List of figures

List of tables

Notations

Roman upper case letters

A_s	Cross section area of steel reinforcement
D_{av}	Average diameter of sample in slump flow test
$E_{c,0}$	Initial secant modulus of elasticity for concrete
E_{ci}	Initial tangent modulus of elasticity for concrete
$E_{c,s}$	Secant modulus of elasticity for steel
E_s	Young's modulus for steel
G_F	Fracture energy
V_f	Volume fraction of fibres
$W_{f,CMOD}$	Are under splitting load-CMOD diagram

Roman lower case letters

f_{cm}	Actual compressive strength at an age of 28 days
f_{ct}	Tensile strength
$f_{ct,sp}$	Splitting tensile strength
$f_{R,i}$	Residual flexural strength
w_1	First opening crack width
w_c	Final opening crack width

Greek letters

α	Shear retention factor
Δu	Displacement increment
ε	Strain
ε_2	Ultimate strain
ε_{cr}	Crack opening strain
η_0	Capacity factor
λ_f	Aspect ratio of fibres
μ	Friction factor
ν	Poisson's ratio
ρ	Reinforcement ratio
ρ_f	Density of fibres
σ	Stress
σ_1	Maximum tensile stress
σ_2	Residual tensile stress
σ_s	Yielding stress
τ	Shear stress

Acronyms

2D	Two-dimensional
3D	Three-dimensional
AR	Alkali-Resistant
CMOD	Crack Mouth Opening Displacement
COIN	Concrete Innovation Centre
EC2	Euro Code 2
FEA	Finite Element Analysis

FEM	Finite Element Method
FIB	Fédération Interantionale dú Beton
FRC	Fibre Reinforced Concrete
GFRC	Glass Fibre Reinforced Concrete
L-D	Load-Displacement
N-R	Newton-Raphson method
NFEA	Non-linear Finite Element Analysis
NFEM	Non-linear Finite Element Method
NFRC	Natural Fibre Reinforced Concrete
SFRC	Steel Fibre Reinforced Concrete, commercial fibres
SNFRC	Synthetic Fibre Reinforced Concrete
LWC	LightWeight Concrete
PE	PolyEthylene
PES	PolyESter
PP	PolyPropylene
PVA	PolyVinyl Acetate
RFRC	Recycled Fibre Reinforced Concrete
SCC	Self Compacting Concrete
TW	Tyre Waste

1 Introduction

1.1 Background

Reinforced concrete is one of today´s most widely used building material, and make up the majority of structures such as bridges, power plants, silos, dams and pavements. The concrete itself has no geometric restrictions, and its constituents are available everywhere. In the later decades, the interest for fibre reinforced concrete has increased substantially. Fibres may partially or totally substitute the conventional steel bar reinforcement, which may bring many advantages. The presence of fibres in concrete can improve certain mechanical performance of concrete i.e increase the tensile strength and the fracture resistance, as well as reduce the plastic shrinkage and thereby improving the durability (Lu, 2015).

At the present, a vast amount of different fibre types are available at the building industry market. Among fibre materials, steel is the most commonly used. In the search of preserving the environment and re-use waste material, fibres produced from recycled materials have come up as an alternative to the commercial fibres specifically produced to reinforce concrete. Various recycled fibre materials are gaining ground, as for instance fibres recovered from used car tyres.

Tyre waste represents a serious problem for several countries in Europe. This is mainly due to improper management of the non-biodegradable material. Consequently, stockpiles of tyre waste are increasing. Huge amounts of wasted tyres are dumped in the landfills, where they are burned. Fires in these dumps are very damaging to the environment, emitting large amounts of heavy smoke containing noxious gases. The fires of tyre are extinguished, and the resultant runoff can cause severe damage to the groundwater. To preserve the environment, a proposal for sustainable and life-cycle assessment way of handling tyre waste, has been introduced to the civil construction field. One solution might be to use wasted tyres as reinforcement in concrete by means of discrete fibres.

Steel fibres recovered from tyre waste could lead to economical advantages, in addition to contribute to the widely known pollution problem concerning tyre waste. On similar basis to industrial steel fibres, the application of recycled steel fibres could contribute to increase the mechanical properties of concrete. However, how effective recycled steel fibres are compared to commercial steel fibres will be investigated in the thesis.

1.2 Aim and limitations

The aim of this thesis is to examine the behaviour of fibre reinforced concrete through nonlinear analysis in the finite element software ATENA. The numerically results will be compared to the experimental results achieved at the laboratory. The mechanical properties of recycled steel fibre reinforced concrete are compared with those of conventional steel fibre reinforced concrete in order to evaluate whether they can be effectively used as reinforcement in concrete applications.

A four-point bending test is recreated in ATENA, where the experimental results serve as input i.e. compressive and tensile strength, modulus of elasticity and fracture energy. The resulting load-displacement curves for the numerical models are then compared to those from the laboratory tests. Crack pattern and crack widths are also investigated and compared to the beams tested at the laboratory. In order to compare the effectiveness of the load capacity of the beams, a reference beam containing plain concrete and conventional reinforcement bars is tested.

1.3 Outline of the thesis

This thesis is divided into 6 chapters and an introductory part briefly describing the background of the features treated in later sections. The aim and limitations for the thesis is described in Chapter 1 as well. Chapter 2 introduces the concept of nonlinear analysis and solution methods used to describe behaviour of composite materials. Solution methods for the software applied in this thesis is also briefly explained.

Chapter 3 dealt with the concept of fibre reinforced concrete (FRC) and general application areas. Different fibre types and shapes are described within this section, including advantages and disadvantages with the use of fibres. In Chapter 4 important properties concerning both plain concrete and fibre reinforced concrete are discussed. It includes determination of the fibres used for the laboratory tests i.e. commercial steel fibres and recycled steel fibres made for tyre waste. In the subsequently section, Chapter 5, the experimental programme is described. Both fresh concrete and hardened concrete is examined through test, and the experimental outcomes are presented.

Chapter 6 deals with the procedure of numerical modelling executed in the finite element software ATENA. An FE analysis is carried out for the beams, to study the behaviour of FRC concrete containing recycled steel fibres made from tyre waste material in comparison to commercial steel fibre reinforced concrete. The analysis and the results are presented in Chapter 7, where the FE-models are compared with the experimental results. Chapter 8 gives final conclusions and suggestions for further work.

2 State of the art

The aim of this thesis is to analyse the behaviour of fibre reinforced concrete with fibres made of recycled tyre waste. The analysis is conducted with the use of finite element method (FEM) software, specialized for concrete structures. In order to investigate and analyse the behaviour of fibre reinforced concrete, it will be necessary to use nonlinear analysis. The concepts of methods and analysis that are to be used in the modelling, is to be explained in this section.

2.1 Nonlinear analysis of concrete structures

The term "nonlinearity" implies that response is not directly proportional to the action that produces it. Nonlinearity is in reality always present to some degree, but the effects are often so small that it can be totally ignored. In general, most of the analysis procedures for new reinforced concrete structures are based on linear-elastic principles. In some situations, however, it will be necessary to analyse structures more accurately in order to predict its structural behaviour.

Nonlinear analysis might be required in cases like strength, safety and integrity assessment of damaged or deteriorated structures, or in cases where old structures are designed in accordance to out-dated codes. In such special situations, structural engineers may therefore assess maximum load capacity, ultimate displacement capacity, ductility, deficient members or failure mechanisms of the structure. Nonlinear analyses are complex and time consuming, and are therefore mostly performed by using specialized computer programs(Güner, 2008). There are various fields of nonlinear analysis, but only finite element method (FEM) is to be considered in this thesis (V. Červenka et al., 2016)

2.2 Finite element analysis

Finite element analysis (FEA), also known as finite element method (FEM), is an effective numerical technique for solving field problems. Such field problems are represented mathematically as differential equations or by integral expressions. However, the majority of such equations cannot be solved analytically and therefore other methods must be applied. With finite element method, approximations of such equations can be established based on different types of discretizations. Each individual finite element represents a small piece of the total structure, where the term structure in general is used for a defined body or region. The elements are connected at points, or so-called *nodes,* and are arranged at a certain way. The specific arrangement of elements is called a *mesh,* and is numerically represented by a system of algebraic equations to be solved for unknown at nodes.

Advantageously, finite element method offers great freedom in selection of the discretization in elements that may be used to discretize both space and the basis functions. Even thought FEA does not provide exact solutions (assuming the FEA is appropriate), the solution can be considerably improved by increasing the number of elements representing the structure i.e. refinement of the mesh. Another advantage by using FEA is that it is applicable to any field problem, without any geometric restrictions. In addition, the material properties in FEA are not restricted to isotropy and

may also change from element to element, or even within an element. This is especially advantageous when studying the behaviour of fibre reinforced concrete and other complex materials (Cook, Malkus, Plesha, & Witt, 2002).

2.3   Nonlinear finite element analysis

Linear analysis is only applicable in the case of small strains, and in order to describe difficult phenomena such as yielding, creep, fatigue and buckling, or interactions between them, nonlinear formulations are applied. However, nonlinear analysis requires further physical and theoretical understanding of the equation-solving processes, which might consist of more than one single strategy. In NFEA it is very common to guess and change strategies several times before the results is satisfactory enough for the analysis. In other words, the effort of the analyst increases substantially when the problem becomes nonlinear.

With respect to structural mechanics, nonlinearity can be divided into *material nonlinearity, contact nonlinearity* and *geometric nonlinearity.* Material nonlinearity involves nonlinear elasticity, plasticity and creep, where the material properties are functions of the state of stress and strain. In contact nonlinearity the contact area between parts changes as the contact forces changes through opening and closing of adjacent gaps. Sliding contact with frictional forces is also a form of contact nonlinearity. The remaining term, geometric nonlinearity, appears when deformation of the member/structure becomes large enough so that equilibrium equations must be written with respect to the deformed structural geometry. Problems like this are of nonlinear category because the stiffness and sometimes the loads as well, become functions of deformation or displacement.

In linear structural equations like equation 2.1, the displacement {D} can be obtained by multiplying the inverse of the stiffness matrix [K] with the load vector {R}, as shown in equation 2.2. Nonlinear problems, however, cannot be solved directly with respect to {D}, because information needed to construct the stiffness matrix and the load vector are not known in advance, see equation 2.3. Thus an iterative process is required to obtain {D} and its associated [K] and {R}, such that the product [K]{D} is in equilibrium with {R}.

$$[K]\{D\} = \{R\} \tag{2.1}$$
$$\{D\} = [K]^{-1}\{R\} \tag{2.2}$$

$$[K(D)]\{D\} = \{R(D)\} \tag{2.3}$$

Although nonlinear analysis gives quite precise solutions, it also poses some disadvantages that are important to be aware of. In NFEA the principle of superposition is not applicable, and the results can therefore not be scaled in proportion to load or superpose results of different loads. This is mainly due to that each load case (or set) requires a separate analysis. Furthermore, a given set of loads may have more than one solution {D}. In order to solve nonlinear equations it is necessary to apply other solution methods, which are be introduced in the following section.

2.4   Solution methods

As previously mentioned, in nonlinear analysis, a single solution of the regular linear equation [K]{D}={R} is inadequate, since [K] and/or {R} is a function of {D}. The displacement {D} becomes dependent on displacement from earlier steps, and a sequence of analysis is required, in which [K] and/or {R} must be updated after each analysis. The problem must be discrete in space by means of finite elements, as well as discrete in time with small portions (increments). When this is the case, the state of equilibrium at the end of each increment can be determined by the use of repeated cycles (iterative solution algorithm). The combination of these two methods is known as an *incremental-iterative procedure*, and will be further discussed.

2.4.1   Incremental method

Nonlinear equations may have multiple solutions, and if a solution is obtained it might not necessarily be the one sought (Cook et al., 2002). The size of the incremental steps plays an important role in the solution procedure, especially when it comes to the incremental-iterative procedure. Too large steps might give more than one solution, and it is therefore essential to use small steps in order to obtain realistic answers. The required increment size, however, depends on the specific problem and its geometry.
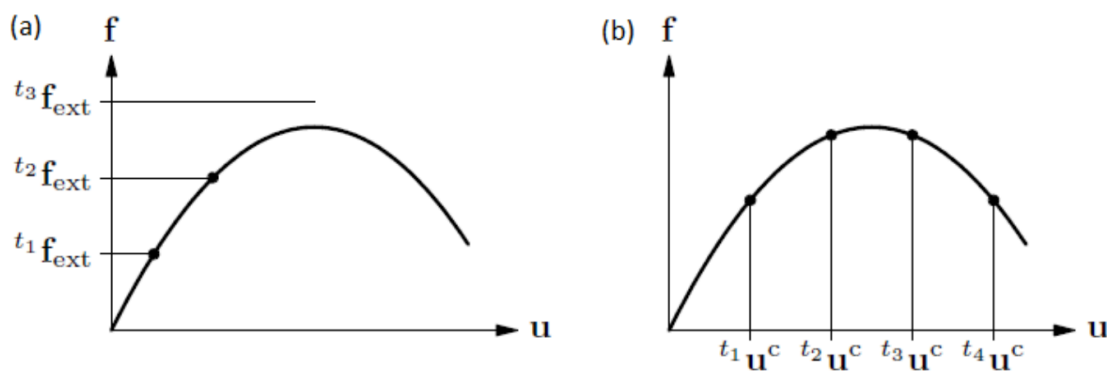
Figure 2-1: Incremental procedures (a) load-controlled (b) displacement-controlled (TNO DIANA)

With the incremental method the load is applied in several load steps. Load control and displacement control are among the most common load incremental procedures. *Both procedures are based on the same concept where the load is increased for each increment, but differs in type of approach. In the case of load control, the load is increased for each increment directly by increasing the external vector f_{ext} as illustrated in*

Figure 2-1(a). With displacement control, the load is rather represented by fixed, prescribed displacements u^c, and not the load itself, see

Figure 2-1(b).

With load control, the increment does not have to be uniform. The unfortunate is that the load can only be applied for each incremental step, which means that the force f

cannot pass limit points. Displacement control, on the other hand, increases the fixed displacement for each incremental step making it possible to pass limit points. Although the displacement control is more stable than force control, it cannot pass turning points.

2.4.2 Iterative procedure

The computer program ATENA has several implemented methods for solving sets of nonlinear equations of finite element model. In order to solve the set of nonlinear equations within an increment, the solution procedure need to iterate until some convergence criterion is satisfied. To do this, the Newton-Raphson (N-R) method or the Modified Newton-Raphson method may be applied. Both methods are very common in computational mechanics, and will therefore be shortly introduced.

Newton-Raphson method

The Newton-Raphson method (N-R method), also known as Newton´s method, is the most robust method for solution of nonlinear algebraic equations (Belytschko, Liu, & Moran, 2000). The N-R method uses the concept of incremental step by step analysis to determine the set of nonlinear equations shown in Equation 2.4.

$$K(p) \cdot \Delta p = q - f(p) \tag{2.4}$$

$$f(k \cdot p) \neq k \cdot f(f) \tag{2.5}$$

$$K(p) \neq K(p + \Delta p) \tag{2.6}$$

where:
q is the vector of totalt applied joint loads,
$f(p)$ is the vector of internal joint forces,
Δp is the deformation increment due to loading increment,
p are the deformations of structure prior to load increment,
$K(p)$ is the stiffness matrix, relating loading increments to deformation increments,
i number of iterations,
k is an arbitrary constant.

Equation 2.4 is nonlinear due to nonlinear properties of the internal forces, as well as nonlinearity in the stiffness matrix, see Equation 2.5 and 2.6 respectively. Equation 2.7 is thus a mathematical description of the structural behaviour only representing one step of the solution. Consequently, by including the i-th iteration within a distinct loading increment, the expression rather becomes:

$$K(p_{i-1}) \cdot \Delta p_i = q - f(p_{i-1}) \tag{2.7}$$

The stiffness matrix K is generally deformation dependent i.e. a function of p. However, this is typically neglected meaning that linearity remains. To begin the iterative procedure, a starting value for the unknown must be chosen, usually the solution from the last time step is selected. Equation 2.8 can now be solved for the unknown deformation increment p_i at load level q using:

$$p_i = p_{i-1} + \Delta p_i \tag{2.8}$$

The solution of the nonlinear Equation 2.7 is obtained by iterating until convergence is achieved. Although the stiffness matrix is calculated for each iteration, making the N-R method computational expensive, it also uses few iterations to reach convergence. To overcome slow convergence due to substantial deviations of the residual from the underlying linear model and roughness of residual, *line search iteration* may be applied. The concept of line search iteration will be explained later in Section 2.4.4. ATENA have several convergence criterions to be checked in which are explained in Section 2.4.5. The regular Newton-Raphson method may be explained as a way of extracting root of a polynomial, and the procedure is depicted in Figure 2-2.
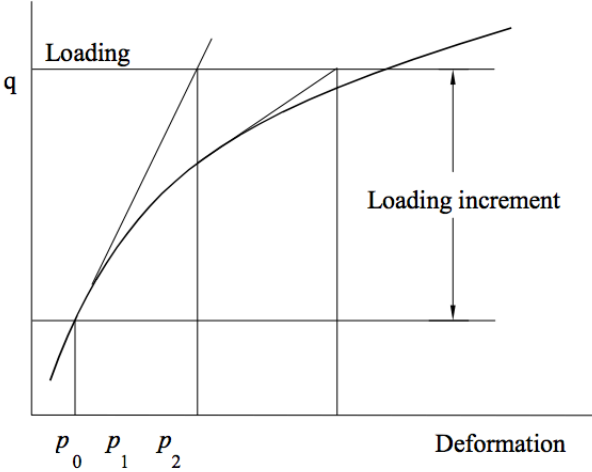
Figure 2-2: Procedure of the regular Newton-Raphson method

Modified Newton-Raphson method
The Modified Newton-Raphson method also applies the *line search iteration.* In difference to the regular N-R method, the Modified Newton-Raphson method (MN-R method) updates the stiffness matrix only one time for each increment, instead of updating K for every iteration. In many cases, the matrix $K(p_0)$ from the first iteration of the step can be used. This simplification can be mathematically expressed by:

$$K(p_{i-1}) = K(p_0) \qquad (2.9)$$

The MN-R method Even though the modified Newton-Raphson method produces significant time saving, it also exhibits worse convergence of the solution procedure than the original N-R method. In other words, the MN-R method converges slower to equilibrium, which means that additional iterations are required as illustrated in Figure 2-3. In practice, a combination of the modified and regular N-R method is the most optimal.
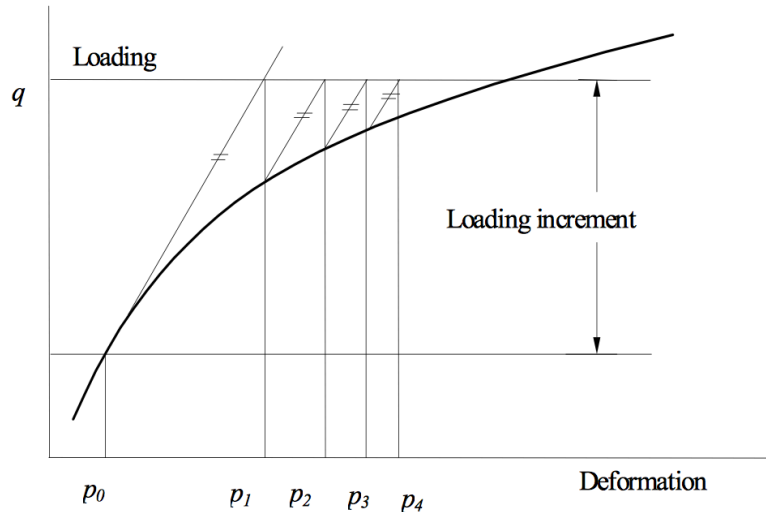
Figure 2-3: Procedure of modified Newton-Raphson method

2.4.3 Arch-Length Method

The Arch-Length (A-L) method is a great alternative to the modified Newton-Raphson method, and is widely known due to its excellent performance. It can be applied for both material non-linearity and geometric non-linearity, and provides robustness as well as computational efficiency. In areas where the traditional N-R method fails, the arch length method can be applied and still provide good results. The ability of changing the load condition during iteration within an increment makes it possible to study stability problems such as snap-through and snap-back phenomena, see Figure 2-4. This means that the A-L method is especially advantageous when running force-controlled analysis.
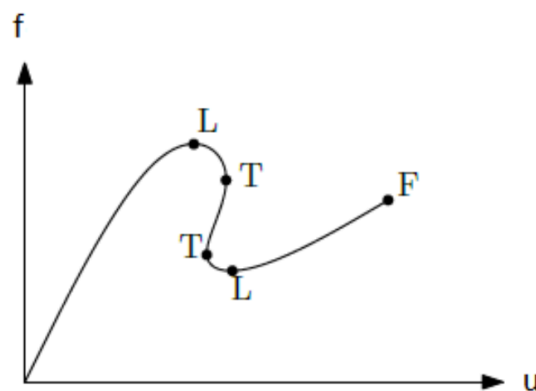
Figure 2-4: Snap-back with limit (L), turning (T) and failure (F) points (TNO DIANA)

Basically, the A-L method observes the complete load-displacement relationship instead of applying a constant loading increment as in the N-R method. In order to do this, it will be necessary to introduce an additional degree of freedom for the loading level i.e. *n* displacement degrees of freedom associated with one loading. The new degree of freedom, usually called λ, can be defined by constraint in many ways in ATENA. The set

of nonlinear equation suitable for iterative solution for the arch-length method will therefore be the following:

$$K(p_{i-1}) \cdot \Delta p_i = \lambda q - f(p_{i-1}) \tag{2.10}$$

$$\lambda_i = \lambda_{i-1} + \Delta \lambda_{i-1} \tag{2.11}$$

$$p_i = p_{i-1} + \Delta p_i = p_{i-1} + (\Delta p_{i-1} + \eta_{i-1}\delta_{i-1}) \tag{2.12}$$

where:
λ is the new loading factor,
η is a new scalar.

As the name indicates, the A-L method uses the arch-length to achieve convergence, see Figure 2-5. ATENA supports various types of arch-length constraints; normal update method, consistently linearized method, explicit orthogonal method and the Crisfield - to mention some of them. The stiffness matrix can either be recomputed for each iteration or be fixed based on the first iteration for all subsequent iterations (V. Červenka et al., 2016). In cases of damp oscillations or arise of convergence problems like near extreme points, the scalar η may come to good use. The scalar makes it possible to accelerate solutions, and will be further explained in Section 2.4.4.
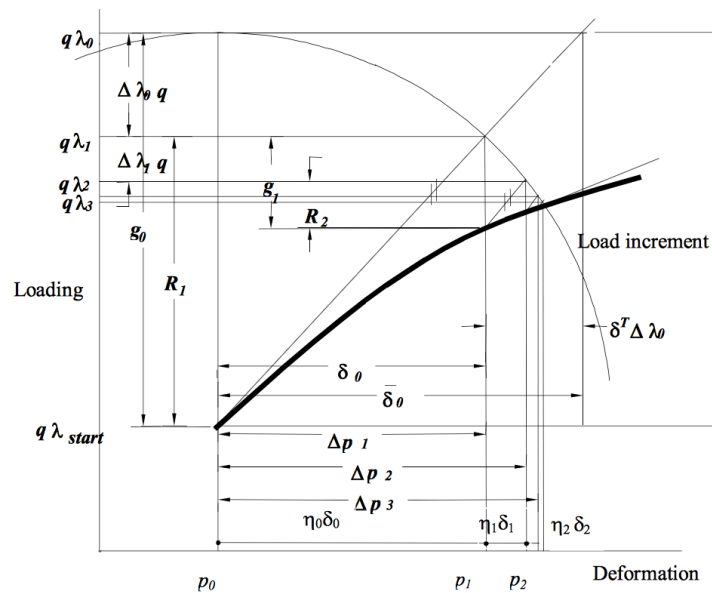
Figure 2-5: The Arc-length method

2.4.4 Line Search Method
The line-search method aims to increase the effectiveness of the Newton-Raphson methods, where convergence is slow. In structures where the nonlinearity is present at high levels, such as in case of cracking, the prediction might be too far away from equilibrium. With the N-R method, the direction of Δp obtained might be optimal, whereas the step size is not (Belytschko et al., 2000).

The first step in the line search method is to calculate displacement increment δ, by any choice of methods. The next step is to set a value for the parameter η', which typically might the increment load from previously steps i.e. typical values between 0.6 and 0.8. The main idea behind η is to minimize the work of current out-of balance forces on displacement increment. Subsequently, the out-of-balance forces can be calculated by linearly interpolating between point p_0 and $p_0 + \eta'\delta$. The parameter η must be obtained by iterating until a specified energy drop is achieved.

2.4.5   Convergence criterions

Iterations are performed within an increment until satisfying results are approached, or eventually until a maximum number of iterations is reached. The iterations must then be stopped somehow, and for this purpose some convergence criterions are established. ATENA support several types of criterions which are presented below:

$$\sqrt{\frac{\Delta p_i^T \cdot \Delta p_i}{p_i^T \cdot p_i}} \leq \varepsilon_{rel.disp} \tag{2.13}$$

$$\sqrt{\frac{(q-f(p_{i-1}))^T \cdot (q-f(p_{i-1}))}{(f(p_i)^T \cdot f(p_i)}} \leq \varepsilon_{rel.force} \tag{2.14}$$

$$\sqrt{\frac{\Delta p_i^T \cdot (q-f(p_{i-1}))}{p_i^T \cdot f(p_i)}} \leq \varepsilon_{rel.energy} \tag{2.15}$$

$$\sqrt{\frac{\max\left(\left(q^k - f^k(p_{i-1})\right)\right) \cdot \max\left(\left(q^k - f^k(p_{i-1})\right)\right)}{\max\left(f^k(p_i)\right) \cdot \max\left(f^k(p_i)\right)}} \leq \varepsilon_{abs.force} \tag{2.16}$$

Displacement changes during the last iteration are to be checked for by the first criterion, see Equation 2.13. The second criterion checks the norm of out-of-balance forces, whereas the third one checks the out-of-balance energy. The fourth criterion controls the out-of-balance forces, not in terms of the Euclid norms, but through the terms of maximum components (V. Červenka et al., 2016).

2.4.6   Nonlinear finite element analysis using ATENA

ATENA offers both the Newton-Raphson method and the Arc-length method to solve the nonlinear equations. It is also possible for the user to define the convergence parameters, and default values are shown in Figure 2-6. Limit for iterations is possible to adjust to get more accurate results for each step, but the greater values the more time-consuming the analysis becomes. It is possible to choose Line search with or without iterations, and to set a limit for line search iteration. The stiffness matrix can be assembled either with each iteration or with for each step. A various solvers can be employed, thereby the default PARADISO linear equation system solver, or sparse iterative solvers (ICCG, DCG). However, in cases where the mentioned solvers cannot give a solution a slower, but more robust equation solver should be applied i.e. LU. Method for the element numbering optimization can be set; with the ability of reducing the program memory requirements i.e. SLOAN or Gibbs-Poole can be selected. Tangent

or elastic stiffness can be chosen, where the elastic stiffness results in more robust convergence, while the tangent stiffness gives faster convergence (V. r. Červenka, Červenka, Janda, & Pryl, 2017).

In this thesis the loading is displacement-controlled, and the Newton-Raphson method is applied. It is in general recommended apply loading with the N-R method up to a nominal level (100%), and then continue overloading with Arch Length solution (Pryl & Cervenka, 2017).
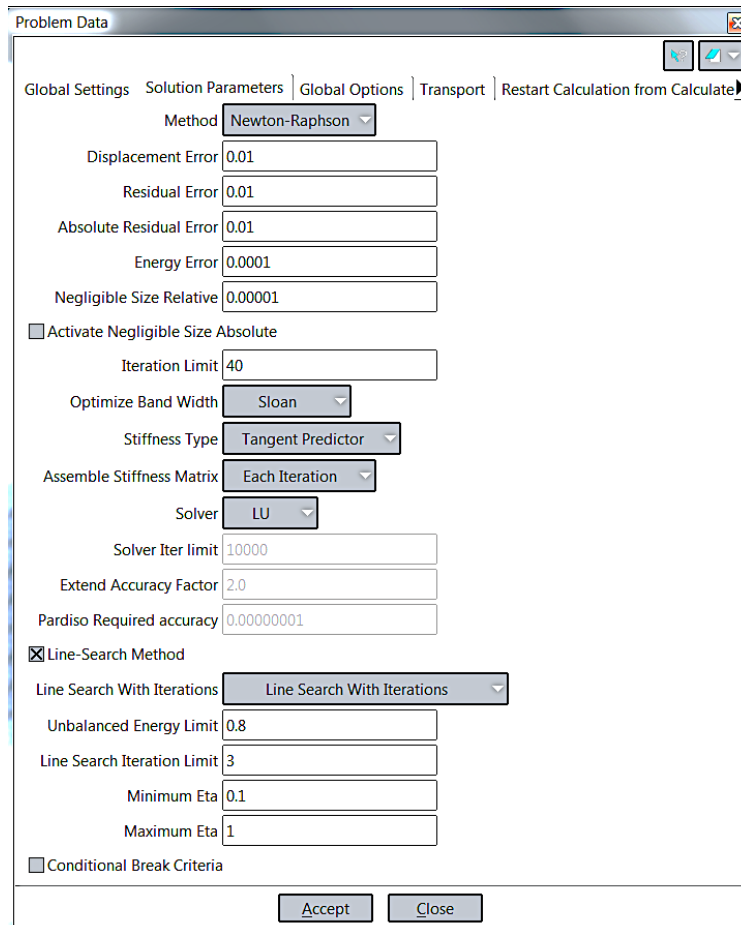
Figure 2-6: Menu for solution parameters in GiD

3 Fibre reinforced concrete

This section gives an introduction to the concept of using concrete as a structural material, and the influence of reinforcing with fibres. Different fibre materials and shapes are discussed.

3.1 Concrete

3.1.1 History and development

"Concrete" as a building material has its origins dating back to ancient time. The use of gypsum is dated all the way back to the Egyptian eras, where the gypsum was used as a binder in the construction of the pyramids. The romans developed further a concrete-like material by mixing burnt limestone, volcanic sand and volcanic rocks. The mixture of the materials resulted in a product, which occurred to be water resistant. Structures as the famous Pantheon temple built in year 126 in Rome and the Colosseum built in 70-80 AD in the centre of Rome, are remarkable examples of the strength and durability that concrete provides (Delphin, 2009).

The modern concrete concept is based on the roman technique of concrete mixing and casting. The major development of the concrete concept, however, started in the beginning of the 19th century.

The British engineer John Smeaton created the forerunner to the modern concrete in the reconstruction work of the Eddystone Ligthhouse in 1756. He carried out research, which lead to a hydraulic cement with the function of being quick drying. The lighthouse was entirely made of interlocked Portland stone and survived severe weather conditions for about 120 years.

Bricklayer Joseph Aspdin from England was the inventor of the Portland cement, which is the fundamental layer for the modern concrete industry. Joseph Aspdin burnt a mixture of limestone and clay, which resulted in a very fine powdered product capable of binding a large content of water. In the modern cement production, similar rocks to the ones at the Portland islands are being used, hence the name Portland cement (Jahren, 2011).

In 1845 Isaac Charles Johnson proved that the optimal cement contained a certain amount of each of the contributing raw materials. He also discovered that a heat temperature at 1400°C was required in order to produce clinker. Johnson contributed to improve the concrete quality further and in the 1880´s when the rotary kiln became invented, England became a leading nation regarding concrete production. The first concrete building with 2 floor levels was raised in 1935 in Swanscombe. The first reinforced concrete structure was raised about 20 years later.

After exporting the modern Portland cement to America, the modern concrete became a revolutionary construction material. Several countries opened factories with the intention of producing their own Portland cement. In the introduction of the 20th century, the production of Portland cement had increased incredibly on world

basis(Espedal, 2015). In Norway, however, about75% of the total accumulated cement consumption has been after 1960.

3.1.2 Concrete technology

As mentioned in the previously section, the concrete concept as a construction material in an old fact. From a technology point of view, however, concrete has varied a lot concerning its constituents. The modern concrete we know today is a mixed composition that may contain 6-8 different constituents. These are listed below:

1) **Coarse aggregate:** crushed or natural particles with diameter larger than 4mm (stone and pebbles)
2) **Fine aggregate:** natural or crushed particles with diameter less than 4mm (sand and gravel)
3) **Cement:** the main contributor to the concrete strength, mainly determined by a ratio expressing the water demand (clinker materials)
4) *Water:* either as liquid or as ice (decreases the curing temperature) which in contact with cement start the hydration process
5) **Admixtures:** chemical agents with the purpose of improving certain properties of the concrete (accelerators, retardations, air- entraining)
6) *Additives:* pozzolans (silica fume, fly ash and blast furnace slag) with beneficial effects on the concrete workability
7) **Plasticizers/ Superplasticizers:** chemical substances that adjusts the consistency of the concrete

Fine and coarse aggregates make up approximately 70% of the total volume in concrete, while the cement paste makes up about 30% of the volume. The remaining constituents are relatively small in comparison.

The composition of concrete strongly depends on the application area. Concrete is commonly used for structures as facades, bridges, road paving, dams, offshore silos, tunnels, rockfall securing and repairs. Usually, concrete is divided into three categories depending on its density. According to NS-EN 206-1, lightweight concrete (LWC) has as density less than 2000 kg/m^3. A lower concrete density is accomplished by adding structural lightweight aggregates with a bulk density in the range of 200-1000kg/m^3. LWC provides less dead load, which is advantageous for bridges and similar structures. Concrete with a density in the range of 2000-2600 kg/m^3 is the most common concrete type for structural purposes. Heavy concrete (HC) is defined as concrete with a density higher than 2600 kg/m^3 and has the advantage of shielding against radioactive radiation. HC is thus mostly used in nuclear power plants and for x-ray equipment in hospitals. Heavy sand and heavy coarse aggregates are often used in order to obtain greater densities.

The term, *workability*, is often used in relation to fresh concrete. It is often referred to as the ease with which concrete can be mixed, placed and consolidated. To facilitate the complex behaviour of concrete, workability is divided into *mobility*, *compactability* and *stability*. Mobility is the ability of concrete to flow and spread out in the formwork – either by rodding or by itself. Compactability is the easiness of the concrete to completely fill the formwork and embedding the reinforcement. The last term, stability, is the ability of concrete to resist excessive bleeding or separation when being worked

with. The workability of concrete is obtained indirectly by its consistency, ranging from very stiff to flowing/wet. Often, the wetter a concrete is, the more workable it is (Maage, 2008). However, there are exceptions.

3.2 Fibre reinforced concrete (FRC)

Fibre reinforcement in concrete usually has the intension of being an addition to the traditionally steel bar reinforcement. Fibre reinforced concrete (FRC) might otherwise be used separately for non-structural components. The fibre reinforcement might vary in material, dimension and shape. The addition of fibres can contribute to increase bearing capacity of the concrete, as well as reducing shrinkage cracking.

3.2.1 Historical development

The concept of adding fibres to reinforce brittle materials has been practiced for thousands of years. Straws were applied to strengthen sun-baked bricks and mud-hut walls, while horsehair was used to reinforce gypsum. Later on, Portland cement mortars have been reinforced with asbestos fibres. The introduction of the modern fibre reinforcement, however, began in the early 1960s. At this moment straight steel fibres were added to the concrete, mainly in pavements. The use of fibres as reinforcement brought difficulties to the mixing and casting process. High amounts of fibres reduced the workability of the concrete dramatically, as the fibres had a tendency to cling together in balls.

During the 1970s further research was made worldwide and fibres of various metals, plastics and glass was introduced to the market (Nawy, 2001). From the 1980s and to the present, fibres have made striking advances. The commercial introduction of superplasticizers and other viscous agents made it possible to adjust the workability of the fibre reinforced concrete. Since the 1980s fibres has been well established as complementary reinforcement with the purpose of increasing both the cracking resistance and the shear and flexural strength (Shi & Mo, 2008).

3.2.2 Fibre reinforced concrete in general

Concrete as a structural material provides good ability to withstand compression and is thus the main property utilized in structures. The tensile strength, however, only makes up 10-12% of the compressive strength of an ordinary structural concrete. When the tensile forces exceed the tensile capacity of the concrete, cracks are generated. Cracks on the concrete surface might result in reduced durability of the structure, as they are considered as weak spots due to increased environmental exposure. In the design of concrete structures, it is therefore assumed that all the tensile forces must be taken care of by the reinforcement. This is traditionally accomplished by using steel rods and stirrups, which transmits the tensile forces through the bond between concrete and the steel bars. The process of designing and placing steel bars before casting is time consuming and requires skilled personnel.

By using fibres as reinforcement instead of regular steel bars, one may gain several outcomes. Fibres are advantageous in the way that it is applied directly in the batching plant or mixed into the concrete at the construction site. The use of fibres in self-compacting concrete (SCC) is especially advantageous due to work relieve as it does not require vibration. In addition, when no vibration is performed, the fibres tend to remain more uniformly distributed (Maage, 2008). This will be discussed further in Section 4.3.

The concrete must, in addition to the strength tolerance, satisfy criterions for shrinkage cracking and cracking when loading. Concrete behaves like is a brittle material, and by adding fibres one may alter the ductility. Consequently, a randomly spaced discontinuous fibre addition should aid in arresting the development or propagation of microcracks generated at an early stage of loading. The fibres contribute to increase the cracking resistance of the concrete as well as the shear and flexural strength, which implies:
- Increased ductility as the material is softened
- A higher fracture toughness is obtained
- The impact resistance is altered as the energy absorption capacity becomes greater

Advantages and disadvantages of using fibre as reinforcement in concrete are summarized in Table 3-1.

ADVANTAGES	DISADVANTAGES
• Possible to cast very thin sections • Avoid misplacement of steel bars, and thus eliminate the problem with thin concrete cover • Reduce corrosion issues (choose corrosion resistant fibres) • Reduce shrinkage cracking • Alter the impact resistance by increasing the ductility of the concrete (energy absorb capacity) • Higher fracture toughness • Less time consuming • Work relief as in turn is health positive	• Difficult to obtain a uniform distribution of the fibres • Can be more costly than regular steel bars • Very varying fibre-matrix bonding

Table 3-1: Summarize of advantages and disadvantages with the use of fibres as reinforcement

3.2.3 Practical use of fibre reinforced concrete

Despite the fact that fibres have proven their ability to improve the mechanical properties of concrete, fibre reinforcement has still not achieved the stage where they are accepted as a replacement of the conventional steel bars (Nawy, 2001). This is mainly due to the lack of accepted guidelines and design codes within this area. Partly it is also due to lack of experience/practice and difficulties with achieving the desired fibre distribution.

Common application areas for fibre reinforced concrete involve overlays on bridge decks, industrial slabs, thin shell structures, highway and airport pavement, explosion-resisting structures, shotcrete application (sprayed concrete) in tunnels and rocks, and nevertheless repairs. In Norway, fibre reinforced concrete is mostly applied for foundations, ground-supported slabs or as shotcrete for rock support. In practice, fibre

reinforcement is predominately used in combination with traditional steel bars for load bearing structures (Kanstad et al., 2011).

With respect to the fibre material added, one may categorize the fibre reinforced concrete into the following groups:
- Steel fibre reinforced concrete (SFRC)
- Glass fibre reinforced concrete (GFRC)
- Synthetic fibre reinforced concrete (SNFRC)
- Natural fibre reinforced concrete (NFRC)

Among the above, steel fibre reinforced concrete and synthetic fibre reinforced concrete are the most commonly used for structural purposes (Kanstad et al., 2011).

3.3 Standards and guidelines for the use of FRC

At the present, there are numerous international standards and regulations available concerning fibre reinforced concrete. Many countries have developed their own regional guidelines for the application of FRC. Some of the international guidelines and recommendations for the use of FRC are to be presented in the following.

The Concrete Society in Great Britain has published technical reports for guidance concerning the design and use of fibre reinforced concrete. The important ones are;
- The Concrete Society: *Guidance for the design of steel-fibre-reinforced concrete*, Technical Report No 63, Surrey, Great Britain, March 2007.
- The Concrete Society: *Guidance on the use of macro-synthetic-fibre-reinforced concrete*, Technical Report No 65, Surrey, Great Britain, April 2007

America has also contributed to the development of fibre technology and research. In 2001 the American Concrete Institute (ACI), Committee 544, released a report on "Fiber Reinforced Concrete".

The German Committee for Reinforced Concrete, DAfStb (Deutscher Ausshuss für Stahl-Beton), published, in 2012, a guideline for regulations of properties and applications of "steel fibre reinforced concrete" (SFRC). The guideline is primarily revised on foundation of DIN EN 1992-1-1 in conjunction of DIN EN 1992-1-1/NA (EC2), DIN EN 206-1 and DIN EN 13670 in conjunction of DIN 1045 part 1-4 (01-2008) covering lacking subjects in the previously guidelines. The guideline forms the basis of technology, specification and production, design and construction, and execution of SFRC, see draft (*Model Code 2010 - First complete draft*, 2010).

In October 2013, the International Federation for Structural Concrete (fib – Fédération internationale du betón) published an e-book edition of the fib Model Code for Concrete Structures 2010. Part 4 in the fib Model Code 2010 treats principles, models and test validation of fibre-reinforced concrete, see (Di Prisco, Colombo, & Dozio, 2013). However, none of the above appears to be encompassing regarding FRC. Furthermore are neither of them appropriate to apply directly as governing regulations for execution and inspection in Norway. The Norwegian centre of research based innovation, COIN (Concrete Innovation Centre), have published a series of reports and proposals to regional guidelines. Among other is; *a proposal to guideline for design, execution and*

inspection of fibre reinforced structures, ref. (Kanstad et al., 2011). It is mainly based on NS-EN 1992-1-1 (EC2) for concrete design rules, NS-EN 206-1 for production and NS-EN 13670 for execution. NS-EN 14651:2005 is the governing regulation for testing of specimens and determination of tolerance.

3.4 Fibres – types, shapes and properties

Fibres come in many different materials and in various geometries. By varying the shape, size, thickness and the dosage of the fibres, one may modify the concrete in order to improve certain properties. This will be discussed further in Section 4.1.

European Standard prEN 14889-1:2004 distinguishes the fibres in accordance to their intended use;
- *Class I*; mainly improve short-term plastic properties of concrete, by controlling plastic shrinkage, settlement cracks and reduce bleeding without adversely affecting the long-term properties
- *Class II*: primarily to improve the durability of the concrete by altering the abrasion and impact resistance, in addition to reduce the scale of damage due to freezing and thawing cycles
- *Class III*; primarily increase the residual strength of the concrete
- *Class IV*; primarily improve the fire resistance of the concrete

Fibres are commonly made from steel, glass or synthetic materials, as well as natural elements. The shape and the cross section of the fibres are mainly dependent on the production method. Usually fibres have round cross sections, while other may be flat, crimped, twisted or deformed. A variety of fibre shapes are illustrated in Figure 3-1 and Figure 3-2. Fibres are classified as microfibres when their lengths are greater than the aggregate in the concrete and when the fibre cross section is larger than that of the cement grains. Otherwise, fibres are categorized as microfibres (Löfgren, 2005). Fibres have a typical length of 6mm to 150mm and thickness in the range between 0.005mm and 0.75mm.

| Straight | Curved | Conical | End hooks | End knobs | Kink-shaped | Irregular | Profiled |
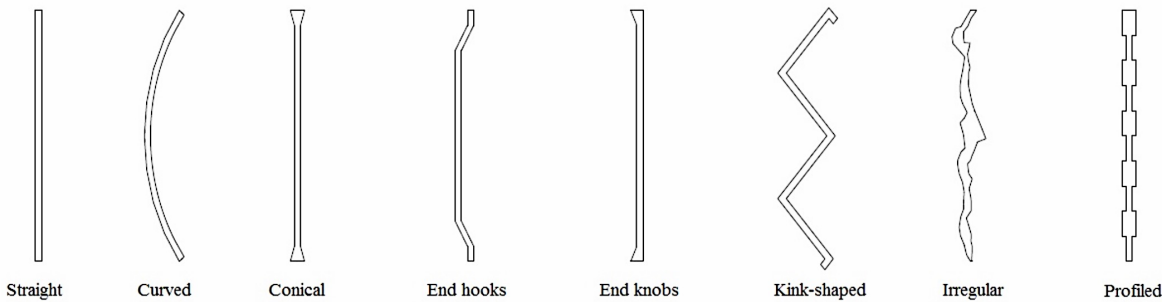
Figure 3-1: A selection of fibre shapes (Kanstad, 2009)
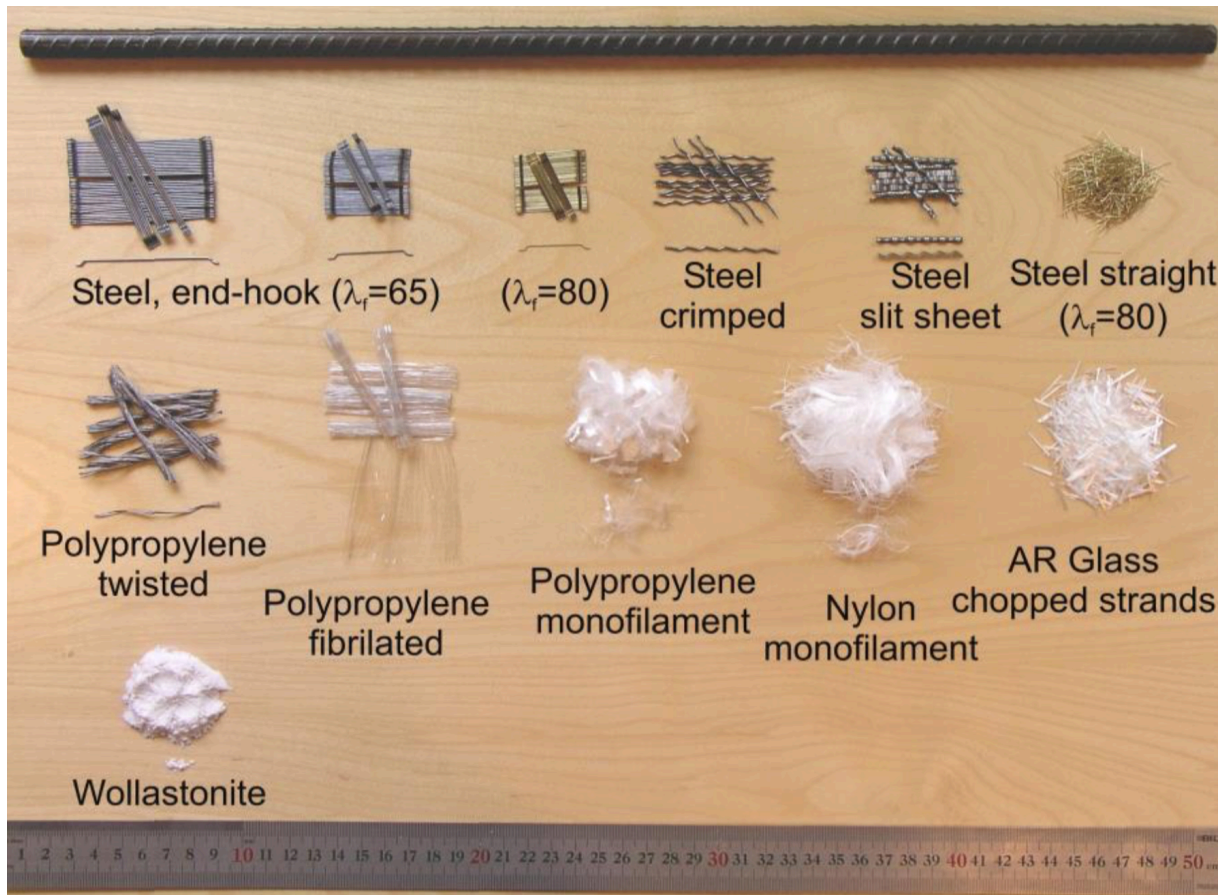
Figure 3-2: Fibres made from different materials depicted (Löfgren, 2005)

The term *aspect ratio* λ_f is often used in relation to fibres, and is a measure of the ratio between the fibre length l and the diameter of its thickness d; $\lambda=l/d$. The aspect ratio typically holds values of 20-100(Vikan, 2007). Another important parameter used to characterize and compare properties of different fibre-reinforced mixtures, is the *volume fraction V_f*. The volume fraction defines the amount of fibres added to the concrete as a percentage of the total volume of the concrete-fibre mixture. In practice the volume fractions varies from 0.25% (20kg/m^3) to 2% (157kg/m^3). Fibres that are to be used in concrete are required to be tested, and its suitability as reinforcing material must be documented (Klausen, 2009).

3.4.1   Steel fibre

Fibres made from steel are relatively short in length, in general from 19mm to 60mm, and with a corresponding aspect ratio between 30-100. Steel fibres are usually of straight, wavy or end hooked shape, with round, flat or crescent cross sections. Steel fibres can, according to prEN 14889-1:2004, be classified into the five general groups;

1) Group I; Cold-drawn wire
2) Group II; Cut sheet
3) Group III; Melt extracted
4) Group IV; Shaved cold drawn wire
5) Group V; Milled from block

There are three important variables that influence the steel fibre performance;
1) The aspect ratio
2) The fibre shape and surface deformation
3) The surface treatment

Normally, a volume fraction of 0.5% and up to 2% of steel fibres is added to the concrete. Additional volume fractions will only lead to reduced workability and requires special techniques for mixing and casting. The steel fibres can, in order to improve the corrosion resistance, be coated with for example zinc(Löfgren, 2005).

3.4.2 Glass fibre
Glass fibres are made from melted glass, and are chopped to various lengths. They are usually very thin and bendable, and will therefore not suffer permanent deformations. The greatest advantage by using glass fibre rather than steel fibre is the low density; about four times lower than steel. The modulus of elasticity and the elongation at fracture, however, is lower than that of steel. Nowadays glass fibres are of alkali-resistant type (AR), which also have shown to improve the long-term durability (Knudsen, Nolte, Gaarder, & Hammer, 2016).

3.4.3 Synthetic fibre
A wide range of synthetic fibre is available at the market, such as polyethylene (PE), polypropylene (PP), polyvinyl acetate (PVA), carbon (high/low), polyester (PES), acrylic and nylon. Fibres made of synthetic materials are often monofilament (large-diameter continuous fibre), fibrillated (continuously networks of fibres, where each individual fibre have branching fibrils) or bundled (strands with several hundreds/thousands filaments of microfibres) (Löfgren, 2005). Alternatively to the randomly distributed fibres, fibres mesh or textiles can be used as reinforcement.
Synthetic fibres are beneficial in the way that they have very low density, where PP-fibres have approximately density of 0.9 versus approximately 7.9 for steel (Maage, 2008). Some of the synthetic fibres such as PP-fibres are hydrophobic (do not absorb water), in addition to being chemically inert. Thin concrete sections are possible to produce, as there is no risk of corrosion of the reinforcing materials in the concrete.

There are also some disadvantages associated to the use of synthetic fibres as reinforcing material in concrete. Synthetic fibres have low ability to bond with the concrete matrix. Furthermore, some of the fibres provide low modulus of elasticity in addition to being expensive.

3.4.4 Natural fibre
Bamboo, coconut coir, sisal, wood cellulose, and vegetables, are examples of natural fibres used as reinforcing materials. Natural fibres are monofilament, strands, crimped and single-knotted. Thin sheets for roofs and walls can be easily made, and provides relatively good mechanical properties to the concrete compared to many of the synthetic fibres. On the other hand, natural fibres are very susceptible to moisture content, resulting in quite varying concrete durability (Vikan, 2007).

3.4.5   Recycled fibres of tyre waste

As a way to preserve the environment, waste material, like used car tyres, might be recycled and re-utilized. Tyres vary in composition depending on the type of vehicle and the severity of use. A car tyre typically contains a tread, a body with sidewalls and beads, like shown in Figure 3-3. The tread is the outer layer in contact with the road, and is supported by the body. The beads are metal-wire bundles covered with rubber, and makes sure that the tyre sticks to the wheel. Tyres are typically made of natural rubber, synthetic rubber carbon, steel, and fabric fillers in the percentage quantities given in Table 3-2.

Rubber compounds - throughout the tyre: treads, sidewalls, etc.

Plies and belts: layers of brass coated steel with rubber

Bead wire: Cords of high tensile steel that give form to the tyre

Casing: Made of metal, rayon, nylon. Polyester cords
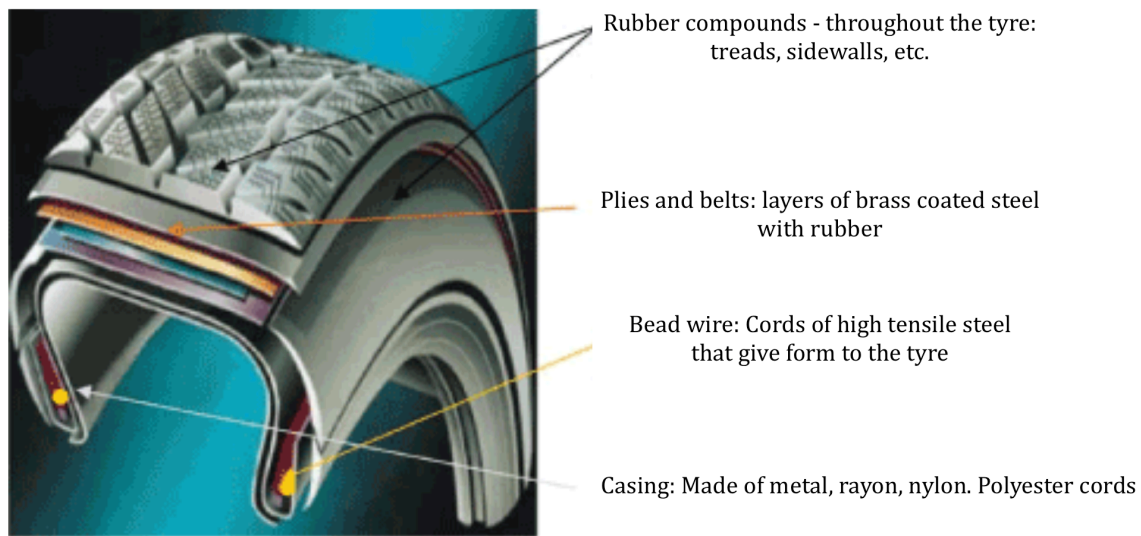
Figure 3-3: A typical tyre composition (Lu, 2015)

The recycling of tyre waste mainly involves three by-products; crumb rubber, steel and fibre. The production of fibres made of waste tyre consist of several steps, as presented in the following:

- *Selection*: collection of suitable tyre for reconstruction
- *Bead wire breaking* (only for truck tyres): extracting bead wires of truck tyres by mechanical action before further processing takes place
- *Cleaning*: tyres are washed inside a washing tank to eliminate traces of soil and other dirt
- *Shredding*: tyres are being cut into smaller pieces, where the cutting action of liberates the rubber from the steel
- *Sieving*: tyre pieces are passed in a sieve with a rotating drum, where material with a size less than 100mm is being selected. The material is then being passed over to a second shredding action, where fibres are being processed up to a suitable size.
- *Granulation*: the shredded tyres are loaded into a granulator and the desired size of the fibres can be selected by passing them through a suitable grid placed in the last part of the granulation system.
- *Electromagnetic separation*: fragments of tyres containing steel fibres, rubber and textile fibres are passed through an electromagnetic separator.

	Passenger tire	Truck Tire
Natural rubber	14%	27%
Synthetic rubber	27%	14%
Carbon black	28%	28%
Steel	14 - 15%	14 -15%
Fabric, fillers, accelerators, antiozonants, etc.	16 -17%	16 -17%
Average weight	new: 11.35 kg	new: 54.43 kg
	scrap: 9.10 kg	scrap: 45.36 kg

Table 3-2: Typical tyre composition by weight (Lu, 2015)

The cleanliness and quantity of the steel fibres strongly depends on the type of equipment utilized. The steel fibres produced in such manner discussed above, have irregular shapes, with variable lengths in the range of 20mm-70mm. A sample of fibres used in this thesis is depicted in Figure 3-4. The mechanical properties of the recycled fibres used in this thesis, are presented in Section 4.2.2, (Lu, 2015).

Figure 3-4: Sample of recycled steel fibres at the laboratory

4 Mechanical properties

This section deals with mechanical properties of fibre reinforced concrete such as compression strength and tensile strength. Additionally, the influence of fibre orientation and distribution will be dealt with. A declaration of the mechanical properties concerning the fibres used in the experiments is also given in this chapter.

4.1 Fibre properties in general

4.1.1 Influencing parameters of fibres

Several physical properties of fibres are considered strongly influence the performance of fibre-reinforced composites. According to the general guideline for design of FRC (Concrete Society, 2007), the most important ones are, ref. (Kanstad et al., 2011):
- Bond and anchorage mechanism
- Fibre length and diameter
- Dosage of fibres (kg/m^3)
- Tensile strength
- Modulus of elasticity

4.1.2 General requirements for fibres

Fibres in concrete matrices are, according to experimental and analytical studies, considered to be effective when (Löfgren, 2005):

- The tensile strength of the fibres is significantly higher than that of the matrix (two or three orders of magnitude).
- The bond strength between the matrix and the fibres is of at least the same order as the tensile strength of the matrix, preferably higher.
- At least three times as high modulus of elasticity in tension for the fibres than that of the matrix.
- The ductility is high enough so that the fibres do not fracture due to fibre abrasion or bending.
- The Poisson ratio and the thermal expansion coefficient are of the same order for both fibre and matrix (avoid debonding).
- The fibres are durable and able to withstand the high alkaline environment.

4.2 Declaration of fibre parameters

All fibres that are to be added to concrete, whether they are applied for structural purposes or not, must be tested and declared. Regulations for material documentation and declaration of fibres are given in the following standards;
- Steel fibres; NS-EN 14889-1: *Fibres for concrete – Part 1: Steel fibres – Definitions, specifications and conformity*
- Polymer fibres; NS-EN 14889-2: *Fibres for concrete – Part 2: Polymer fibres – Definitions, specifications and conformity*

The above regulations and principles are also to be applied for fibres made from other

materials than steel and polymers. In this thesis both commercial steel fibres and recycled steel fibres made from tyre waste are used.

4.2.1 Commercial steel fibres

There is a lot of information available for the commercial steel fibres that are used at the laboratory. The fibres are hooked-end, with the particular purpose of arresting cracks. Advantageously, these fibres have the ability to anchor and resist a greater pull-out load than straight fibres, see Figure 4-1. Some of the most important parameters are shown in Table 4-1. For further details see (MAPEI, 2015).
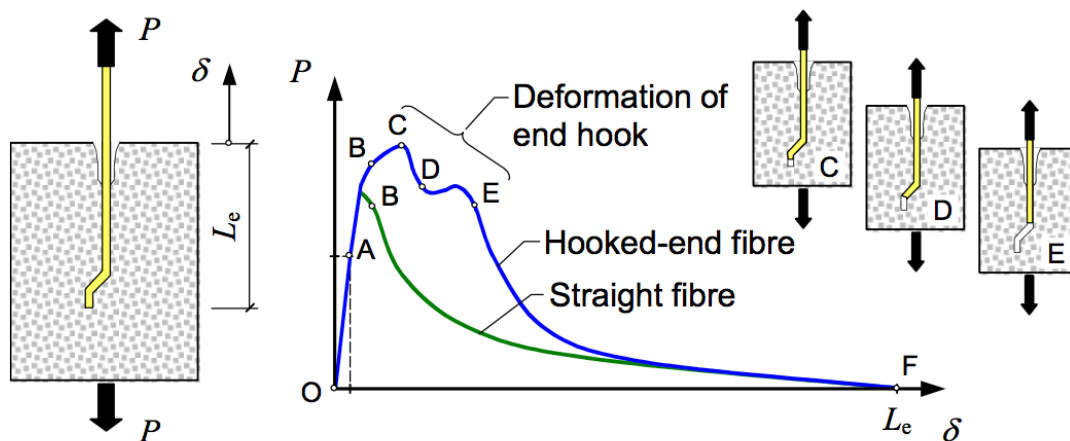
Figure 4-1: Typical fibre pull-out behaviour for hooked-end and straight fibres (Löfgren, 2005)

Steel fibre DE 35/0.55N	
Length	35mm (±10%)
Diameter	0.55mm (±10%)
Aspect ratio	63.5
Tensile strength	1250MPa (±15%)
Application area	Very suitable for thin concrete layers and shotcrete

Table 4-1: Steel fibre parameters (MAPEI, 2015).

4.2.2 Recycled steel fibres from tyre waste

Very little information came along with the recycled steel fibres. In order to determine important parameters of the recycled fibres, a series of test were conducted. Through the tests, the aspect ratio, density, composition and tensile strength of the fibres was determined. Figure 4-2 shows the recycled steel fibres at the laboratory.

Figure 4-2: Sample of recycled steel fibres made from tyre waste

Aspect ratio (l/d)
To determine the aspect ratio, an amount of 100 fibres were randomly handpicked from the container. Some of the fibres were of much greater lengths and diameter than the rest of the fibres, and it was therefor decided to not include them in the tests. Neither were the improper fibres used for casting. The aspect ratio (length-diameter ratio) was determined by measuring each individual fibre length and diameter. A statistical representation of the frequency of the fibre aspect ratios is shown in

Figure 4-3. The red line represents the cumulative percentage of the total amount of samples at any given point. Average values and standard deviation for fibre lengths, diameter and aspect ratio were calculated and are given in Table 4-2.
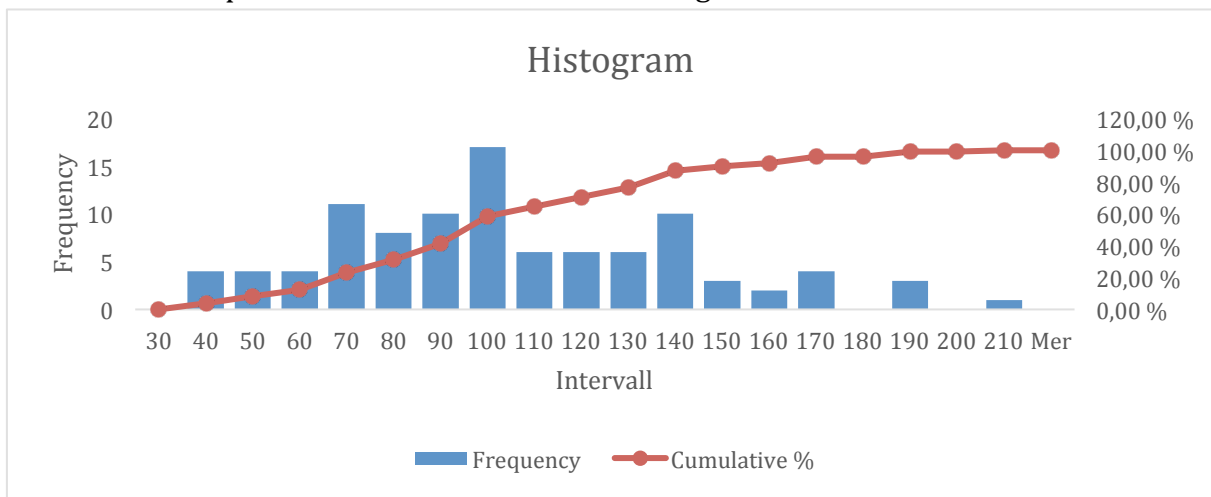
Figure 4-3: Aspect ration distribution of recycled steel fibres

	Length [mm]	Diameter [mm]	Aspect ratio
Mean	37.31	0.42	100.38
Median	34.00	0.33	97.06
Standard deviation (STD)	11.80	0.22	37.47
% STD	31.6%	52.4%	37.3%

Table 4-2: Average values and deviation for fibre length, diameter and aspect ratio

In comparison with the commercial steel fibres, the recycled steel fibres have a significantly different aspect ratio. The shapes of the recycled fibres are irregular, which means a let predictable pull-out behaviour than the commercial steel fibres.

Density

The density of a material compound can reveal great information about the material composition. Since the fibres are added to the concrete with respect to the volume fraction, the density becomes of a great importance for the concrete recipe. Since there was no measuring device specifically designed for density test available at the laboratory, the test was improvised to some extent. Before the density could be measured, the fibres were placed in a drying cabinet at 100 degrees Celsius overnight. Following, a stable frame with a scale was placed over a bucket filled with water. The dried fibres were added to a sieve, where they stayed in between two very fine layers. The sieves were attached to the scale by means of strings, in such way that the sieves were hanging freely above the bucket. The sieves were weighted while submerged both before and after the fibres were added. Thus, the density of the fibres alone could be obtained by the principle of Archimedes:

$$\rho_f = \frac{w_d}{\frac{w_d - w_s}{\rho_w}} \tag{4.1}$$

where:
ρ_f is the density of the fibres,
w_d is the weight of the dry weight of the fibres,
w_s is the submerged weight of the sieves, and
ρ_w is the density of the water.

The density was carried out for two samples, with the average value of 3014 kg/m³.

Fibre composition

Fibres made from tyre waste, contains other material components besides steel, such as nylon, rubber and textile. Since the steel is the reinforcing component, it is of interest to determine the pure steel contamination. To do this, pyrolysis was performed.

In order to avoid moisture to interfere with the test results, fibres were placed in a drying cabinet at 100 degrees of Celsius overnight. The fibres were weighted before and after drying. Following, the pyrolysis was performed by drying the material up to 600 degrees of Celsius, with the condition of no access to oxygen. At this temperature, all other material besides steel either evaporates or dissolves into finer particles. After the

pyrolysis, the steel fibres were extracted from the rest of the materials by means of a magnet. By carefully holding the magnet over the sample, the steel fibres were able to adhere to the magnet and be easily transferred to another bowl. The bowl containing pure steel fibres was then weighted, and the percentage of steel content and remaining materials could therefore be determined. Table 4-3 summarizes the obtained results. In average, the steel content makes up about 91.7%, whereas other materials (nylon, rubber, carbon) represent the remaining 8.3% of the recycled fibre content.

	Sample 1	Sample 2	Sample 3
Weight wet [g]	901.6	1245.3	967.7
Weight wet [g]	897.7	1239.1	960.2
Weight after pyrolysis [g]	843.1	1161.8	899.0
Weight after magnet [g]	832.0	1142.3	882.2
Pure steel content [%]	92.28	91.73	91.16
Other materials [%]	7.72	8.27	8.84

Table 4-3: Material composition obtained from the tests

Tensile strength

The characteristics of fibres play an important role for the effective mechanical and damage behaviour of the composite. Tests were therefore conducted in order to make an overall estimation of the tensile strength of the recycled fibres. The test fibres were randomly selected. The test was performed by mounting clamps in both end of a single fibre in a vertical stretching machine. Both length and diameter is measured in advance. An axial load is applied, resulting in elongation of the fibre. The load is applied until failure, where both loading and displacement are monitored. The ultimate tensile strength could then be calculated (Ilankeeran, Mohite, & Kamle, 2012).

However, an average estimation of the tensile strength turned out to be difficult to determine. The results were quite varying, and therefore no precise pattern was obtained. There are many reasons for this, such as storing fibres outside exposed to corrosion. Another reason might be due to the deformed shapes, making the material weaker at certain areas and thus reducing the tensile strength. Tyres may also contain different types of steel depending on the manufacturer, which again means variations in steel quality. In addition, loading history of the steel material also influence the fibre strength parameters.

The average yielding strength obtained is 870MPa, with a very high corresponding standard deviation of 584 MPa. The results for tensile strength testing are given in Appendix A.

4.3 Orientation and distribution of fibres

The aim of this thesis is to investigate the behaviour of fibre reinforced concrete, in which means to analyse the load-carrying capacity. The analysis is based on varying the fibre type and quantities added to the concrete, and examine the concrete response to loading. Consequently, it will be necessary to study how the fibre orientation affects the load-carrying ability of the FRC.

The orientation of fibres in concrete has a great influence on the mechanical performance of fibre reinforced concrete. The objective of the technology regarding distributed reinforcement is to achieve direct and random (free) orientation of the fibres in the concrete body. Optimal fibre orientation is when the fibres are normal to the crack, and the crack occurs at the middle of the fibre. However, this is seldom the case in FRC elements and must therefore be taken into account when designing.

There are several factors influencing the fibre orientation and distribution in fibre reinforced concrete. Firstly, the fibre orientation is very restricted to the geometry of the FRC element. Free fibre orientation occurs to be more limited for smaller cross-sections than for elements with large dimensions. Especially restricted are thin-walled fibre reinforced components such as flat sheets and plates. According to several analyses, the effect of constrained orientations occurs in members where the dimensions are less than five times the fibre length.

Secondly, the method of placement, the equipment used (e.g. pumping), and the properties of the fresh concrete (resistance against fibre segregation) play an important role concerning the fibre orientation.

The angles of inclination of the fibres relative to the surface of the concrete element, range from 0° to 90°, assuming that all the dimension of the element is considerably greater than the fibre length. Different techniques of discrete fibre orientations are visualized in Figure 4-4(Löfgren, 2005).
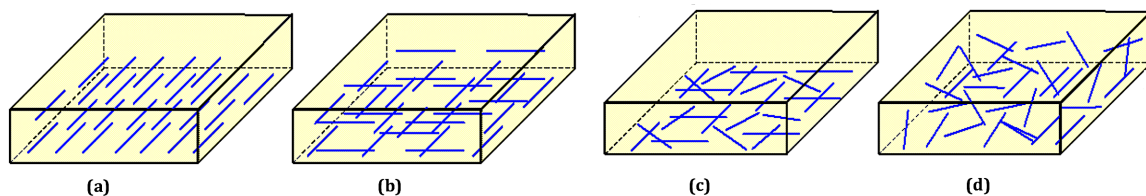
Figure 4-4: Representation of various discontinuous fibre orientations (Löfgren, 2005)

(a) *Discontinuous biased with 1-D fibre orientation*
(b) *Discontinuous biased with 2-D fibre orientation*
(c) *Discontinuous with plane-random fibre orientation*
(d) *Discontinuous with random fibre orientation*

4.4 Strength classes

For concrete the compressive strength is the main quality criterion in focus. The strength of the concrete is the ability to resist stress without any failure occurring in the material. In design codes other concrete properties are often expressed in terms of the compressive strength. According to NS-EN 1992-1-1 the different compressive strength classes are defined by a prefix "B" for normal concrete, followed by a number equal to the characteristic compressive cylinder strength of the concrete at 28 days (f_{ck}). In Norway the compressive strength of a concrete may also be expressed and documented by the strength tested on cube specimens. The compressive strength classes for concrete and their characteristic cylinders and cube strength are shown in Table 4-4.

	Strength classes							
	B20	**B25**	**B30**	**B35**	**B40**	**B50**	**B60**	**B70**
Cylinder, Compressive strength	20	25	30	35	40	50	60	70
Cube, Compressive strength	25	30	37	45	55	67	68	78
Tensile strength $f_{ctk,0.05}$	1,5	1,8	2,0	2,2	2,5	2,9	3,1	3,2

Table 4-4: Strength classes and characteristic strength for both normal concrete and fibre reinforced concrete ((Kanstad et al., 2011)

Compressive strengths in the range between 20-40MPa are considered to be moderate-strength concrete, and are the most common used for construction purpose. Low-strength concrete (strength <20MPa) and high-strength concrete (strength>40MPa) are mostly used for special applications (Mehta & Monteiro, 2006).

Fibre reinforced concrete is characterized by its compressive strength in the same way as for normal concrete. Additionally, fibre reinforced concrete is categorized by its residual tensile strength at 2.5mm crack width as shown in Table 4-5. A fibre reinforced concrete of B30-R1.5 has a characteristic compressive cylinder strength of 30 N/mm^2 and characteristic residual tensile strength of 1.5 N/mm^2 at a crack width of 2.5mm (Kanstad et al., 2011).

Residual tensile strength class	R0,5	R0,75	R1,0	R1,5	R2,0	R2,5	R3,0	R3,5
$f_{ftk,res\ 2.5}$	0,5	0,75	1,0	1,5	2,0	2,5	3,0	4,0
$f_{R,3}$(*2.5mm*)	1,3	2,0	2,7	4,0	5,4	6,7	8,1	10,8

Table 4-5: Examples of residual tensile strength classes with characteristic residual tensile strength and residual bending tensile strength for FRC (Kanstad et al., 2011).

4.5 Compressive properties

In general, the presence of moderate amounts of fibre in concrete matrix does not affect the compressive strength significantly. On the other hand, the addition of fibres does influence the tensile strength of the concrete, causing a less brittle failure (Døssland, 2008).

The stress-strain relation of non-reinforced concrete exhibits nearly linear elastic response up to about 30% of the total compressive strength. Subsequently follows a gradual softening up to the maximal compressive strength. Beyond the compressive strength of the concrete, the stress-strain relation exhibits strain softening until failure takes place by concrete crushing.

The behaviour is highly dependent on the type of fibre added, the size and properties of the fibres, and the volume fraction of fibres added. Not at least does the composition of the matrix affect the stress-strain relation. A general conclusion is that conventional fibres at moderate dosages (<1%), does not affect the pre-peak properties. For microfibres or larger volume fractions (>1%), however, it will be possible to increase the compressive strength. The effect of fibres in terms of compression is illustrated in Figure 4-5 (Löfgren, 2005).
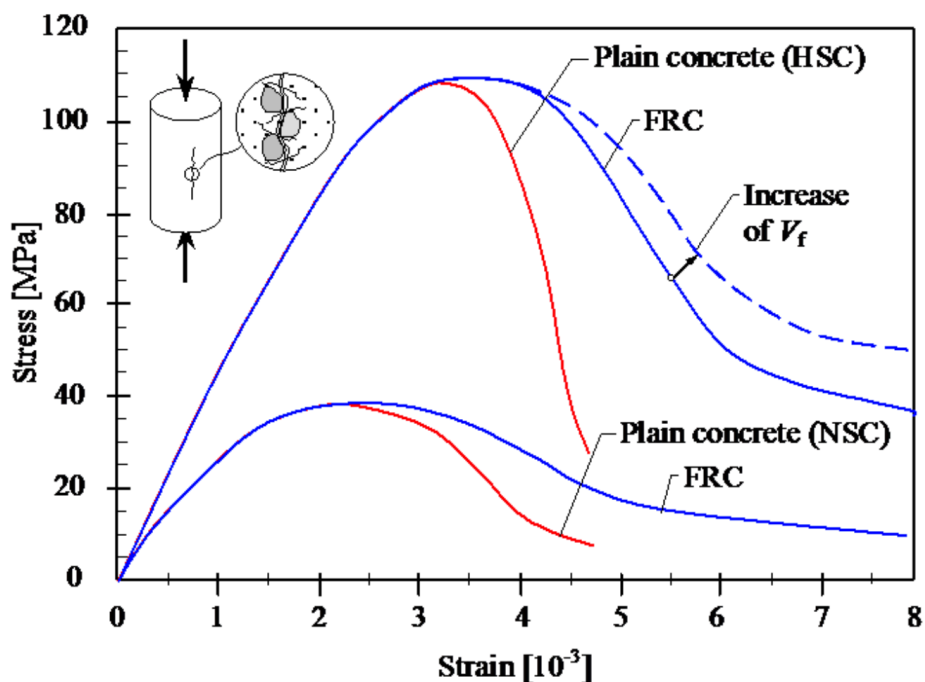
Figure 4-5: Stress-strain relation for plain concrete and concrete with various amounts of fibres added (Löfgren, 2005)

4.6 Tensile properties

As pointed out in the previous subsection, the addition of fibres affects the tensile behaviour of the concrete (Kanstad et al., 2011). With moderate addition of fibres, it is mainly the ductility, which is affected, not the tensile strength itself. Thus, for ordinary concrete with moderate fibre content the effect on the peak stress, f_t, can be neglected see Figure 4-6 below (Døssland, 2008). What makes fibres special in comparison to traditional steel reinforcement in concrete is that the fibres continue to provide relatively stable tensile strength to the concrete, even after cracks are generated. In normal reinforced concrete, the ability to withstand tensile forces is considerably reduced after cracks have developed a width of 0.3mm.

The case is somewhat different for fibre reinforced concrete. When a crack has initiated, the fibres will have the ability to transfer stresses across the crack, relieving stress concentration. As the crack mouth opening displacement (CMOD) becomes greater, fibres will experience plastic deformation when being pulled out of the concrete matrix. Fibres that have been completely drawn out of the concrete matrix have reached the limit of ultimate failure. The stress-strain diagram for fibre reinforced concrete will therefore have a rather different development, behaving more ductile and with residual capacity after the peak is reached. The residual tensile capacity will be further discussed
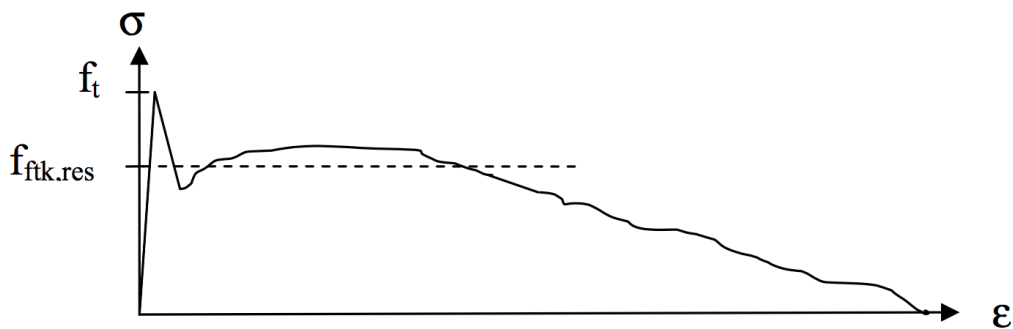
Figure 4-6: Typical tensile behaviour for steel fibre reinforced concrete (Døssland, 2008).

in the following (Löfgren, 2005).

4.6.1 Residual tensile strength

The ability of providing relatively stable tensile strength to the concrete after cracking, is referred to as residual tensile strength. The residual tensile strength for FRC is generally determined from flexural tests on notched prisms or by four-point bending test, which is fully described in Section 5.4.4.

The characteristic residual tensile strength, $f_{ftk,res\ 2.5}$, of the fibre reinforced concrete is defined as the tensile force resultant per unit area for a consistently crack with a crack width of 2.5mm. According to COIN Project report 29-2011, the residual tensile stress can be expressed as 0.37 times the characteristic residual bending capacity determined by bending tests of standardized beams (f_{Rk3}):

$$f_{ftk,res\,2.5} = 0.37 \cdot f_{Rk,3} \tag{4.2}$$

The characteristic residual tensile strength can be obtained from the following expression:

$$f_{Rk,3} = f_{R,i} - k \cdot s \tag{4.3}$$

where
$f_{R,i}$ is the residual flexural strength,
k is a factor that is set to 1.7 as described in NS-EN 14651, see chapter 8.2.2. NS-EN 14651,
s is the standard deviation from the test values.
The residual flexural strength for concrete with known volume fraction of fibres can be partly determined by theory and partly by performing tests of the specific concrete;

$$f_{ftk,res\,2.5} = \eta_0 \cdot v_f \cdot \sigma_{fk,av} \tag{4.4}$$

where
η_0 is the capacity factor, which indicates how much of the fibre forces that is effective normal to the crack plane (usually set to 1/3 for fibres with 3D random orientation),
v_f is the known volume fraction of fibres added to the concrete
$\sigma_{ft,av}$ is the average stress in all fibres across cracks, measured by pull-out test of single fibres (Kanstad et al., 2011).

4.6.2 Strain softening and strain hardening
Cement-based materials like fibre-reinforced concrete, is often divided into two separate categories, depending on the tensile behaviour. Either the concrete is strain softening (quasi-brittle material) or it is classified as pseudo strain hardening, see Figure 4-7.
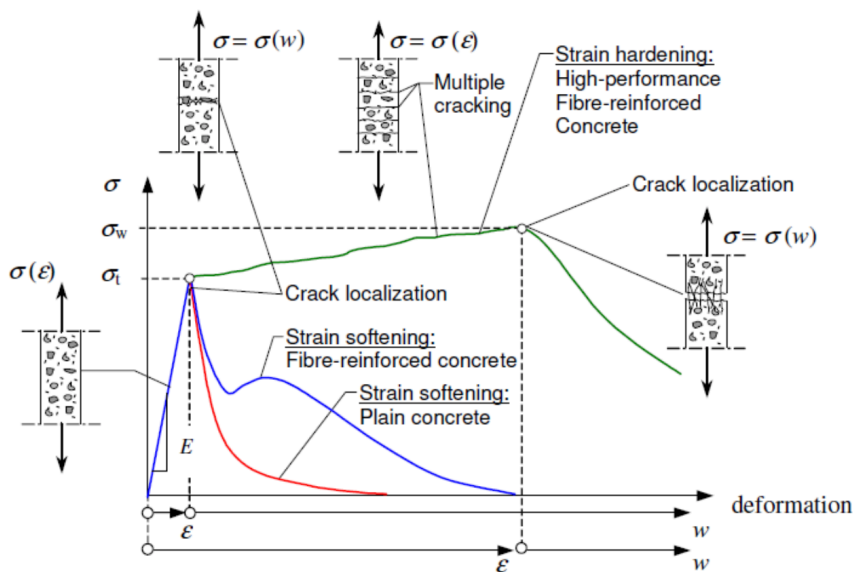
Figure 4-7: Classification of tensile behaviour of cement-based materials (Löfgren, 2005)

Strain softening is defined as the loss of load-carrying capacity of the concrete, after the maximum load is reached. For strain softening materials, the post-peak behaviour is fully dependent on a single localised crack, causing the stress in the concrete matrix to decrease. Plain concrete is a strain softening material, whereas high performance fibre-reinforced concrete (HPFRC) is as strain hardening material. Several researches have shown through experiments that the stress-crack deformation curve of plain concrete lie in a relative narrow band when the stress is normalized with respect to the tensile strength. The tensile fracture behaviour can be determined by the tensile strength, and then be used in a crack model. In the case of high performance FRC the stress-strain curve shows a quasi-strain hardening behaviour, in which means that the post-cracking strength appears to be larger than the cracking strength.

In this thesis the focus will lie on ordinary concrete with fibre content up to 1%. A typically stress-strain behaviour of fibre reinforced concrete is illustrated by the blue curve in Figure 4-8(a). This type of material acts as strain softening, but in more ductile manner than the plain concrete. The fracture energy and the shape of the stress-crack opening curve are highly dependent on type and amount of fibres added. Theoretical crack models include important properties as the tensile strength, the modulus of elasticity, fracture energy G_F and the shape op the σ-w curve, see Figure 4-8(b). However, the total fracture energy is of no interest since the stress-free crack opening, w_c, occurs at very large CMOD for FRC (Löfgren, 2005).
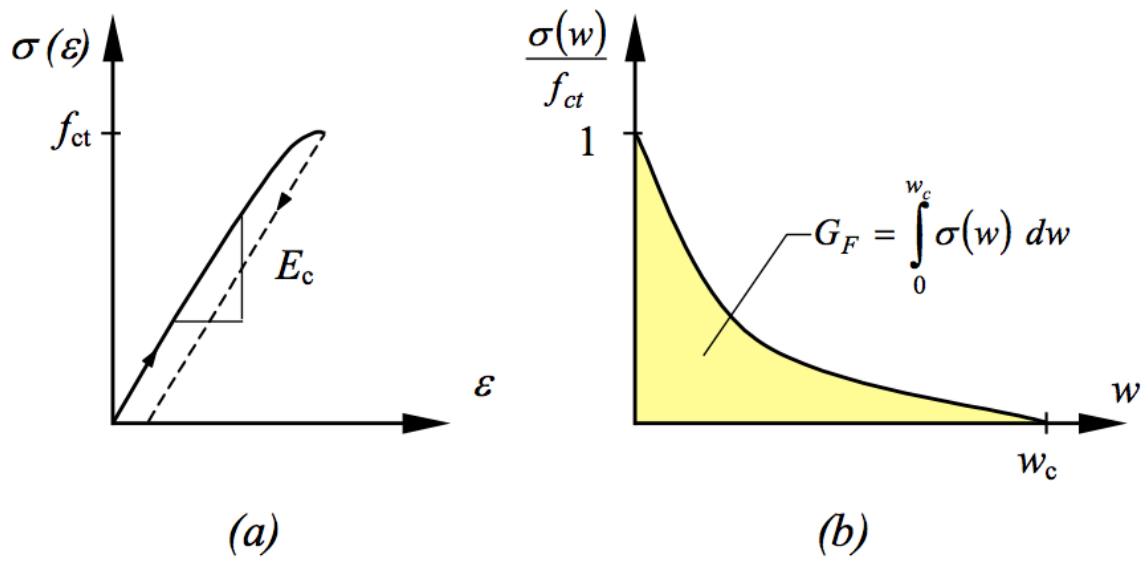
Figure 4-8: Description of tensile behaviour for theoretical crack model (Löfgren, 2005)

(a) stress-strain curve
(b) stress-crack opening curve

5 Experimental programme

The experimental programme will be dealt with in this section. It includes mixture design, casting process, and testing of both fresh and hardened concrete. It should be emphasized that the three bachelor students P. R. Hovind, B. Mikalsen and J. W. Pedersen primarily performed the laboratory work.

5.1 Introduction

To be able to model the realistic behaviour of fibre reinforced concrete, certain properties must be obtained. The necessary properties must therefore be conducted through laboratory tests of fibre reinforced concrete components. The aim is to determine parameters such as the compression strength, the modulus of elasticity, splitting tensile strength and fracture energy. Not at least is it necessary to establish the stress-strain behaviour of FRC.

Various tests were performed for both fresh and hardened concrete, and are summarized in Table 5-1. The tests will be explained in Section 5.3 and Section 5.4.

TESTS
FRESH CONCRETE

• Air content
   • Density
   • Slump measure and slump flow

HARDENED CONCRETE

• Compression test
   • E-modulus test
   • Splitting tensile test
   • 4-point bending test (4PBT)
   • Wedge splitting test (WST)

Table 5-1: Overview of laboratory experiments conducted on fresh and hardened concrete

Table 5-2 gives an overview of the casting programme. In total, 5 different concrete recipes were used:
- 0.0% RFRC   0.0% recycled fibre reinforced concrete
- 0.5% RFRC   0.5% recycled fibre reinforced concrete
- 1.0% RFRC   1.0% recycled fibre reinforced concrete
- 0.5% SFRC   0.5% steel fibre reinforced concrete
- 1.0% SFRC   1.0% steel fibre reinforced concrete

MATERIAL	SPECIMEN GEOMETRY AND QUANTITY				
	Cylinders			Cubes	Beams with reinforcement bars
	Compressive strength	Modulus of elasticity	Splitting tensile strength	Fracture toughness	Stress-strain curve
0.0% RFRC	3	3		3	1
0.5% RFRC	3	3		3	1
1.0% RFRC	3	3		3	1
0.5% SFRC	3	3		3	1
1.0% SFRC	3	3		3	1
TOTAL	30			15	5

Table 5-2: Schematic overview of casting elements

5.2 Mix design

B30 is one of the most common concrete classes used for construction purpose, and it was therefore desirable to design such concrete. Originally, the concrete was designed with Industrisement Cem I 52,5. However, because of mislabelling at the laboratory, the cement turned out to be Standard FA Cem II/B-M 42,5R. The mix composition for beams and cylinders is given in Table 5-3, and the composition for cube specimens is given in Table 5-4. The concrete is designed with a water/cement ratio of 0.59. The ratio between gravel and sand is set to 0.55, and the matrix volume is 300 litre/m^3. To avoid problems due to segregation, it is chosen to use normal concrete instead of self-compacting concrete. However, it should be noted that SCC have other motivating advantages (Maage, 2008).

COMPONENTS	Material amount in kg				
	0.0% RFRC	0.5% RFRC	1.0% RFRC	0.5% SFRC	1.0% SFRC
Gravel 8-16mm (Velde)	196,504	185,986	183,81	185,162	183,81
Sand 0-8mm (Årdal)	243,756	229,24	225,774	231,374	229,574
Cement STD FA	77,55	72,856	73,612	73,61	73,612
Water	41,67	40,594	41,838	37,888	38,038
Dynamon SX-N (SP)	0,62	0,582	0,588	0,588	0,588
Recycled fibres (RF)	0	3,376	6,752	0	0
Steel fibres (SF)	0	0	0	8,736	17,472
Total (litres)	236	224	224	224	224

Table 5-3: Mix composition of concrete for cylinder and beam specimens

COMPONENTS	Material amount in kg				
	0.0% RFRC	0.5% RFRC	1.0% RFRC	0.5% SFRC	1.0% SFRC
Gravel 8-16mm (Velde)	47,461	19,839	18,053	18,185	18,052
Sand 0-8mm (Årdal)	60,028	24,802	22,394	22,979	23,14
Cement STD FA Cem II 42,5R (Norcem)	18,73	7,887	7,23	7,229	7,23
Water	8,91	4,047	3,89	3,467	3,144
Dynamon SX-N (Mapei)	0,15	0,063	0,058	0,058	0,058
Recycled fibres (RF)	0	0,362	0,663	0	0
Steel fibres (SF)	0	0	0	0,858	1,716
Total (litres)	57	24	22	22	22

Table 5-4: Mix composition of concrete for cube specimens

Two different types of fibres were used, and the volume fraction of the two fibre types was varied from 0% to 1.0%. Table 5-5 shows some of the fibre characteristics.

	Fibre type	
	Steel fibres DE 35/0.55N	Recycled fibres from tyre waste
Manufacturer	Mapei	Ragn-Sells Däckåtervinning AB
Shape	End-hooked, cylindrical	Irregular, deformed
Length (mean)	35mm (± 10%)	37.3mm (±31.6%)
Diameter (mean)	0.55mm (± 10%)	0.42mm (± 52.4%)
Aspect ratio (mean)	63.5	100.4 (± 37.3%)
Average strength	1250 MPa (±15%)	-

Table 5-5: Properties of the fibres used

In advance of casting, moulds and traditional steel reinforcement had to be prepared. The maximal capacity of the jack load of the bending test machine was about 400kN. To make sure all the beams would reach failure, the reinforcement was designed with significant less capacity. Without taking the fibre contribution into account, the beams were calculated to fail at a loading of 109.7kN. The longitudinal reinforcement and stirrups were tied up and attached with steel wire. Further details of formwork and reinforcement are given in Section 5.3.4.

Before mixing, the moisture content of the sand was measured and the concrete recipe was consequently updated. The test was conducted in order to not overestimate the water demand, which decreases the concrete quality.

Following the mixing of constituents was executed. Firstly, fine- and coarse aggregate, as well as cement was added to the concrete mixer while rotating. Subsequently, the fibres were added while the mixer was rotating – this in order to obtain a uniform distribution of fibres. To reduce interlocking of fibres, fibres were separated by hand and added to the mix at an approximately constant rate. In contrary to the commercial steel fibres, the recycled fibres contained rubber, which made it harder to separate the fibre from each other. The process of manually twisting and pulling the fibres from each other was time-consuming, and for larger quantities more efficient methods should be applied.
Finally, water and superplasticizer were added. After adding all the components, a break of about two minutes took place, before continuing to mix the composite for three more minutes. The mixing procedure is illustrated in Figure 5-1:
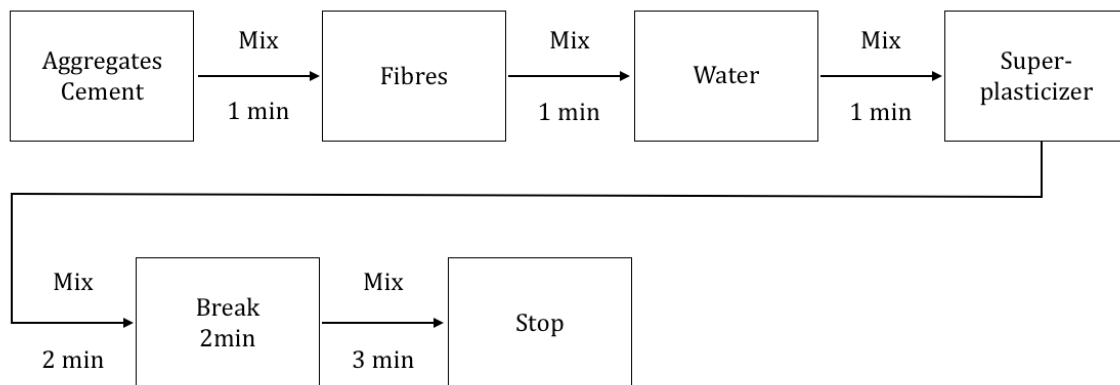
Figure 5-1: Mixing procedure

5.3 Properties of fresh concrete

Several tests were performed at the laboratory to check the rheological properties of the fresh concrete, recall Table 5.1.

5.3.1 Density control

The densities of the different concrete mixes were checked in accordance to *NS-EN 12350-6:2009 -Testing fresh concrete, Part 6: Density* (Standard Norge, 2009b). The densities were determined by weighting a container with a known volume. In this case, the same bowl as for the air content measurement was used. Thereafter the container was filled with concrete and weighted again. A glass plate was used to make sure that the concrete filled the exact volume of the container, by smoothing out the concrete surface to the top of the bowl. Following, the density could be obtained by subtracting the mass of the empty bowl from the mass of the bowl when filled with concrete, and divide it by the volume:

$$D = \frac{m_2 - m_1}{V}$$

(5.1

where
m_1 is the mass of the container when empty (kg),
m_2 is the mass of the container when filled with concrete (kg),
V is the known volume of the container (m³).

5.3.2   Air content
The air content is measured in accordance to *NS-EN 12350-7:2000 Testing fresh concrete Part 7: Air content Pressure method* (Standard Norge, 2009c). A special 8-litre test bowl with an airtight lid was used to measure the air content of the concrete samples, see Figure 5-2. The test bowl was filled with three equal layers of concrete, each layer vibrated with a rod. After rodding, a glass plate was used to smooth out the concrete surface to the level of bowl top, and the top bowl flush was stroked completely off. The air-and watertight lid with a measuring device was clamped to the top of the test bowl and then filled with water. The water then entered the bowl, forming a thin layer on top of the concrete surface. A pump and a pressure gauge mounted on the top of the lid, made it possible to create a pressure inside the bowl. Consequently the concrete was compressed, and the volume change could therefore be measured as the air content.

Figure 5-2: Equipment for measuring the air content and the density of the concrete samples.

5.3.3   Slump test and slump flow
Slump measure and slump flow are two very common methods for testing the workability and the rheology of concrete. The tests give an indication whether the

concrete satisfies the desired properties for casting or not. From a technology point of view, it is essential that the concrete will be able to flow and fill out the formwork.

The slump test of the fresh concrete was performed according to *NS-EN 12350-2:2000 Testing fresh concrete Part 2: Slump-test (Standard Norge, 2009a)*. The test was carried out by filling a standardized slump cone with concrete in three layers, each layer vibrated with a rod. After vibrating the fresh concrete, the concrete was levelled to the top of the slump cone by rolling the rod over the base. The cone was removed by raising it vertically, slowly and carefully. The concrete was then able to spread out and slump by the action of gravity. The slump was measured as the distance between the top of the slumped concrete and the level of the top of the metal cone, see Figure 5-3.
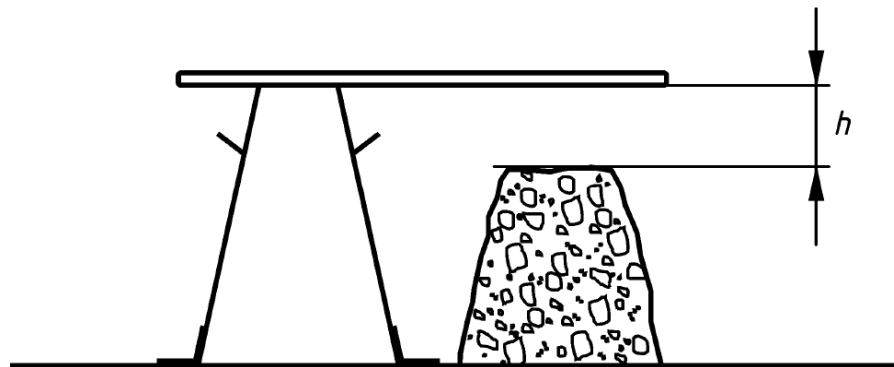
Figure 5-3: Slump measurement (Standard Norge, 2009a)

Additionally, the slump flow was measured. This method is particularly used for highly workable concrete such as self-compacting concrete. The slump flow is simply measured as the diameter of the concrete after subsidence in conventional slump test. The slump flow is measured as the average diameter of the sample:

$$D_{av} = \frac{D_1 + D_2}{2} \tag{5.2}$$

Figure 5-5 and Figure 5-4 show the standardized slump cone and the slump flow of one of the concrete samples respectively. The slump flow test also gives a visually good indication of the concrete rheology. Advantageously, the slump flow test makes it easy to detect phenomena such as segregation and bleeding.

Figure 5-4: Slump flow measure of 0.5% RFRC sample.

Figure 5-5: Standardized slump cone used for slump measure and slump flow test

5.3.4 Casting

Cylinders

For each concrete recipe, 6 cylinders were casted, which in total made up 30 cylinders. The cylinder specimens were casted in formwork made of metal, and were of standard dimensions d=150mm and h=300m. To prevent the concrete from sticking to the walls when hardening, the moulds were oiled.

Cubes

In total, 15 cube specimens were casted for the wedge splitting test – 3 specimens of each recipe. The cube were also casted in metal formwork, with dimensions of s=150mm. A 3D printed plastic model of dimensions 25x40x150mm was placed at the bottom of the moulds, in order to create a notch for the wedge-splitting test, see Figure 5-6.
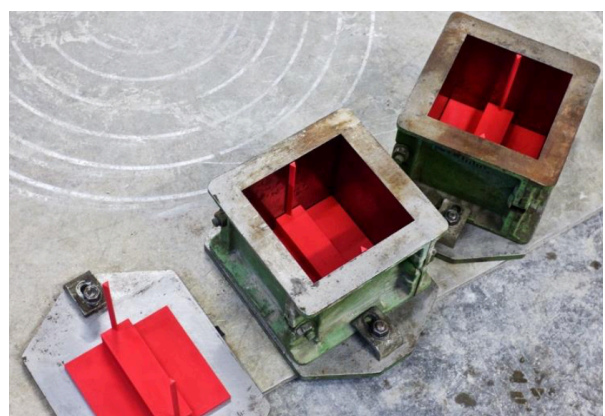
Figure 5-6: 3D-printed model made of plastic and placement in moulds

Beams

With respect to each concrete recipe, one beam was casted – in total 5 beams. The formwork for the beams was made of wood, forming the following dimensions for the beam specimens: *wxhxL*=250x300x2200mm. All beams were reinforced with conventional steel bars. The longitudinal reinforcement consists of five bars with a length of 2150mm. The three lower bars were of diameter 16mm, whereas the two upper bars were of diameter 12mm. The longitudinal reinforcement is attached to stirrups with a diameter of 8mm diameter. Stirrups were designed with a height of 250mm, width of 200mm, and were placed with a spacing of 150mm throughout the beam. All beams were designed with a concrete cover of 25mm. A sketch of the reinforcement location is shown in Figure 5-7. Additional reinforcement was used to stabilize the reinforcement frame as shown below. However, since they do not contribute to the bending capacity of the beam in any significantly manner, they are neglected for structural modelling.
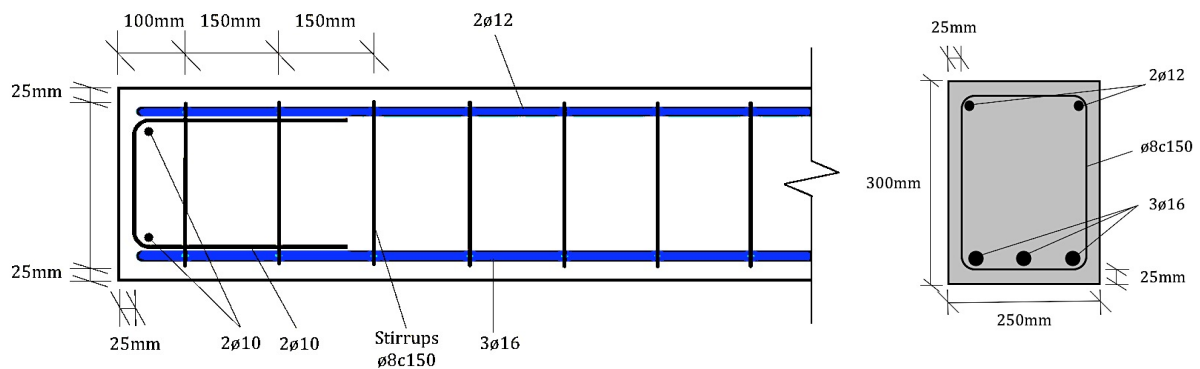
Figure 5-7: Placement of ordinary reinforcement in longitudinal- and cross-sectional direction

The beams were casted satisfactorily at the laboratory as shown in Figure 5-9 and Figure 5-8.

Figure 5-9: Formwork and reinforcement bars for the beam specimens.

Figure 5-8: Completely casted beam.

5.3.5   Curing conditions and curing time

The beams were taken out of the formwork at different times, between 1-14 days after casting. Unfortunately, none of the beams were covered with water-resistant tarpaulin after casting. Instead, the beams were placed under the roof outside the laboratory at the University of Stavanger, fully exposed to changing weather and temperatures.

Optimal curing conditions for the cylinders and cubes would have been to store them fully submerged in water after taken out of the formwork. However, this was not the case for any of the specimens. The cylinders were demoulded 2-4 days after casting, while the cubes for the WST were demoulded 22-28 hours after casting. Both cylinders and cubes were stored at the laboratory in the condition of room temperature (20 degrees of Celsius).

Common curing time for concrete is 28 days, and the tests were scheduled with respect to this. However, due to lack of equipment, many of the tests were delayed. The table below shows the curing time for the different test specimens.

	0.0% RFRC	0.5% RFRC	1.0% RFRC	0.5% SFRC	1.0% SFRC
Cylinders	42	45	39	42	42
Cubes	39	28	28	28	28
Beams	43	42	39	42	42

Table 5-6: Curing time for the different test specimens

5.3.6 Comments on the fresh concrete

Table 5-7 summarized the experimental results for fresh concrete. As one can see from the table below, the densities varied from 2317kg/m³ -2407kg/m³. The values show a tendency to increase with respect to increasing amount of fibres. The densities of samples containing steel fibres, appears to be greater than for the corresponding amounts of recycled fibres (for the cube specimens).

Tests	Beams and cylinders					Cubes for WST				
	0% RFRC	0.5% RFRC	1.0% RFRC	0.5% SFRC	1.0% SFRC	0% RFRC	0.5% RFRC	1.05% RFRC	0.5% SFRC	1.0% SFRC
Air content (%)	-	0.99	2.47	2.13	2.60	1.38	2.10	2.45	1.63	-
Density (kg/m³)	2360	2396	2317	2357	2368	2332	2320	2322	2394	2407
Slump (mm)	-	215	183	165	50	231	215	214	205	40
Slump flow (mm)	535	430	385	357.5	205	570	442.5	415	475	247.5

Table 5-7: Experimental results for fresh concrete (lack of values for air content is due to improperly condition of measurement equipment, and lacking slump measure due to very flowable matrix).

The higher volume fractions of fibres, the more it seemed to affect the workability of the concrete samples. The slump measures varied a lot, likewise for the slump flow measures. According to *NS-EN 1350-8:2010*, a concrete is classified as self-compacting concrete when the slump flow measure is about 650mm or greater. The samples with plain concrete gave the highest slump flow values, and the consistency of the matrix was wetter than desired. In addition the fresh concrete showed sign of segregation in the concrete mixer – probably because of too much addition of superplasticizer. The samples containing 0.5% and 1.0% recycled fibres acted in more viscous manner. The samples containing commercial steel fibres acted even more viscous. The consistency of the concrete containing 1.0% was very stiff, beyond what desired.

Attention should therefore be given to the concrete mixes containing 1.0% fibre, where the workability was the poorest. During the casting of the two beams, phenomena of fibre clustering appeared. When removing the framework, the surface of these two beams appeared to have rough surfaces, as shown in Figure 5-10. It is likely to think that this situation might influence the bearing capacity of the beams.

Figure 5-10: 1.0% SFRC beam with rough surface.

5.4 Properties of hardened concrete

Certain information will be necessary to determine for creating FRC material model. FRC parameters that serve as an input material model in ATENA, must be determined from laboratorial tests, e.g.:

- Compression tests on cubes or cylinders
- Three- or four-point bending test (4-point bending is preferred)
- Test for the elastic modulus (fracture test)

The above tests will therefore be discussed in the following (Prochazkova, Cervenka, Janda, Pryl, & Mikolaskova, 2016).

5.4.1 Compression test - cylinders

To determine the compressive strength of plain and fibre reinforced concrete, compression tests were performed. Compression test was conducted on cylinder specimens in accordance to *NS-EN 12390-3:2009 Testing hardened concrete Part 3: Compressive strength of test specimens (Standard Norge, 2009d).* However, the curing conditions are deviating, as the cylinders were stored in dry conditions at room temperature (20°C) rather than submerged in water. The test is basically performed by loading cylinder specimens until failure, by means of a compression-testing machine, see Figure 5-11. The specimens were subjected to uniaxial loading perpendicular to the direction of casting, see Figure 5-11. The load was applied with a constant rate of

0.05mm/s. The fracture load is recorded and the compressive strength of the specimens could be obtained by using the following formula:

$$f_c = \frac{F}{A_c} \tag{5.3}$$

where
f_c is the compression strength in MPa (N/mm²), F is the fracture load in N, and
A_c is the cross section area of the cylinder exposed to compression loading in mm².

Figure 5-11: Compression testing machine.

Typical fracture pattern for cylinders under uniaxial compression are illustrated in Figure 5-12 (Maage, 2008).
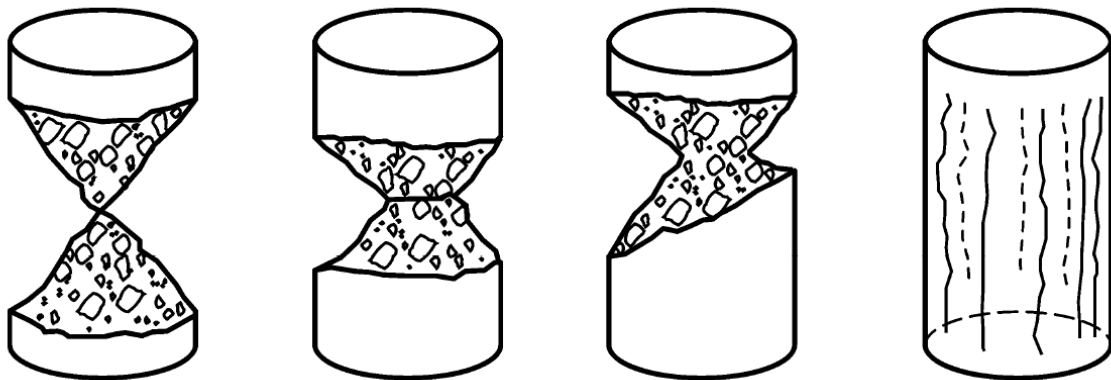
Figure 5-12: Satisfactory fracture patterns for cylinders under uniaxial compression (Standard Norge, 2009d).

Outcome of the test

The compressive strengths from the tests are shown in Table 5-8. When comparing the average compressive strengths by a visual representation, a much clearer pattern can be seen, see Figure 5-13. The compressive strength appears to increase with increasing fibre content.

Cylinder	0.0% RFRC		0.5% RFRC		1.0% RFRC		0.5% SFRC		1.0% SFRC	
	F (kN)	f_c (MPa)	F (kN)	f_c(MPa)	F (kN)	f_c(MPa)	F (kN)	f_c(MPa)	F (kN)	f_c (MPa)
C1	512.06	28.98	529,54	29,97	588,12	33,28	596,78	33,77	613,06	34,69
C2	521.72	29.52	524,39	29,67	574,55	32,51	617,16	34,92	610,35	34,54
C3	514.12	29.09	568,09	32,15	580,39	32,84	602,53	34,10	637,35	36,07
Average	515.97	**29.19**	540,7	**30,6**	581,0	**32,9**	605,5	**34,3**	620,3	**35,1**

Table 5-8: Compressive strength obtained from compressive test on cylinder specimens
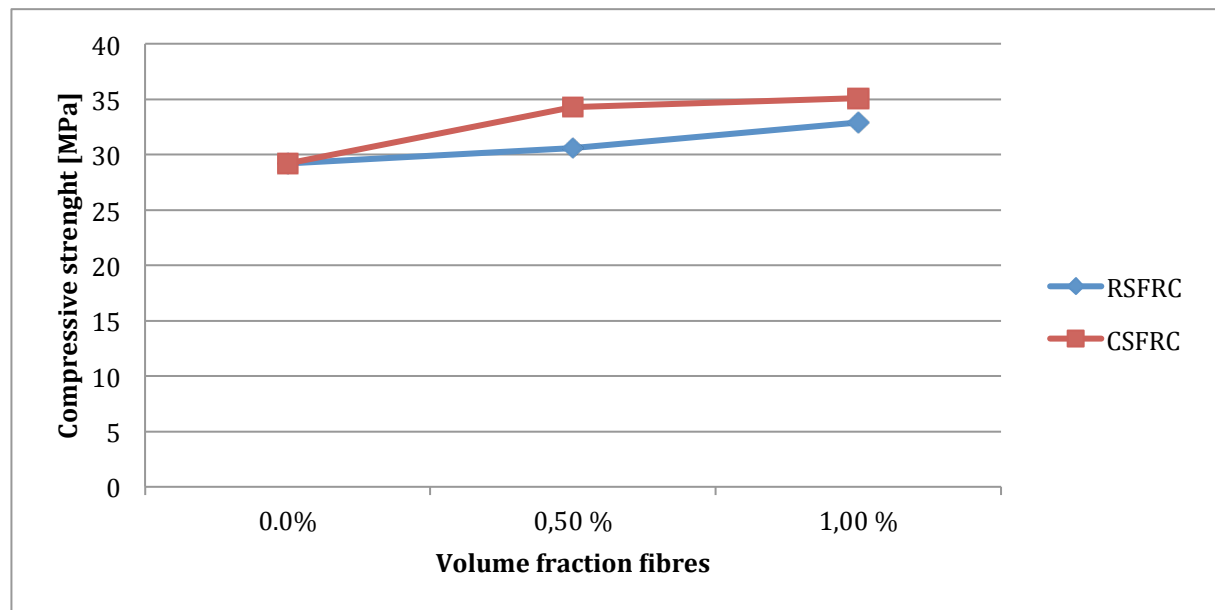
Figure 5-13: Average compressive strength pattern of cylinders

5.4.2 Modulus of elasticity

The modulus of elasticity describes a materials ability to resist deformation. Tests to determine the modulus of elasticity is performed; this to investigate how the presence of various fibre types and fibre content affects the behaviour of concrete. The test is performed according *to NS-EN 12390-13:2013 – Testing hardened concrete, Part 13: Determination of secant modulus of elasticity* in compression (Standard Norge, 2013).

Each test series consists of 3 identical cylinder specimens. The test is conducted by subjecting cylinder specimens to longitudinal compressive stress, in varying load cycles. The strain response is measured by means of two extensometers, placed on the cylinder surface, in the vertical direction as shown in Figure 5-14.

Prior to the test, the test specimen is subjected to three initial load cycles. The load is varied from the lower initial stress σ_{10} to the upper initial stress σ_1, where each cycle is held stable for 20 seconds. The pre-test was carried out to make sure the two extensometers gave measured values with less deviation than 20%. The test was able to continue if the criterion was complied. Following, the specimen was subjected to cyclic loading, varying from the upper stress σ_2 and the lower stress σ_{02}. The loading is applied in three cycles, and is held stable for 20 seconds each. The loading values are given in Table 5-9. A general measuring procedure of the stress-strain relation is illustrated in Figure 5-14.
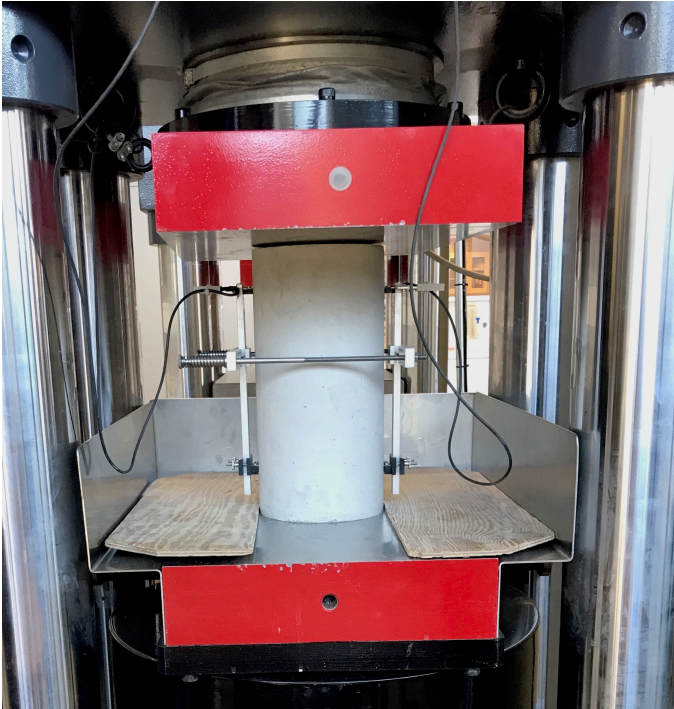
Figure 5-14: Measuring modulus of elasticity of a cylinder specimen subjected to compressive loading.

	Stresses [MPa]	Range [MPa]
Preload stress	0.7% F_{nom}	1.05
Lower stress	1.0% F_{nom}	1.63-1.73
Upper stress	10	10.1-10.3

Table 5-9: Stresses applied to determine secant modulus of elasticity

The modulus of elasticity is defined as the ratio between stress and the strain until the point where unloading is irreversible. At this point, the plasticity state is entered. The initial and stabilized E-modulus for each sample can be calculated by the formulas:

$$E_{C,0} = \frac{\Delta\sigma}{\Delta\varepsilon_0} = \frac{\sigma_a^m - \sigma_b^m}{\varepsilon_{a,1} - \varepsilon_{b,0}} \qquad (5.4)$$

$$E_{C,S} = \frac{\Delta\sigma}{\Delta\varepsilon_S} = \frac{\sigma_a^m - \sigma_b^m}{\varepsilon_{a,3} - \varepsilon_{b,2}} \qquad (5.5)$$

where $E_{C,0}$ is the initial secant modulus of elasticity in GPa (secant slope of the stress-strain curve at first loading),
$E_{C,S}$ is the stabilized secant modulus of elasticity in GPa (secant slope of the stress-strain curve after three load cycles),
σ_p is the pre-load stress level in MPa,
σ_a is the upper stress level in MPa,
σ_b is the lower stress level in MPa,
$\varepsilon_{a,n}$ is the average strain at upper stress on loading cycle n in ‰,
$\varepsilon_{b,n}$ is the average strain at lower stress on loading cycle n in ‰, and
t is the time in s.

The strains are defined as

$$\varepsilon_{a,n} = \frac{\Delta L_{a,n}}{L_0} \qquad (5.6)$$
$$\varepsilon_{b,n} = \frac{\Delta L_{b,n}}{L_0} \qquad (5.7)$$

where
$\Delta L_{a,n}, \Delta L_{b,n}$ represents the registered change in length at the upper and lower stress respectively,
L_0 is the initial gauge length of instrument in mm.
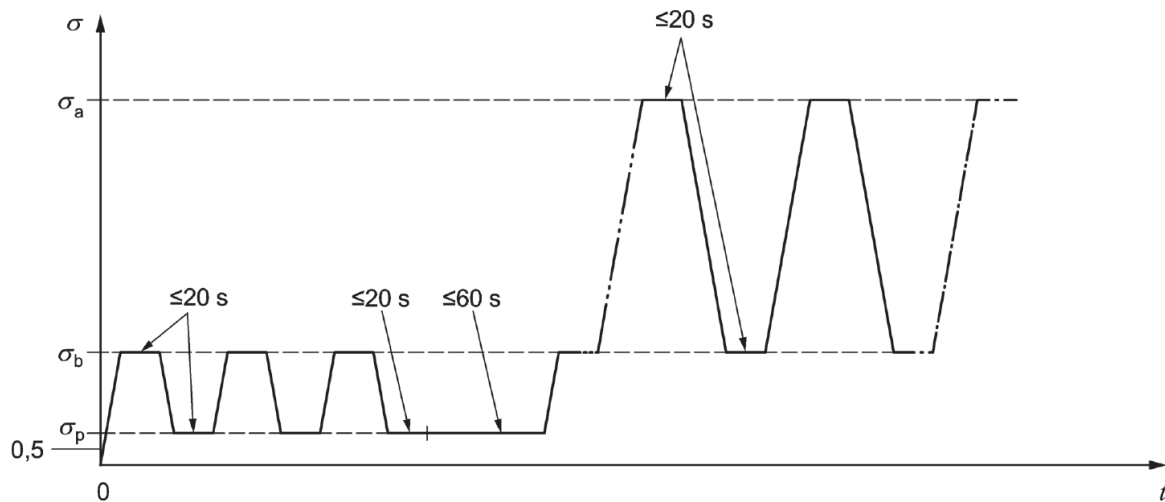
Figure 5-15: General procedure of measuring E-modulus (Ahmadyar, 2011)

Outcome of the test

Stress and strain values are measured and the corresponding E-modulus is then calculated by Formula 5.4 and 5.5. 3 cylinders are used to measure the average modulus of elasticity for each test series, and are highlighted in blue in Table 5-10. It should be noted that the E-modulus varies a lot within each batch, resulting the average values to vary uncharacteristically.

Cylinder	0.0% RFRC		0.5% RFRC		1.0% RFRC		0.5% SFRC		1.0% SFRC	
	E0 (GPa)	Ec (GPa)	E0 (GPa)	Ec (GPa)	E0 (GPa)	Ec (GPa)	E0 (GPa)	Ec (GPa)	E0 (GPa)	Ec (GPa)
C1	21,14	26,01	15,33	21,95	21,79	25,61	22,08	26,23	23,63	27,76
C2	21,24	25,82	27,04	31,33	22,14	25,20	23,80	28,43	21,40	26,59
C3	19,52	24,52	21,71	26,77	19,92	24,45	21,18	25,40	21,20	25,48
Average	20,63	25,45	21,36	26,69	21,28	25,09	22,35	26,69	22,08	26,61

Table 5-10: Modulus of elasticity obtained through tests

5.4.3 Tensile test

Several methods can be applied in order to characterize the tensile behaviour of fibre reinforced concrete. The most common tests are:
- Uniaxial tension test or indirect tensile test
- Flexural test
- Panel test or plate test

(Löfgren, 2005)

5.4.3.1 Tensile splitting test - cylinders

Determination of the splitting tensile strength of cylindrical specimens are performed according to *NS-EN 12390-6:2009 – Testing hardened concrete, Part 6: Tensile splitting strength of test specimens* (Standard Norge, 2009e). The same specimens used to determine the modulus of elasticity (non destructive test) are used for the splitting tensile test. All the cylinders were tested within 39-45 days of curing.

With the splitting tensile test, the tensile strength, f_t, of concrete can be determined indirectly. The test is conducted by placing cylinder specimen of standard dimensions (DxL=150mmx300mm) horizontally between the surfaces of a compression-testing machine, see Figure 5-16. Following, the load is applied diametrically and uniformly along the length of the cylinder. The specimens are subjected to loading until failure occurs along the vertical diameter. The loading is applied at a rate of 3534 N/s, and the failure load is registered.
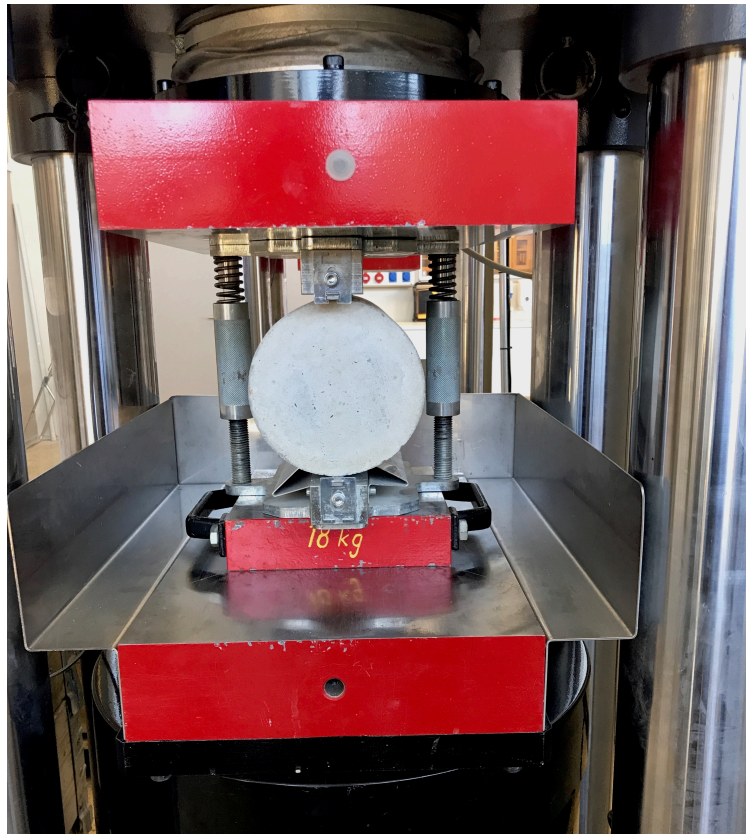
Figure 5-16: Splitting tensile test of cylinder specimen

The test specimens were under this condition forced split into two parts due to indirect tensile force generated by the Poisson's effect, see Figure 5-17. By assuming that the concrete specimens behaves elastically, the tensile strength can be obtained from the following expression:

$$f_{ct} = \frac{2 \cdot P}{\pi \cdot D \cdot L} \tag{5.8}$$

where
f_{ct} is the tensile splitting strength in MPa,
P is the compressive load at failure in N,
D is the diameter of the cylinder specimen in mm,
L is the length of the cylinder specimen in mm.
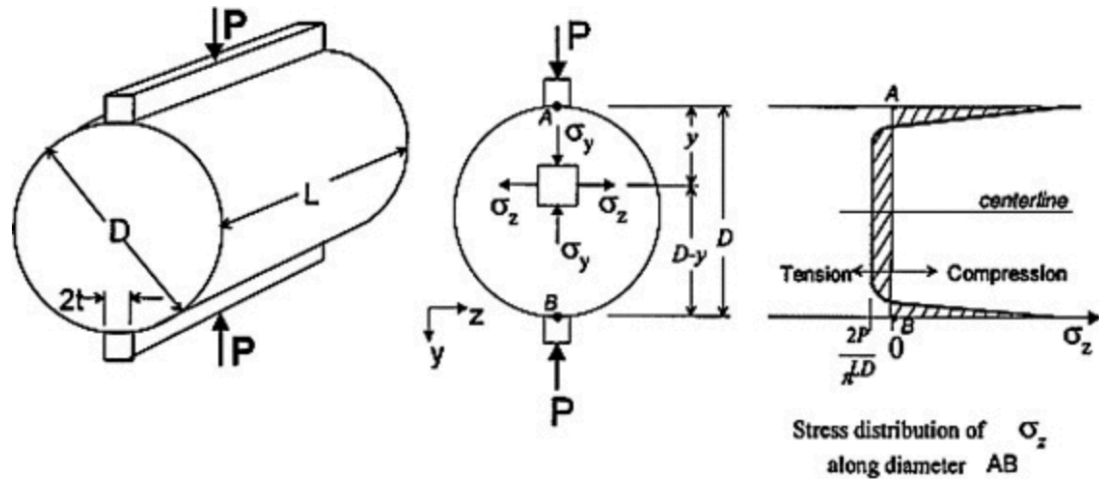
Figure 5-17: Schematic illustration of the load situation for cylinder specimens ("Concrete Cylinder Splitting Tensile Strength Test [2] [Picture]," 2015)

In general, for plain concrete one can expect a tensile strength up to about 10% of the design compression strength. This means:

$$f_{t,plain} = 0.10 \cdot f_{ck} = 0.10 \cdot 30 \frac{N}{mm}^2 = 3.0 N/mm^2 \qquad (5.9)$$

For fibre reinforced concrete, it is reasonable to assume a greater tensile strength, up to about 15% of the compression strength (Maage, 2008).

Outcome of the test
The results from the splitting tensile test are shown in Table 5-11. The average tensile strengths of the samples are calculated by using Formula 5.8 and are marked in bold. As one can see from the results, all the average tensile strengths, $\sigma_{t,av}$, are less than 10% of the respective average compression strengths, $\sigma_{c,av}$.

Cylinder	0.0% RFRC		0.5% RFRC		1.0% RFRC		0.5% SFRC		1.0% SFRC	
	F (kN)	σ (MPa)	F (kN)	σ (Mpa)	F (kN)	σ (Mpa)	F (kN)	σ (Mpa)	F (kN)	σ (Mpa)
C1	168,25	2,38	171,33	2,42	188,40	2,67	196,20	2,78	207,05	2,93
C2	147,47	2,09	168,95	2,39	168,95	2,39	202,63	2,87	210,87	2,98
C3	145,99	2,07	207,28	2,93	170,76	2,42	208,72	2,95	212,68	3,01
Average	153,90	**2,18**	182,52	**2,58**	176,04	**2,49**	202,52	**2,87**	210,20	**2,97**
$\sigma_{t,av}/\sigma_{c,av}$		7,5%		8,4%		7,6%		8,4%		8,5%

Table 5-11: Results from slitting tensile strength test

5.4.4 Four-point bending test – beams (4PBT)

5.4.4.1 Beam types

The aim of the four-point bending test is to determine the residual flexural tensile strength of the reinforced concrete beams. In order to be able to make comparisons of the test results, the concrete quality is kept constant for all samples. The varying factor for the five test beams is the type and amount of fibre reinforcement. Table 5-12 summarizes the test beams and their respective reinforcement:

Test beam	Conventional reinforcement	Fibre type	Fibre content
1	Yes	Recycled steel fibres	0.0%
2	Yes	Recycled steel fibres	0.5%
3	Yes	Recycled steel fibres	1.0%
4	Yes	Commercial steel fibres	0.5%
5	Yes	Commercial steel fibres	1.0%

Table 5-12: Test beams and their respective reinforcement

5.4.4.2 Test setup

In total, 5 beam specimens were tested in four-point bending. The test beam is basically placed on two supports and then subjected to two point loads, thereby the name four-point bending test.

The beam is resting on two steel roller supports, making the beam able to rotate around its own axis and thus preventing warping. The test specimen is subjected to two equal and symmetrically placed point loads by means of a loading beam with two roller bearers attached to its bottom. Furthermore, the load is applied at a constant rate at 2mm/min forcing the test beam to bend. The physical deflection and loading data is monitored and recorded by measuring devices and then transferred to a computer program. In addition camera devices (DIC-system) were used to record the crack pattern development. A schematic illustration of the test setup is shown in Figure 5-18.
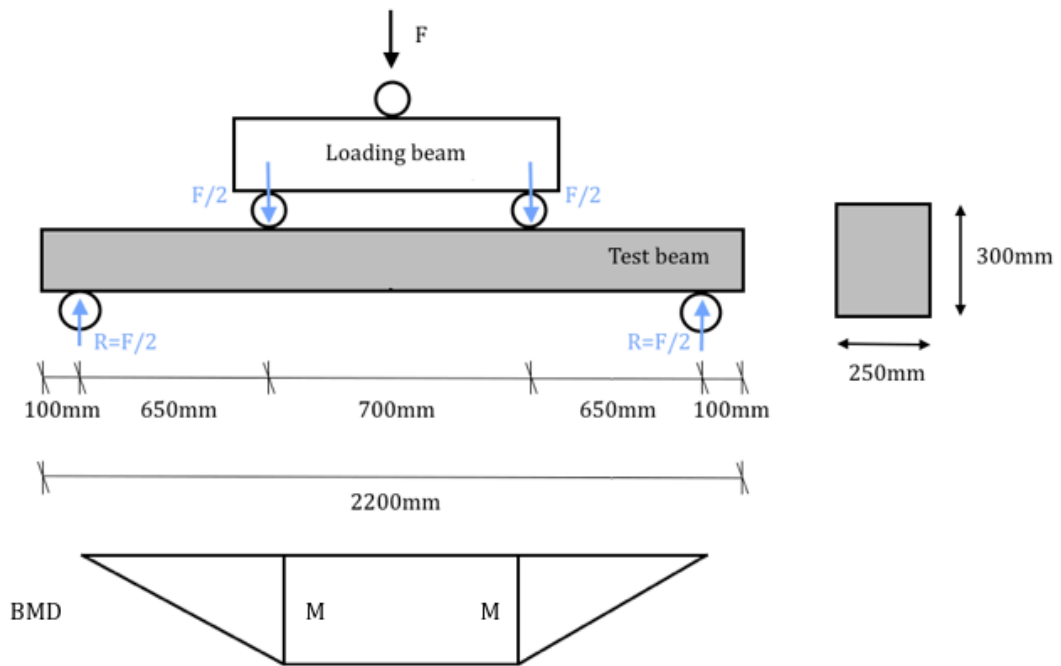
Figure 5-18: Illustration of the test setup for four-point bending test

The beams were tested at the laboratory within 39-43 days after casting, and the equipment used to perform the tests is shown in Figure 5-19. With the four-point bending test, the maximum bending moment will be distributed along the beam length between the two point loads at the mid span, as shown in Figure 5-19. Thus, cracking and failure were likely to occur at the weakest point within this area (assuming no shear failure). By simple calculations, the beam is expected to fail at total loading of 202kN, see Appendix C.

Figure 5-19: Four-point bending test of beams at the laboratory
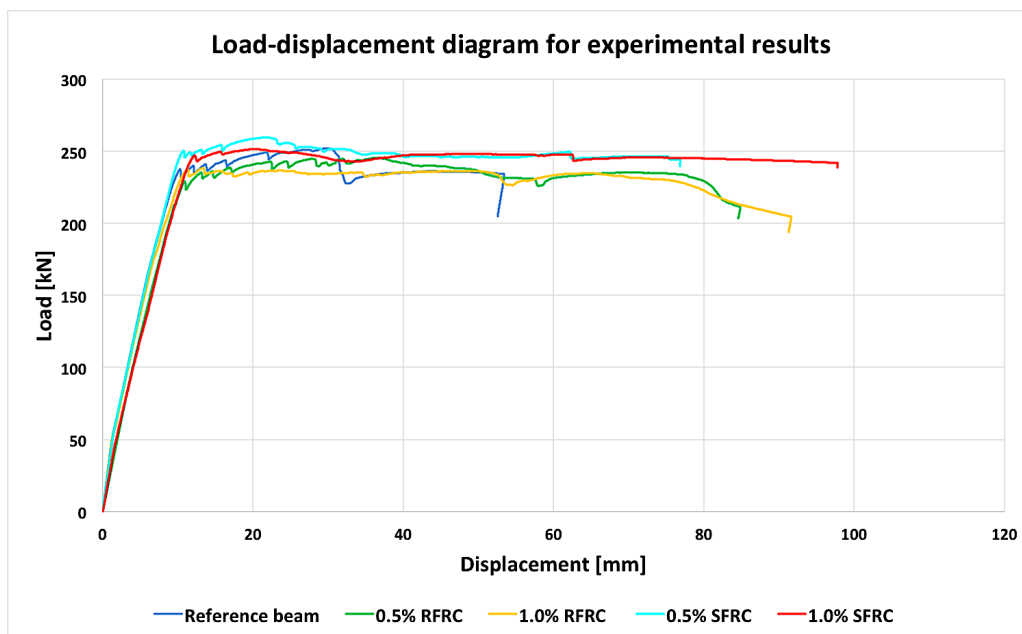
Figure 5-20: Load-displacement diagram for beams tested in four-point bending

5.4.4.3 Outcome of the tests

Table 5-13 shows experimental results from the four-point bending test.

BEAMS	0.0% RFRC	0.5% RFRC	1.0% RFRC	0.5% SFRC	1.0% SFRC
First peak load [kN]	236.1	228.0	237.8	248.4	243.4
Displacement at first peak load [mm]	10.1	11.7	11.3	11.4	12.7
Maximum load [kN]	2512.0	245.3	238.4	259.6	251.5
Displacement at maximum load [mm]	29.6	36.6	13.3	21.8	20.3
Failure at displacement [mm]	≈54.7	≈84.8	≈91.6	76.9	97.7

Table 5-13: Load and displacement values obtained with 4-point bending test

Figure 5-20 displays the load-displacement behaviour of the beams from the laboratory tests. Due to some flaws with the bending test machine, the beams appeared to deflect even before loading was applied. In both theory and practice, a beam is not able to bend without loading. A tangent of the increasing part of the L-D curves is extended, and the whole graph is shifted such that the intersection with the horizontal axis becomes the new origin.

5.4.5 Wedge-splitting test (WST) - cubes

To determine the tensile fracture behaviour of fibre reinforced concrete, wedge-splitting test (WST) was performed. The test is performed according to the method described in NT Build 511 (NORDTEST METHOD, 2005). The curing conditions for the cube specimens, however, were not in accordance to NT Build 511, as they were rather stored in dry condition (20°C).

For each test series, three cube specimens were tested – in total 15 cubes. The test specimens were tested within 28-30 days after casting. A 3D printed model was placed in the formwork when casting the cubes, making sure that specimens got the desired geometry for the test (groove and guide notch). Right before testing, a starter notch was wet sawn to into the specimens to ensure crack propagation at the symmetry axis, see Figure 5-21.
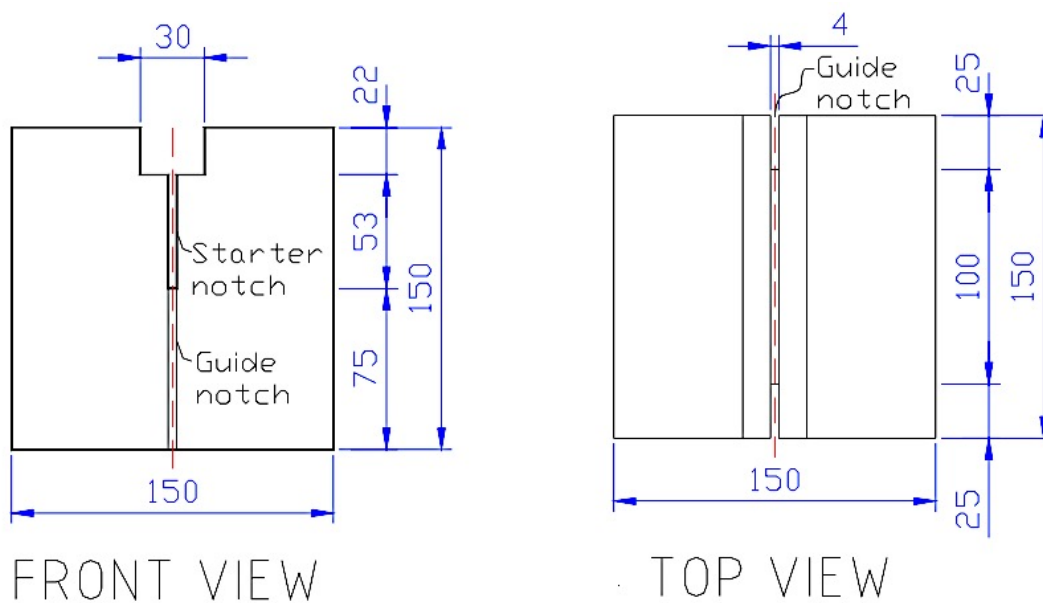
Figure 5-21: Specimen geometry (150x150x150mm³)

Prior to the test, two steel platens are placed partly on top of the specimen and partly into the groove. A vertical load F_v is applied, in which through the roller bearing on the steel-loading device is transformed to a horizontal splitting load F_{sp}. F_v is applied at a constant rate of 0.15mm/min. To record the crack mouth opening displacement (CMOD), a clip gauge is placed into the starter notch. Both the vertical loading F_v and the crack mouth opening displacement (CMOD) are monitored during the test with a frequency of 10 Hz. Figure 5-23 shows an overview of the test setup, while Figure 5-22 illustrates the principle of the splitting load.

Figure 5-23: Schematic overview of the equipment and test setup
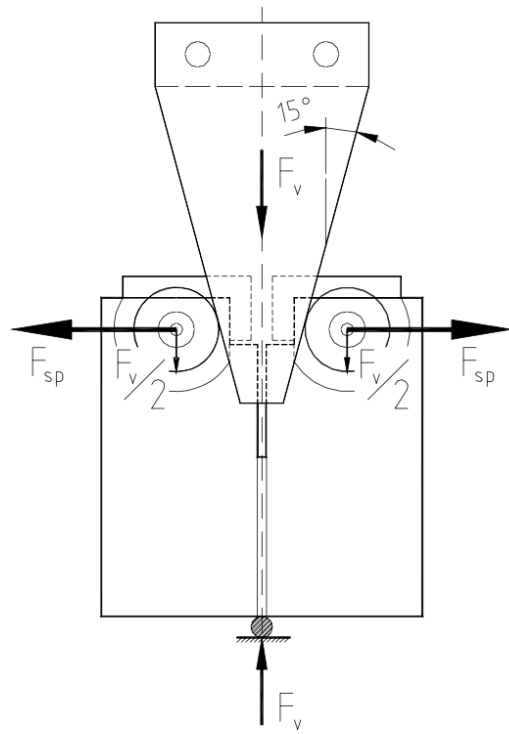
Figure 5-22: The principle of applying the splitting load

The applied horizontal splitting force F_{sp} can be related to the vertical applied load F_v as:

$$F_{sp} = \frac{F_v}{2 \cdot \tan(\alpha)} \qquad (5.10)$$

where
α is the angle between the wedge and the vertical load line in equal to 15°, and
F_v is the vertical load in kN.

The friction μ for the roller bearings is of insignificant influence, and is neglected in this case. In addition to the regular measuring devices monitoring the applied load F_v and CMOD, a Digital Image Correlation (DIC) system is used. The DIC system recorded images of the specimens during testing. Independently on the regular measuring devices, the DIC system also measured CTOD and CMOD. With the information from the DIC system, a more throughout analysis of the fracture behaviour can be performed.

	Average max F_v [N]	Average max F_{sp} [N]
0.0% RFRC	1830.0	3414.8
0.5% RFRC	1723.3	3215.8
1.0% RFRC	1813.3	3383.7
0.5% SFRC	2060.0	3844.0
1.0% SFRC	2810.0	5243.5

Table 5-14: Results obtained from the WST
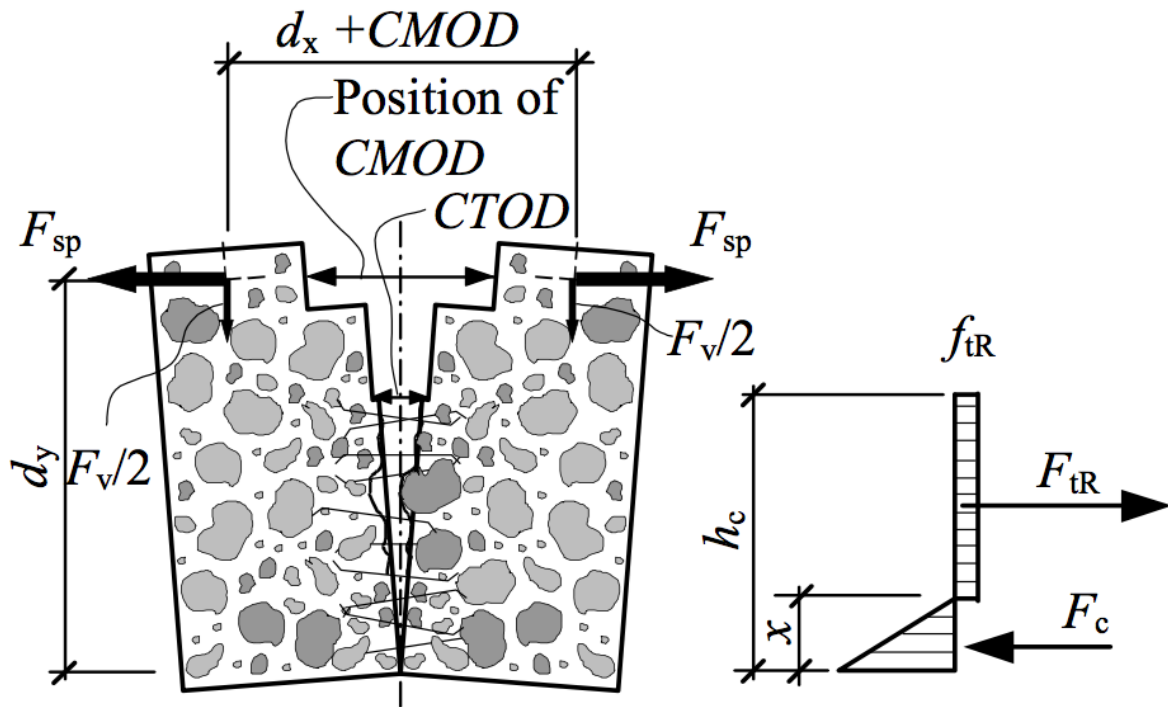
Figure 5-24: Cracked specimen with illustration of CMOD and CTOD

In the WST, the "true" crack opening or so-called crack tip opening displacement (CTOD) is not measured directly. CTOD is of particular importance when evaluating the fracture parameters, and can usually be expressed in terms of the relationship to CMOD. By calculating the area under the F_{sp}-CMOD diagram, the work of fracture W_f can be obtained. The dissipated energy during fracture, $W_{f.CMOD}$, for a certain CMOD can be normalized by the total ligament area A_{lig} at complete fracture. This intermediate fracture energy $G_{f.MOD}$ can therefore be obtained by the following formula:

$$G_{f.CMOD} = \frac{W_{f.CMOD}}{A_{lig}}$$

(5.11)

where
$W_{f.CMOD}$ is the total area under the splitting load-CMOD curve, and
A_{lig} is the area of the ligament (expected total cracked area).

Outcome of the test

Figure 5-25 displays the average F_{sp} - *CMOD* curves of the specimens for each batch. The work of fracture W_F can be determined from the area under the splitting load-CMOD diagram. As previously mentioned, the specific dissipated energy G_F can be calculated as the fracture work divided by the ligament area. Unfortunately, not all the specimens were completely fractured. As one can see from the curves, some of the curves have reached the stage where the *CMOD* increases at a constant splitting load. However, the curves can serve as a qualitative indicator when comparing the FRC compositions. Both curves for samples containing commercial steel fibres displays notably high values for fracture toughness compared to the rest samples.
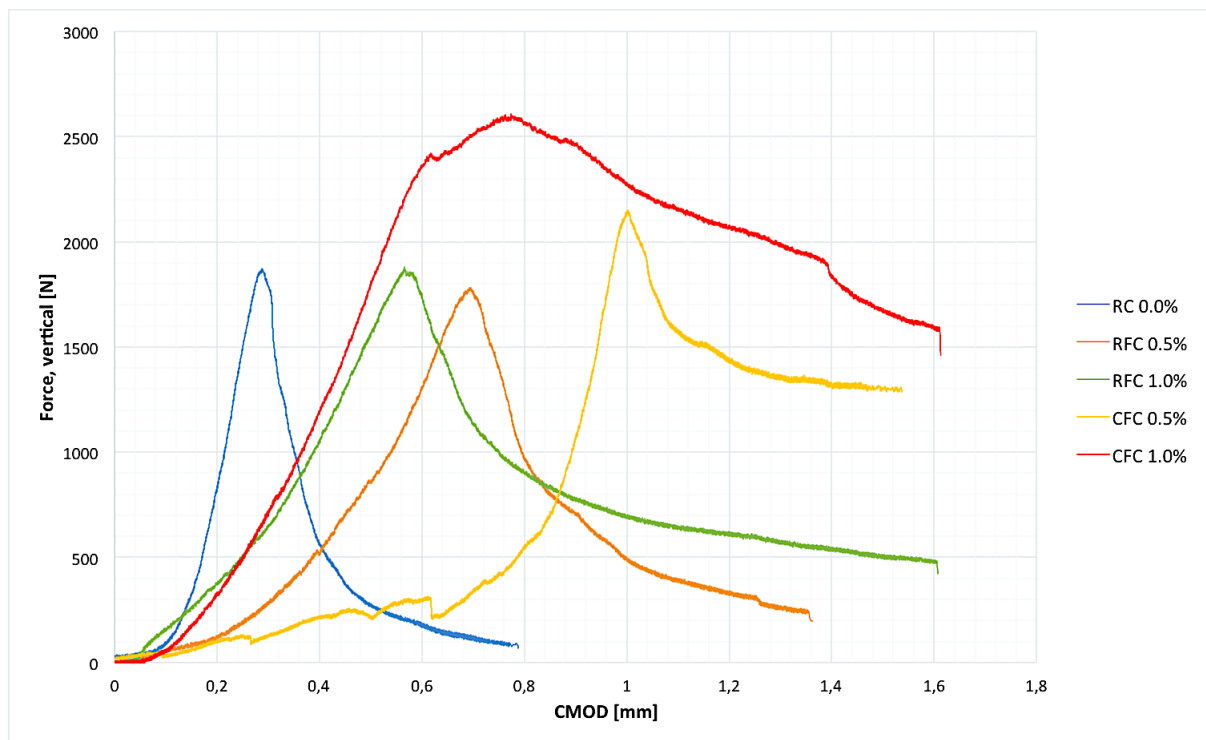
Figure 5-25: Average load-CMOD curves of specimens for each batch obtained with WST

It should be pointed out that the recording was carried out separately, and was manually assembled together at a later point in time. This might have led to uncertainties due to various start-and ending points of the experiments. Due to this, the computed curves may not display the relation between splitting load and CMOD in accurately manner.

The fracture energy cannot be precisely calculated for 0.5% and 1.0% SFRC. For simplification, the first crack width and the largest crack width can be determined by employing the bilinear crack model, ref. Figure 5-27.
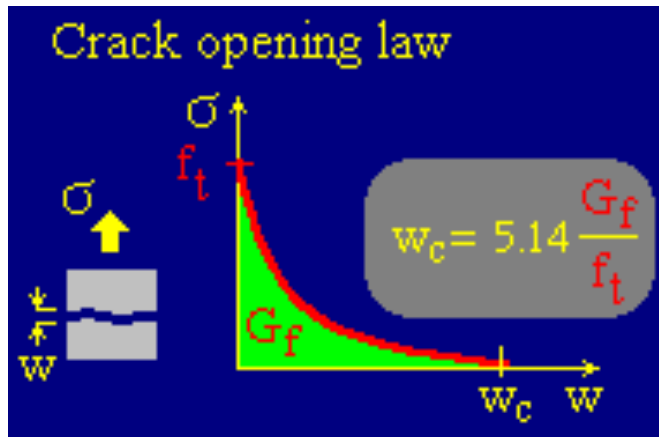
Figure 5-27: Exponential crack opening law in ATENA
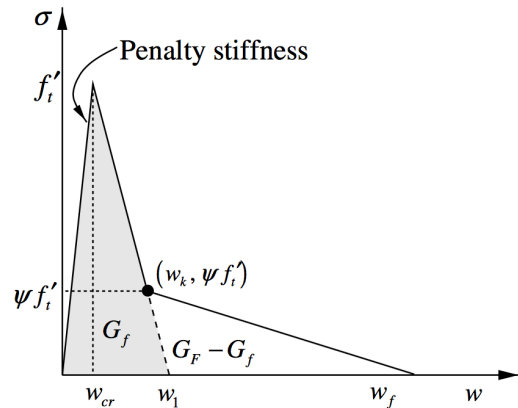
Figure 5-26: Bilinear softening curve for concrete(Park, Paulino, & Roesler, 2008)

With this method, an initial tangent is obtained manually, as well as the tangent for the softening region. From these values, it is possible to determine the final crack opening width w_c, and following by assuming the relationship shown in Figure 5-26, the average fracture energies G_F can be calculated. The roughly calculated values are given in Table 5-15.

	0.0% RFRC	0.5% RFRC	1.0% RFRC	0.5% SFRC	1.0% SFRC
w_1 [mm]	0,4162	0,9137	0,8772	1,2773	2,6215
w_c [mm]	0,9354	1,7105	3,0001	6,2538	3,4030
Fracture energy G_F [MN/m]	340,883	592.660	1096,854	2616,696	1726,078

Table 5-15: Estimated crack widths and fracture energies using data from WST

It should be noted that this is only a rough approximation of the fracture energies and this method will not be suitable for design purpose.

6 Numerical modelling

This section describes the procedure of modelling and constructing beam in four-point bending condition in the FE software ATENA. Various solution methods implemented in ATENA were explained in Section 2.4, and some of them are used to solve the nonlinear analysis.

6.1 Introduction

The numerical modelling and analysis in this thesis is executed in the software ATENA and GiD. ATENA- GiD is a finite element based software specifically designed to analyse both plain and reinforced concrete structures. Basically, GiD is used for the data preparation and mesh generation, while ATENA is used for the analysis part itself. The GiD is a general-purpose pre- and post-processing tool for a variety of numerical problems.

ATENA can simulate real structural behaviour such as cracking, crushing and reinforcement yielding, by using non-linear finite element analysis (NFEA). Fracture mechanics and plasticity theories lies the foundation to the non-linear material models implemented in the software. Advantageously, ATENA offers special numerical models for FRC species such as ductility, high toughness and shape of tensile softening branch. In addition, ATENA supports creep, moisture, and dynamic and static analysis (Cervenka Consulting, 2017, 12.02).

6.2 Finite element model

To get a better understanding of the structural and fracture behaviour of fibre reinforced concrete, nonlinear analysis is applied. GiD is used for the preparation of the four-point bending model. The model is derived from the software manuals and theory documentation developed by Cervenka Consulting (Prochazkova et al., 2016). The procedure of modelling, as well as assumptions and simplifications, will be presented in the following.

6.2.1 Four-point bending test in GiD

The static model of the four-point bending situation is shown in Figure 6-1.
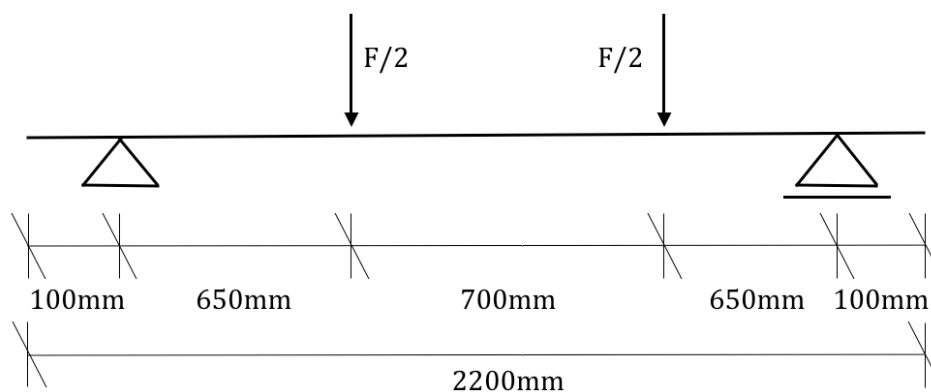
Figure 6-1: Illustration of the four-point bending situation to be created in ATENA-GiD

6.3 Geometry definition

6.3.1 Beam

Since the beam is symmetric about its mid point, only half of the concrete beam is modelled in GiD. By only considering symmetrical half of the body, the size of numerical model is reduced and the computational analysis will thus be less time-consuming. In this case, the left side of the beam is created.

Firstly, the geometry of the beam is defined by means of four points located in the xy-plane. The created points are then connected by straight lines, and are then assigned into a rectangular surface. Following, the rectangle is extruded in z-direction, creating a volume (light blue lines indicate volume, pink lines indicate surfaces, while the dark blue lines are only straight lines). The geometry of the 3D beam created in GiD is shown in Figure 6-2.
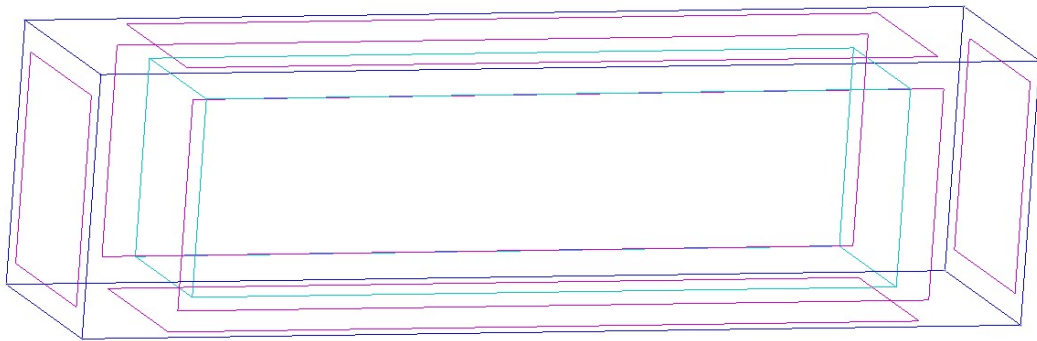
Figure 6-2: Half the beam constructed in GiD as a volume (blue lines represents straight lines, surfaces is represented by pink lines, and the light blue lines represents a defined volume).

6.3.2 Steel plates

The beam is simply supported by steel roller bearings in the physical experiments. To avoid local concrete crushing, the load is applied through steel plates (Kabele & Cervenka, 2010). The supports are designed as plates with quadratic/square cross-section of 1.5mm·1.5mm. Two steel plates are created, one functioning as a support and the other for the loading. The plate representing the pinned support is located 100mm from the left beam end. The other steel plate is copied from the previous, and is located on top of the beam at a distance of 350mm from the mid span of the beam. The plates are assumed perfectly bonded to concrete. The location of the steel plates at the half of the beam is shown in Figure 6-3 below.

6.3.3 Reinforcement

All beams are reinforced with the conventional steel bars and stirrups. The beam is designed with a concrete cover of 25mm. Five longitudinal reinforcement bars are created as straight lines with the length of 1075mm. The three lower bars are of Ø16, while the two upper bars are of Ø12. All the stirrups are designed as straight lines, forming a rectangular with connections in the corners. Stirrups have a diameter of 8mm, and a spacing of 150mmm between each. The reinforcement is shown in Figure 6-3 (material model is applied to make the reinforcement more visible).
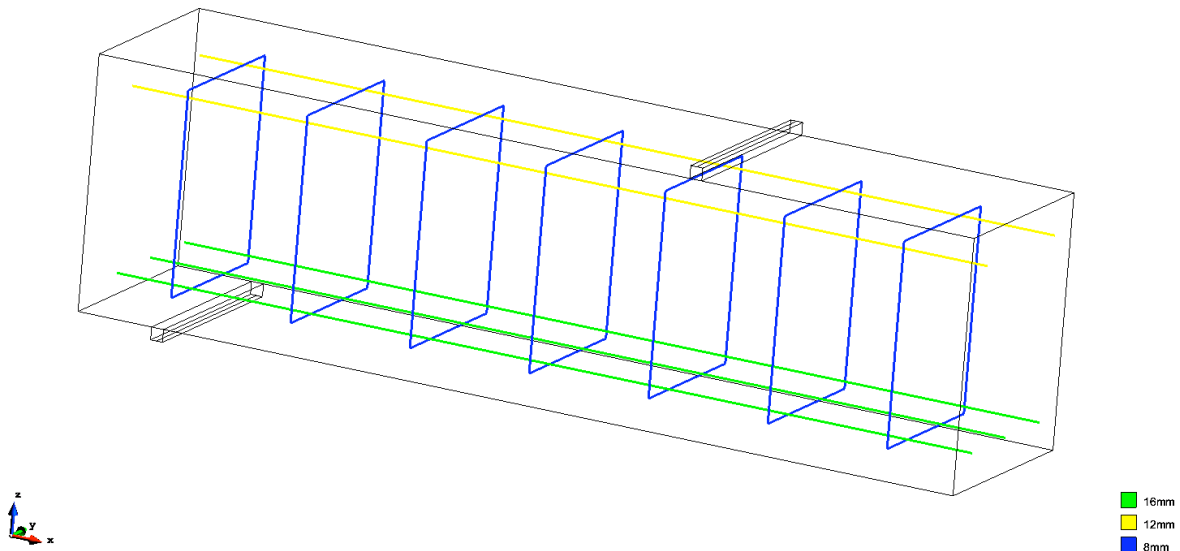
Figure 6-3: Constructed reinforcement in GiD with assigned materials

6.3.4 Layers

The created components can be assigned to different layers. Components can be selectively displayed, making it easier to work with in GiD. Five different layers are therefore created – concrete beam layer, steel plates layer and three reinforcement layers with respect to the different dimensions (8mm, 12mm, 16mm).

6.3.5 Boundary conditions

Only half of the beam is considered. Thus, the symmetry axis is simulated with constrained horizontal displacement i.e. x-direction.

The beam model is supported by the bottom steel plate in vertical direction i.e. z-direction. The bottom steel plate is constrained in both y- and z-direction.

6.3.6 Loading

The loading can be applied in two different ways, either as displacement-controlled or load-controlled, recall Section 2.4.1. The optimal choice of load steps is obtained by an "incremental-iterative-process", and is of crucial importance for the outcome of the analysis. Displacement-controlled analysis is used in this thesis. Loading is applied as a prescribed vertical displacement at the middle point on top of the loading plate in constant increments of 0.001m.

6.3.7 Monitors
Monitors can provide important output information about the state of the structure. To compare the computed results with the experimental results, the overall response of the beams is recorded at two monitoring points. One monitor is located at the top plate, recording the vertically applied load. The other monitor is located at the bottom of the beam at the mid span, and records the displacement response in z-direction.

6.3.8 Contact surfaces
To ensure a consistent model for the analysis in ATENA, fixed contact surfaces were assigned. The top surface of the beam is assigned a fixed contact surface to the top steel plate, and the bottom beam surface is assigned fixed contact surface to the bottom steel support. Figure 6-4 displays all the conditions for the beam model.
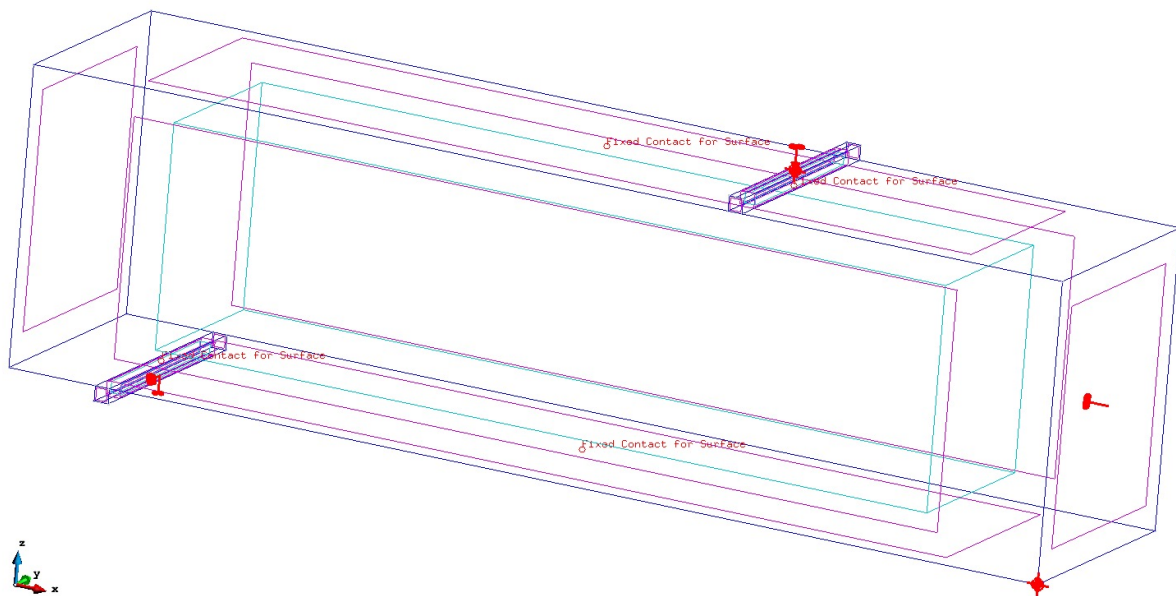
Figure 6-4: Beam with applied conditions in GiD

6.4 Intervals – loading history
The loading history in GiD consists of intervals. The beam is prescribed a displacement of 0.001m. From experimental results, it is known that the beam is likely to fail at deflection between 0.06-0.08m. The predefined displacement must therefore be multiplied with approximately 80 times to reach failure. The load should not be applied to the beam all at once, and the interval is in this case divided in 100 load steps.

6.5 Material models

6.5.1 Loading and supporting steel plates
Loading and supporting steel plates are made from steel material. Since it is assumed that the loading is not high enough to cause plastic deformations of the plates, an elastic

material was used for the steel plates. The steel plates are assigned to the material *SOLID Elastic* in GiD. The input parameters are given in the table below.

Material type		SOLID Elastic	
Material prototype		CC3ElasticIsotropic	
Young's modulus	E_s	200	GPa
Poisson's ratio	ν	0.3	

Table 6-1: Input parameters for loading and supporting steel plates

6.5.2 Reinforcement

The reinforcement can be modelled as discrete bars or as smeared reinforcement. Modelling the reinforcement as smeared is a simpler method, and will be discussed in the following section.

6.5.2.1 Discrete reinforcement

When modelling the reinforcement as discrete bars, the predefined material **Reinforcement** from **1D Reinforcement** is selected. Three reinforcement material models are predefined according to Eurocode 2 – one for each reinforcement type (Ø8, Ø12, Ø16). All reinforcement is of quality **B500NC** and is defined as reinforcement class **C** i.e. dimensioning limit of strain ε_{ud}=3.0.%, ε_{uk}= 7.5% according to EC2, table NA.3.5(901). The safety format is set to **mean** for all reinforcement. Input parameters for the reinforcement are summarized in Table 6-2.

Material name		1DReinforcement	
Material prototype		CCReinforcement	
		Bilinear	
Young's modulus	E_s	200	GPa
Characteristic yield strength	f_{xk} σ_y	500	MPa
Reinforcement class		C	
Safety format		Mean	
Hardening		Elastic-perfectly plastic	
Longitudinal reinforcement area Ø16	$A_{s,Ø16}$	$2.01062 \cdot 10^{-4}$	m²
Longitudinal reinforcement area Ø12	$A_{s,Ø12}$	$1.13097 \cdot 10^{-4}$	m²
Stirrups area Ø8	$A_{s,Ø8}$	$0.50265 \cdot 10^{-4}$	m²

Table 6-2: Material properties for reinforcement bars

The ultimate stress and strain values for reinforcement class C is manually inserted in accordance to EC2, due to improper values to calculate the bilinear law for the reinforcement i.e. k value is set to 1.015 instead of 1.15. Four stages of steel behaviour can be modelled based on the multi-line law: elastic state, yield plateau, hardening and fracture, see Figure 6-5. In this thesis a bilinear law is assumed for the discrete steel

bars, with elastic-perfectly plastic behaviour. Two points are defined within the multi-line law in order to apply bilinear behaviour of steel bars.
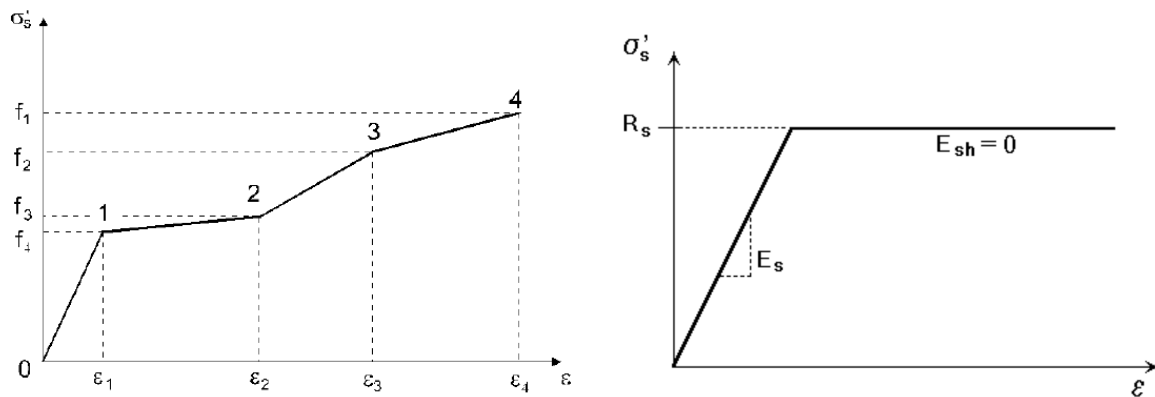
Figure 6-5: Multi-line law and bilinear law for steel bar reinforcement

6.5.2.2 Smeared reinforcement

The **Reinforced Concrete** material model is used to define a composite material, consisting of a volume material (concrete) and smeared reinforcement (1D material) in one or more directions. For smeared reinforcement uniaxial stress is assumed, and the formulation of stress-strain is used. The spacing s of the smeared reinforcement is assumed infinitely small, and the stress in the smeared reinforcement is evaluated in the cracks.
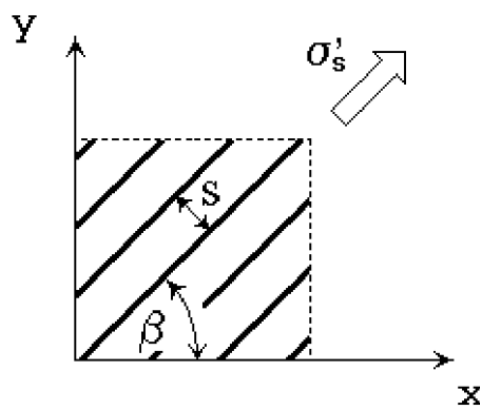
Figure 6-6: Illustration of the concept of smeared reinforcement

Reinforcement ratio

The reinforcement ratio is the reinforcement cross-section area divided by the total area of the beam section:

$$p = \frac{A_s}{A_c} \tag{6.1}$$

It is calculated for each smeared reinforcement direction, always considering the corresponding section perpendicular to that direction. Inputting the value 1 in a direction activates that particular direction for smeared reinforcement. In this case, the stirrups are placed every 150mm and the reinforcement ratio in horizontal direction and vertical direction becomes:

$$p_{hor} = \frac{n \cdot A_s}{b \cdot c} = \frac{2\pi \cdot \frac{(0.008m)^2}{4}}{0.30m \cdot 0.15m} = 0.002234 \tag{6.2}$$

$$p_{vert} = \frac{2\pi \cdot \frac{(0.008m)^2}{4}}{0.25m \cdot 0.15m} = 0.002681 \tag{6.3}$$

For the longitudinal steel bars in the horizontal direction the reinforcement ratio in both directions becomes:

$$p = \frac{3\pi \cdot \frac{(0.016m)^2}{4} + 2\pi \cdot \frac{(0.012m)^2}{4}}{0.25m \cdot 0.30m} = 0.011058 \tag{6.4}$$

Likewise for the discrete reinforcement, the smeared reinforcement is modelled as elastic perfectly plastic material.

Additionally, the fibres can be represented with smeared reinforcement. In 3D the fibres should be defined in 7 directions; the three main axes and 4 pointing in the middle of the octants. Unfortunately, this model is no good in capturing the fibre bond influence, but gives an overall response including the strain hardening phenomena (Pryl & Cervenka, 2017). A reinforcement ratio and direction is defined for each layer of smeared reinforcement. Fibre orientation can be assumed isotropic, and 1/7 of the total reinforcement ratio corresponding to the fibres can be applied in each of the 7 directions.

6.6 Mesh generation

The beam model is constructed in 3D with quadratic hexahedral isoparametric elements, see Figure 6-7. The elements are computed as plane quadrilaterals, and are directly expanded in the third dimension. The designation hexahedral refers to a brick element consisting of six surfaces in total. Additionally, the element geometry can be generated. The Geometrical Non- Linearity is set to linear, which means that the deformed shape from the previous step is used. In GiD, linear element can be assigned by selecting the checkbox for Non-Quadratic Element. Linear elements are not selected in this case. The volume is manually divided into elements by structuring the mesh i.e. assigning numbers of elements in each direction.
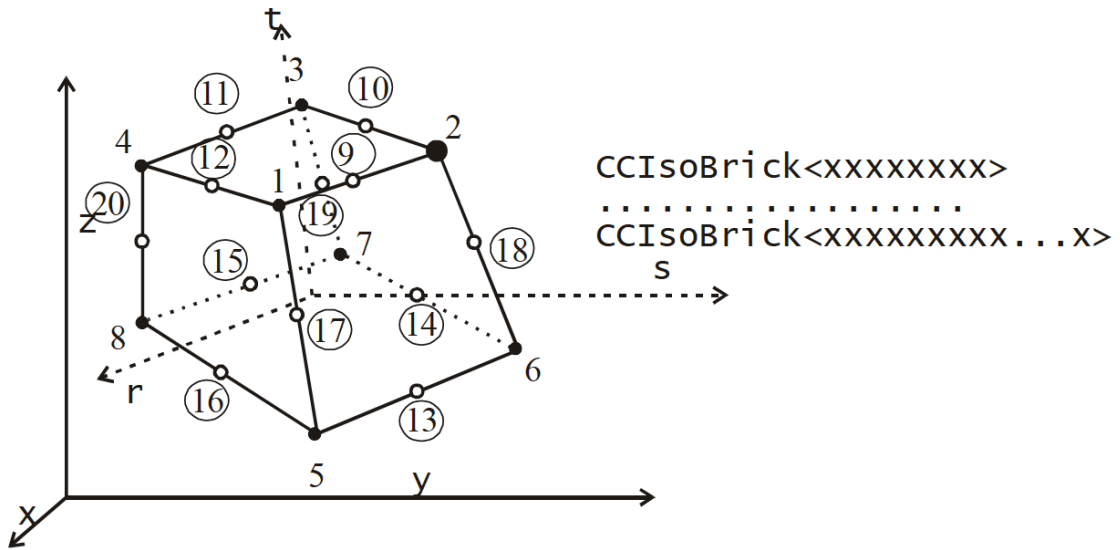
Figure 6-7: Hexahedral isoparametric element with modified numbering corresponding with ATENA format. CCIsoBrick <xxxx...> is the material code used in ATENA, and the number of nodes are referred in <>

Other finite element types are also available in ATENA. For the steel plates, triangular mesh is used. Tetrahedral elements are assigned, and are illustrated in Figure 6-8.
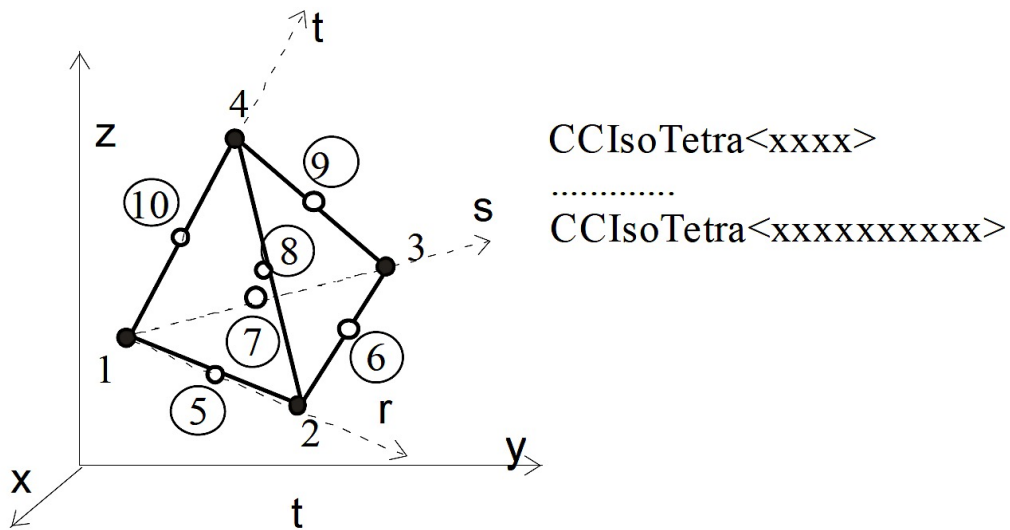
Figure 6-8: Geometry of tetrahedral element

The mesh quality influences the quality of the analysis to a great extent. It should be born in mind that refining only important parts of the model can save a lot of process-time and disk space (V. r. Červenka et al., 2017). The size of the element is varied for the concrete beam, with the first try with 0.050m and 0.025m. The generated mesh of the model in GiD is shown in Figure 6-9 and Figure 6-10.

The beam is divided into elements by manually assigning number *n* of elements in each principal direction, using the formula:

$$n = \frac{L_{beam}}{L_{elements}} \tag{6.5}$$
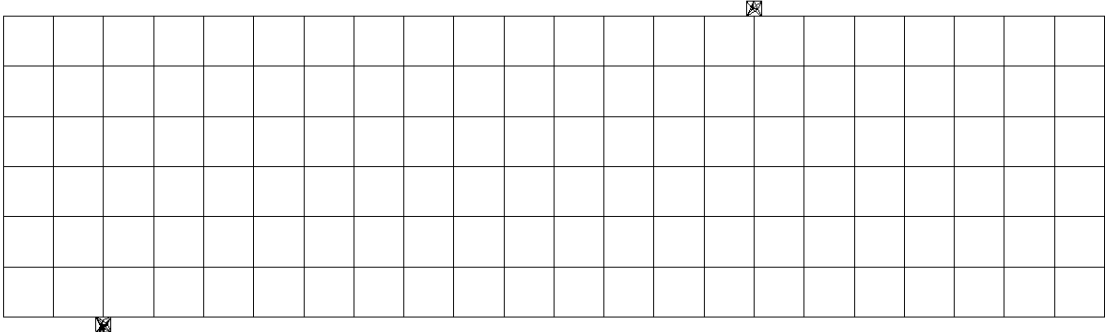
Figure 6-9: Finite element mesh with element size of 0.05m
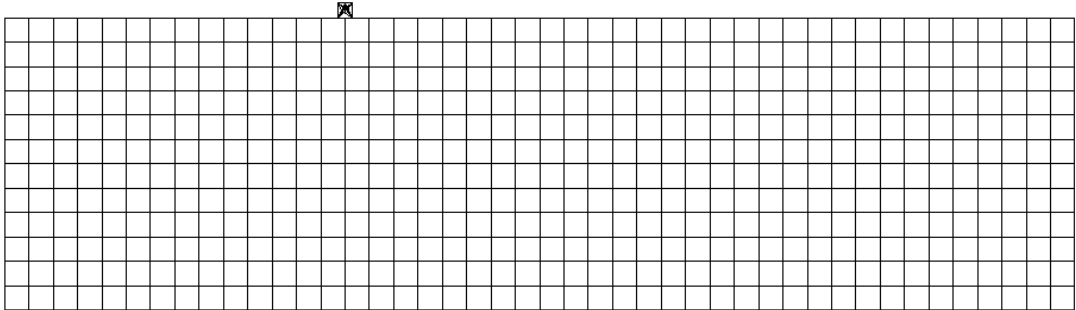
Figure 6-10: Finite element mesh with element size of 0.025m

6.7 Material models for FRC

In general, there are three ways to model fibre reinforcement in ATENA. The following are:

1. a) The normal **CC3DNonLinCementitious2**
   b) The **CCSBETA**
2. Represent the fibre with the *smeared* reinforcement **CCCombinedMaterial**
3. The **CC3DNonLinCementitious2User** (Sajdlová, 2016)

The material model **CCSBETA** is preferred when working in 2D. Since it is desired to model in 3D in order to analyse the crack formation in comparison to experimental results, the **CC3DNonLinCementitious** models is rather used. The three **CC3DNonLinCementitious** are material models that includes both plasticity model (concrete crushing) and fracture model (cracking). The **CC3DNonLinCementitious** assumes hardening regime before the compressive strength is reached. In the **CC3DCementitious2** material model includes a purely incremental formulation, instead of a total fracturing formulation.

CC3DNonLinCementitious2User allows the user to define laws for selected material laws. This includes material laws such as diagrams for tensile- and softening behaviour, shear retention factor and the effect of lateral compression on tensile strength. In this thesis it is chosen to use the material models i.e. **CC3DNonLinCementitious2** which is the simplest model.

6.8 Stress-strain law - basic

The uniaxial law can describe the nonlinear behaviour of concrete. It is described by means of effective stress σ_c^{ef} and the equivalent uniaxial strain ε^{eq}. In most cases the effective stress represents the principal stress. Figure 6-11 shows the complete uniaxial stress-strain diagram for concrete in both compression and tension.
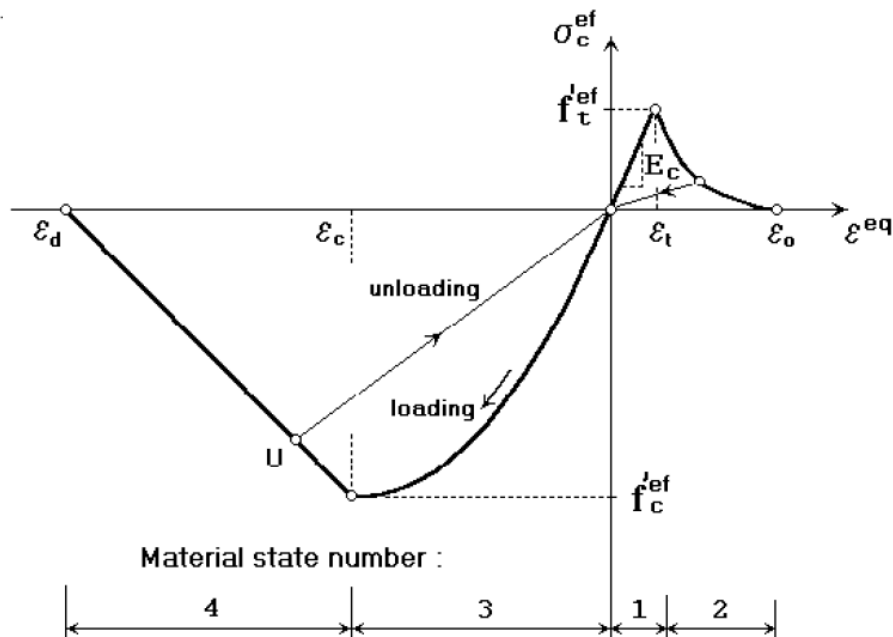
Figure 6-11: Uniaxial stress-strain law for nonlinear behaviour of concrete (V. Červenka, Jendele, & Červenka, 2016)

69

6.8.1 Biaxial stress failure criterion

Concrete is likely to fail in both tension and compression. For biaxial stress state, the strength of the concrete is predicted by assuming a proportional stress path, see Figure 6-12Figure 6-12. In the tension-tension state, the tensile strength is assumed constant and equal to the uniaxial tensile strength f'_t. In the tension-compression zone, the failure function continues linearly from $\sigma_{c1}0=$ to $\sigma_{c2}=f'_c$ (V. Červenka et al., 2016).
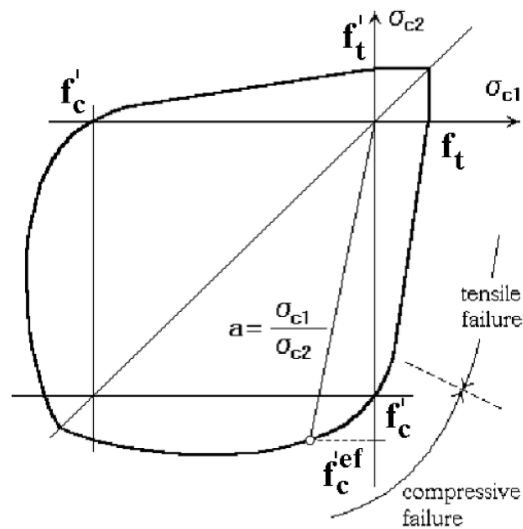
Figure 6-12: Biaxial failure function for concrete

It is assumed linear elastic behaviour for concrete in tension containing no cracks.

6.9 Fracture process

Usually, the process of crack formation is divided into three stages, see Figure 6-13. The un-cracked stage takes place before the tensile strength is reached. After reaching the peak tensile strength, crack starts to form in the process zone. Within this stage, the stress starts to decrease due to a bridging effect. After complete stress release, the crack opening continues without the stress. The cracked stage is finally reached. If the loading is removed in the process zone, the crack is able to close itself. The behaviour is increased with the presence of fibres in the concrete matrix.
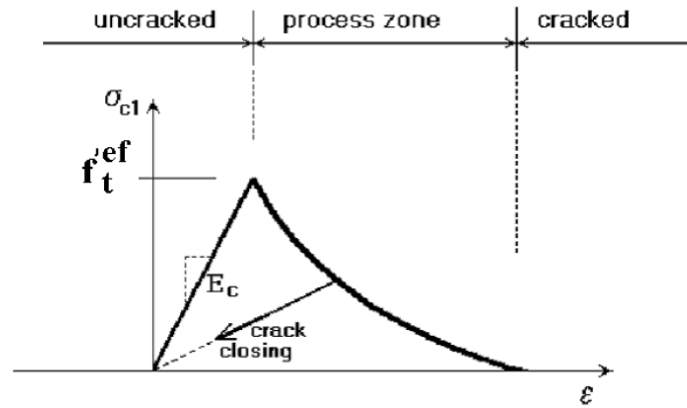
Figure 6-13: Stages of crack formation

Cracking can be modelled either as discrete or as smeared. For the chosen material model, the smeared crack model is used. The crack width is calculated as a total crack opening displacement within the crack band:

$$w = \varepsilon_{cr} \cdot L'_t \tag{6.6}$$

where
w is the crack width
ε_{cr} is the crack opening strain, and
L'_t is the failure band for tension.

6.9.1 Smeared cracking

There are two possible approaches for smeared crack modelling: *fixed crack model* or *rotated crack model*. Both are adopted in the material model **Cementitious2User**, and are based on similar fundamentals. In the two smeared concepts, a crack is formed when the principal stress exceeds the tensile strength. Cracks are assumed uniformly distributed within the element. The orthotropic stress-strain law is introduced for further loading, and the element mesh will therefore be continuous after cracking.

For the fixed crack model, the direction of cracking is governed by the principal stress direction at the moment of crack initiation. After crack initiation, the direction is fixed and represents the material axis of the orthotropy. The weak material axis m_1 is set normal to the crack direction, whereas the strong material axis m_2 is parallel with the cracks, see Figure 6-14Figure 6-14. However, the strains axes ε_1 and ε_2 do not need to coincide with the axes of orthotropy m_1 and m_2. Due to this fact, shear stress τ is produced, as well as the respective non-principal stresses σ_{c1} and σ_{c2}.

71
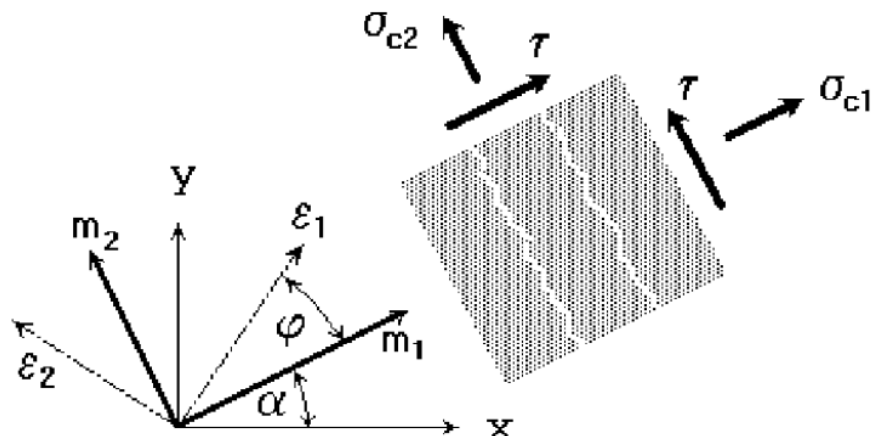
Figure 6-14: Fixed crack model illustrating stress-strain state

Unlike the fixed crack model, the rotated crack model supports the fact that the direction of principal stress coincides with the direction of principal strain. No shear strain is produced, and the crack plane can therefore be described only with the two normal stress components, see Figure 6-15. During loading, the direction of cracking will rotate with respect to principal strain axis rotation. A tangent shear modulus is used to ensure co-axility of the principal strain axes with the material axes (V. Červenka et al., 2016). Usually, the rotated crack model is recommended for very large finite elements such as shells subjected to loading in changing direction.
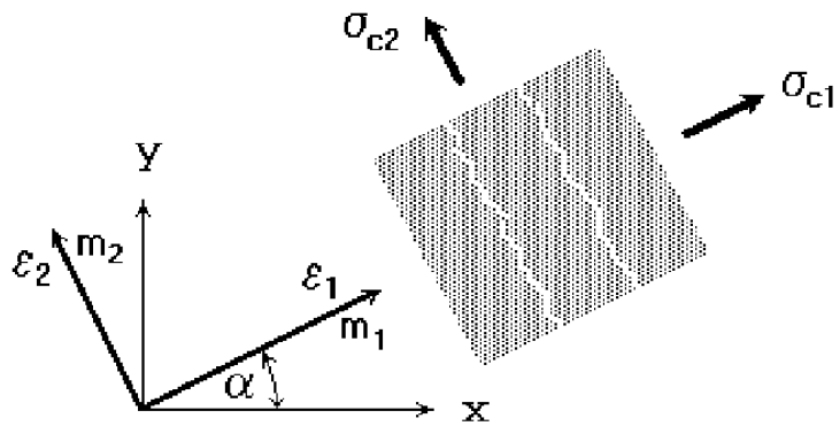
Figure 6-15: Rotated crack model for stress and strain state

6.9.2 Crack modelling

In this thesis it is chosen to use the fixed crack model. The concrete cracking is based on the Rankine-Fracturing model, which in case of fixed crack model means that stress and strains are converted into the principal directions at the onset of cracking. A fully fixed

72

crack model is obtained by inserting the value 1.0 e.g. 0.7 fixes the crack direction as soon as it opens so far that the softening law drops to 1.0 times the initial tensile strength. With the fixed crack model, the cracking pattern of the models displays similar to that of the cracking pattern obtained from laboratory results. In the fixed crack model a shear retention factor r_g can be selected, but the shear factor is not activated in this thesis.

6.10 Modelling tensile behaviour of fibre reinforced concrete

6.10.1 Modelling the tensile behaviour of FRC in this thesis

As previously mentioned, the rotated crack model is used to describe the tensile behaviour of fibre reinforced concrete. Before cracking, it is assumed linear elastic behaviour for concrete in tension. The equivalent uniaxial stress-strain law and the biaxial failure influences the initial steepness diagrams in ATENA, see

Figure 6-16. After the peak is reached, the tension softening area is reached, and the diagrams are constructed with respect to an exponential crack opening law as shown in *Figure 6-17*.
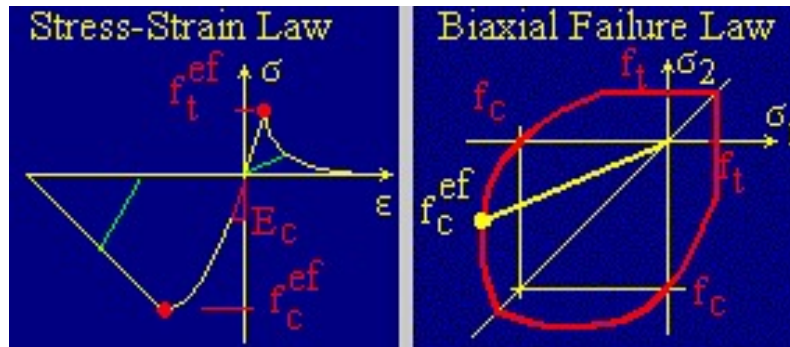
Figure 6-16: Constitutive laws controlling the initial steepness of the diagrams in ATENA
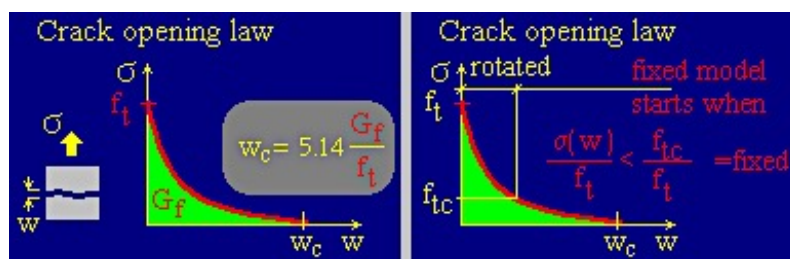
Figure 6-17: Crack opening law controlling tension softening after the peak is reached

6.10.2 More sophisticated method to model tensile behaviour of FRC

The tension behaviour of FRC in the process zone of cracks, recall Section 6.9, can be defined by the user with a tension function, see Figure 6-19. The usual stress-strain constitutive law is used for the first part of the diagram. When exceeding the localization strain ε_{loc}, the material law assumed for the characteristic crack band width $L_{c,h}$ is changed to the actual crack band width L_t. At this point, the region of tension softening is entered. The tensile function will can be modified through the analysis to obtain the best fit of load-displacement diagram of the beams in four-point bending.
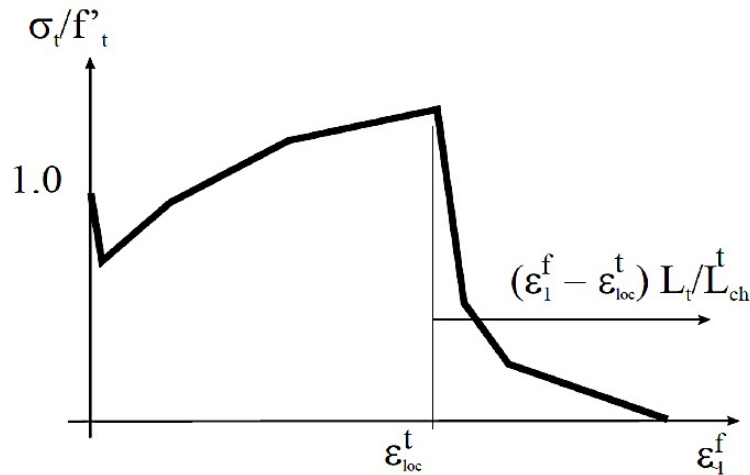
Figure 6-18: Example of user defined compression function (left) and shear function (right)

The tension characteristic size describes the failure band in tension. By recommendation, the characteristic tension length is set equal to the length of the finite element length, which in this case is 0.050m or 0.025m.

In addition, the compressive behaviour and shear stress behaviour can be defined by the user, see Figure 6-18.
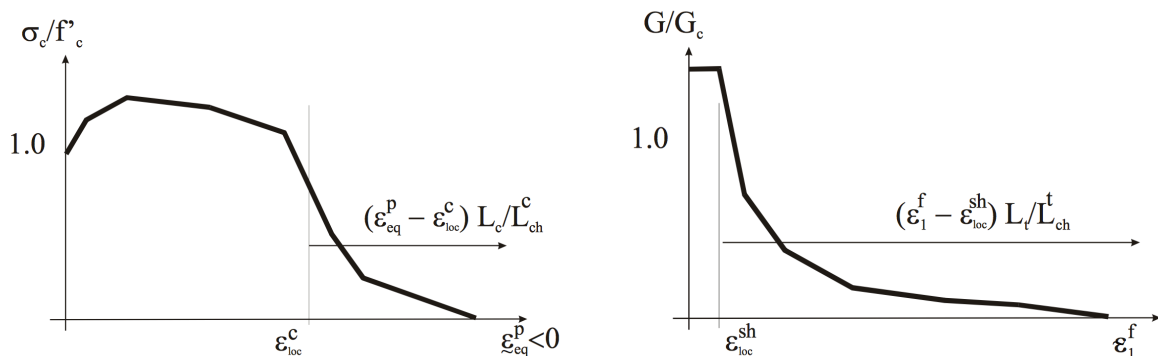
Figure 6-19: An example of user defined tension function

6.10.3 Input parameters for the material model Cementitious2

In the material prototype **Cementitious2** there are several parameters that must be inserted for the stress-strain law and the biaxial failure law. The input values influences the pre-peak behaviour of the beams i.e. the steepness of the L-D diagrams before reaching yielding.

Usually, a Poisson value of 0.2 is recommended for concrete, and is therefore the value chosen for all models (*Model Code 2010 - First complete draft*, 2010). The average compression strength obtained from compression tests serves as input for the models.

The Young's modulus inserted in this material model, is the initial tangent modulus of elasticity at the origin of the stress-strain diagram, not the secant modulus as obtained from the experimental tests, see Figure 6-20. As a first try to determine the tangent modulus of elasticity, stress-strain curves were created from the acquired values measured directly from the compression tests on cylinders. In order to do so, it was assumed a constant length of the specimen of 300mm, even thought this is not correct as the specimen becomes compressed. However, the slope of the diagrams did not seem properly, as the E-modulus obtained was too low to represent the tangent modulus of elasticity. As a second try, the values measured with the DIC system was used to find the slope   of the

$$\frac{\sigma_c}{f_c} = -\frac{k \cdot \eta - \eta^2}{1 + (k-2) \cdot \eta}$$
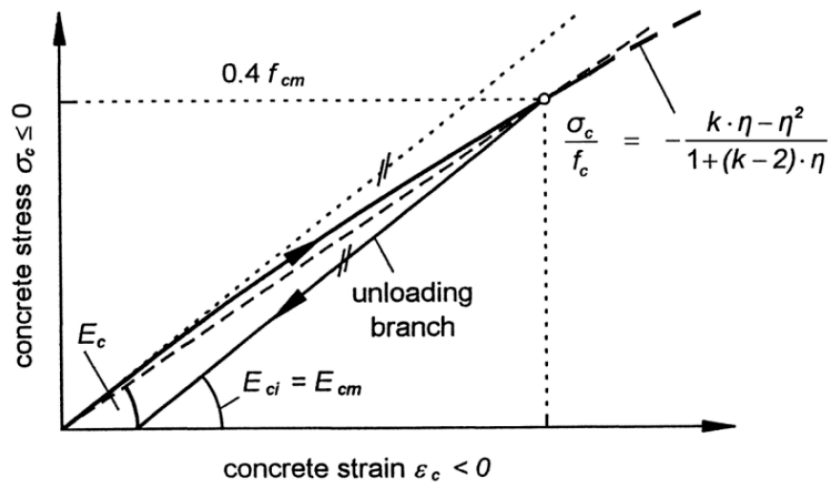
compression diagrams. A virtual extensometer was placed in the middle section of the cylinders, and a stress-strain curve could be obtained using the software DaVis. Unfortunately, the output diagrams were too unstable at the beginning of the curves to determine the slope.

Hand-calculations to determine the slope of the diagrams from DaVis showed that the curves were too steep to represent the initial modulus of elasticity, see Appendix E. As a final try, the tangent modulus of elasticity were calculated according to *fib* Model Code 2010 (*Model Code 2010 - First complete draft*, 2010). The tangent modulus of elasticity E_{ci} are calculated from the following formula:

$$E_{ci} = E_{c0} \cdot \alpha_E \cdot \left(\frac{f_{cm}}{10}\right)^{\frac{1}{3}}$$ (6.7)

where
E_{c0} is equal to $21.5 \cdot 10^3$ MPa,
α_E is 1.0 for quartzite aggregates, and
f_{cm} is the actual compressive strength at an age of 28 days in MPa.

And the actual compressive strength is the average compressive strength acquired from experimental results:

$$f_{cm} = f_{c,av}$$ (6.8)

Another value to be entered in the basic tab for material prototype **Cementitious2**, is the direct tensile strength. The splitting tensile strength $f_{ct,sp}$ is obtained through experimental tests, and the direct tension f_{ct} can according to EC2 (3.12) be calculated as:

$$f_{ct} = 0.90 \cdot f_{ct,sp}$$ (6.9)

According to Model Code 2010, new research has shown that the direct tensile strength can be set equal to the splitting tensile strength. CEB-fib Model Code 2010 is also used to determine the fracture toughness for plain concrete as the following:

$$G_F = 73 \cdot f_{cm}^{0.18}$$ (6.10)

where
G_F is *Figure 6-20: Definition of different moduli of elasticity according to fib* the fracture
energy *Bulletin 55 (Model Code 2010 - First complete draft, 2010)* in MN/m
and f_{cm} is the
average compressive strength obtained through testing in MPa. The fracture energy obtained with rough calculations using the diagrams from the WST test matches the fracture energy using the above formula, recall Table 5-15.

7 Analysis and results

7.1 Introduction

7.1.1 Necessary information for creating a FRC material model
Laboratory results are necessary to create FRC material models. The following experimental data are used:
- Average compressive strength, f_c
- Average tangent modulus of elasticity, $E_{c,s}$
- Average tensile strength, f_t
- Load-displacement curves from 4-point bending test

7.1.2 Determination of FRC material parameters
The experimental results serves as input values in order to develop the FRC material model. Parameters such as average cylindrical compressive strength and average Young's modulus are direct input values. The tensile parameters and the tensile function, however, are more problematic. The results from the four-point bending tests of the beam are therefore utilized for parameter determination. An inverse analysis of the load-displacement diagram is necessary to identify the tensile parameters correctly. The procedure to determine FRC material model parameters can be explained by the following steps:
1. Initial setup of the tensile parameters in GiD (average tensile strength, tension function)
2. Run the analysis in ATENA
3. Export the load-displacement diagram from ATENA to an Excel file
4. Make a comparison of the load-displacement curves from calculation and experimental results
5. If the difference between the diagrams is within the user accuracy limits, the determination of FRC model is completed.

   → If not, the input parameters must be modified in order to achieve better results. The analysis must re-run and the results must then again be compared with the experimental results. The modification of parameters goes on until the results are satisfactory (Sajdlová, 2016).

7.2 What to investigate

- The pre-peak and post-peak development of the load-displacement diagrams using different material models
- Crack initiation – first generated crack
- Crack pattern and crack widths
- Comparison to the experimental results

Comments

Due to lost data from the DIC system for four of the beams, only the beam containing 0.5% recycled steel fibres will be analysed. A comparison of crack pattern and crack widths computed in ATENA will be compared to the experimental ones. For the other beams, only a visually comparison of crack pattern will be conducted.

7.3 Reference beam

To analyse how the fibres influences the properties of concrete, a reference beam is constructed in ATENA. The aim is to find the best fit to the experimental load-displacement (L-D) diagram, by varying certain parameters. Average values obtained from the compression test, splitting tensile test, and calculated tangent E-modulus serve as input values for the models. Table 7-1 to Table 7-4 shows the input parameters.

Material type		CC3DNonLinCementitious2	
Elastic modulus	E_{ci}	30730.2	MPa
Poisson's ratio	ν	0.2	
Compressive strength	f_{cm}	29.9	MPa
Tensile strength	f_{ct}	2.18	MPa
Fracture energy	G_F	134	N/m
Crack model		Fixed	

Table 7-1: Material properties of concrete

Material type		Reinforcement	
		Bilinear	
Elastic modulus	E_s	200	Gpa
Yield strength	σ_Y	500	MPa
Ultimate strain	ε_u	7.5	%
Hardening		Perfectly plastic	
Geom. type		Normal	

Table 7-2: Material properties of reinforcement

Solution method	Newton-Raphson
Stiffness/update	Tangent/each iteration
Number of iterations	30
Line search	On, with iterations
Solver	LU

Table 7-3: Solution parameters

Finite element type	Quadrilateral and Tetrahedral
Element shape smoothing	On
Optimization	Sloan
Finite element size	0.05m or 0.025m

Table 7-4: Finite element mesh

As pointed out previously, the load- displacement curves obtained through laboratory result appears to have some initial freeplay/local plastization. The additional displacements are subtracted to make the data comparable to the FEM.

Various parameters were varied to study the influences on the L-D curves i.e the element size, shrinkage, dowel effect, and representation reinforcement as smeared or discrete.

7.3.1 Element size

Two different finite element sizes are used; 0.05m and 0.025m. The analysis with 0.05m FE size runs relatively fast, while when using element size of 0.025 the crack pattern becomes more realistic with the consequence of a slower running analysis. Figure 7-1 displays the L-D curves for the ATENA models using the two different FE size in comparison to the experimental result.
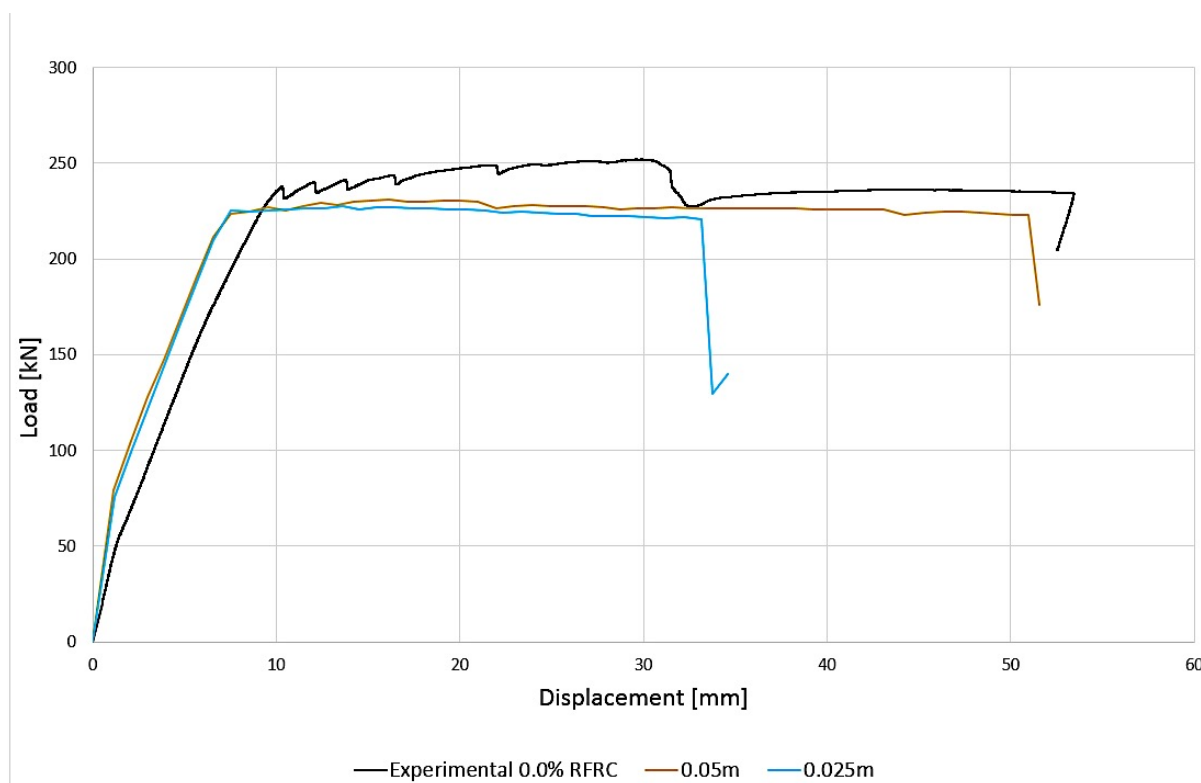
Figure 7-1: Load-displacement diagram with different element size

From the above diagram, the beam modelled with the smallest element size, gives a better fit to the experimental diagram. As a consequence, the analysis also runs much slower. Crack pattern are more realistic for the smallest finite element size as well.

7.3.2 Shrinkage -

Shrinkage is a well-known phenomenon in concrete. Shrinkage can occurs due to different factors, and are divided into plastic shrinkage, drying shrinkage, autogenous shrinkage and carbonation shrinkage (Maage, 2008). The autogenous shrinkage occurs relatively quickly after casting, when the concrete develops its strength. Only the autogenous shrinkage will be accounted, this due to the fact that the beams were tested short time after casting i.e. 40-42 days after casting in contrary to design life of 50 or 100 years. According to EC2, the autogenous shrinkage can be chosen as $5.5 \cdot 10^{-5}$. When taking shrinkage into account in ATENA, the recommended value of $-5.5 \cdot 10^{-5}$ is applied to the concrete structure as initial strain in all directions. Alternative way of taking the shrinkage into account is to reduce the input tensile strength. ATENA Troubleshooting Manual recommends reducing the tensile strength to ½ to 1/10 of the original f_t (Pryl & Cervenka, 2017).
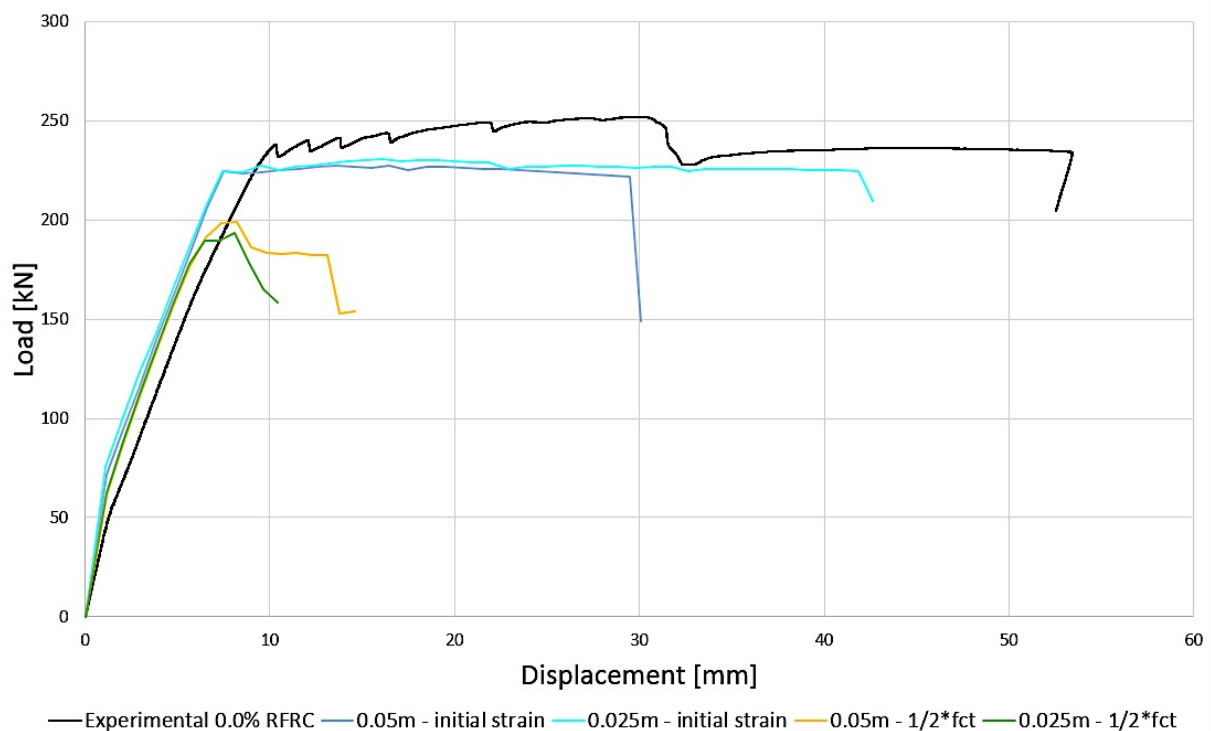
Figure 7-2: Load-displacement curve with applied shrinkage

As can be concluded from the above diagrams, is that taking shrinkage into account affects the length of the diagrams. In particular, the diagrams for reducing the tensile strength to the half of the original one, the initial stiffness of the curve becomes more similar to the experimental diagram. However, they fail too early and the deformed shape of the beam has an unrealistic shape.

7.3.3 Smeared / discrete reinforcement

The beam is designed with reinforcement both as discrete bars and as smeared. The procedure of calculating the reinforcement ratio was discussed previously in Section 6.5.2.2. Smeared reinforcement for the two different FE size are analysed, and the obtained L-D curves are shown in Figure 7-3.
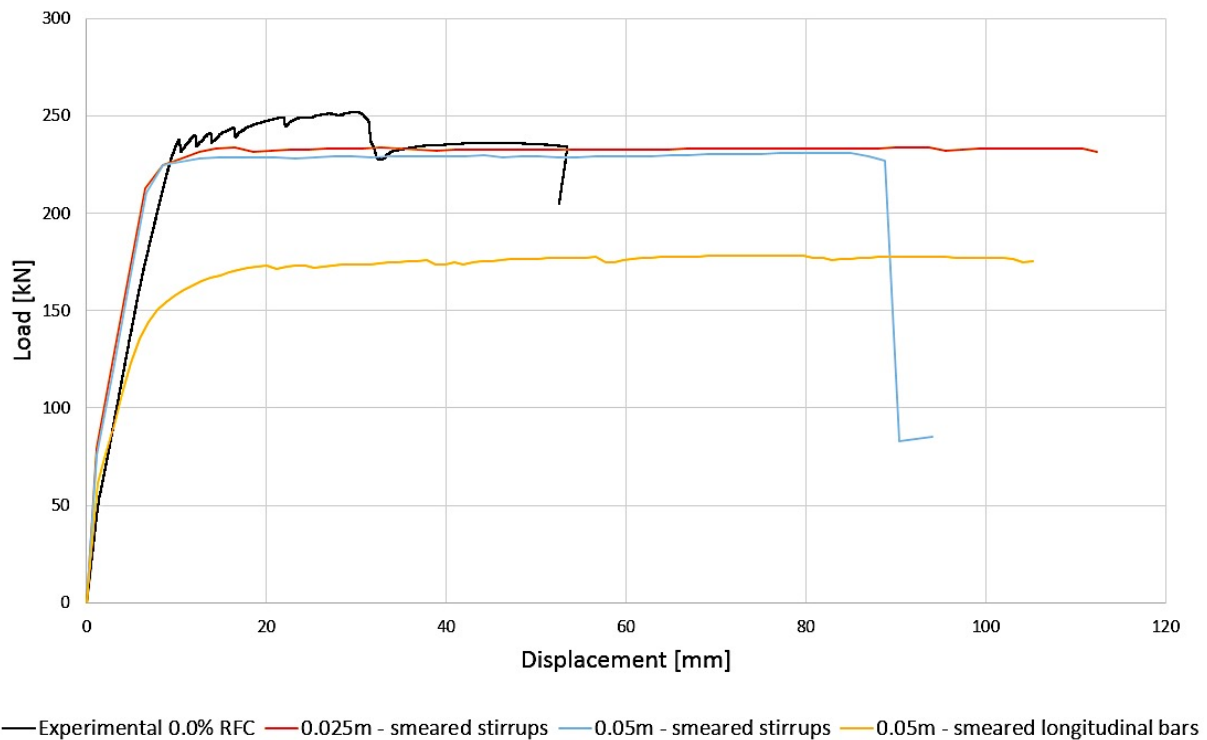
Figure 7-3: Representing reinforcement as smeared with different FE size

By representing the stirrups as smeared, the diagrams appear to smoothen out. However, they are way too long in comparison to the experimental curve. When it comes to representing the longitudinal bars as smeared in x and z direction, the L-D curve does not seem to have sufficient load capacity, and the curve is also too long before reaching failure. On the other hand, the steepness of the curve matches the experimental result better than the other.

7.3.4 Dowel effect

The longitudinal reinforcement might contribute to increase the shear strength of the beam. To consider this effect, the lower longitudinal bars are represented as smeared reinforcement in direction perpendicular to the steel bars. The reinforcement ratio corresponds to the bar volume of lower longitudinal bars distributed evenly over the whole beam volume i.e. reinforcement ratio 0.00842 is added in vertical direction (Pryl & Cervenka, 2017).
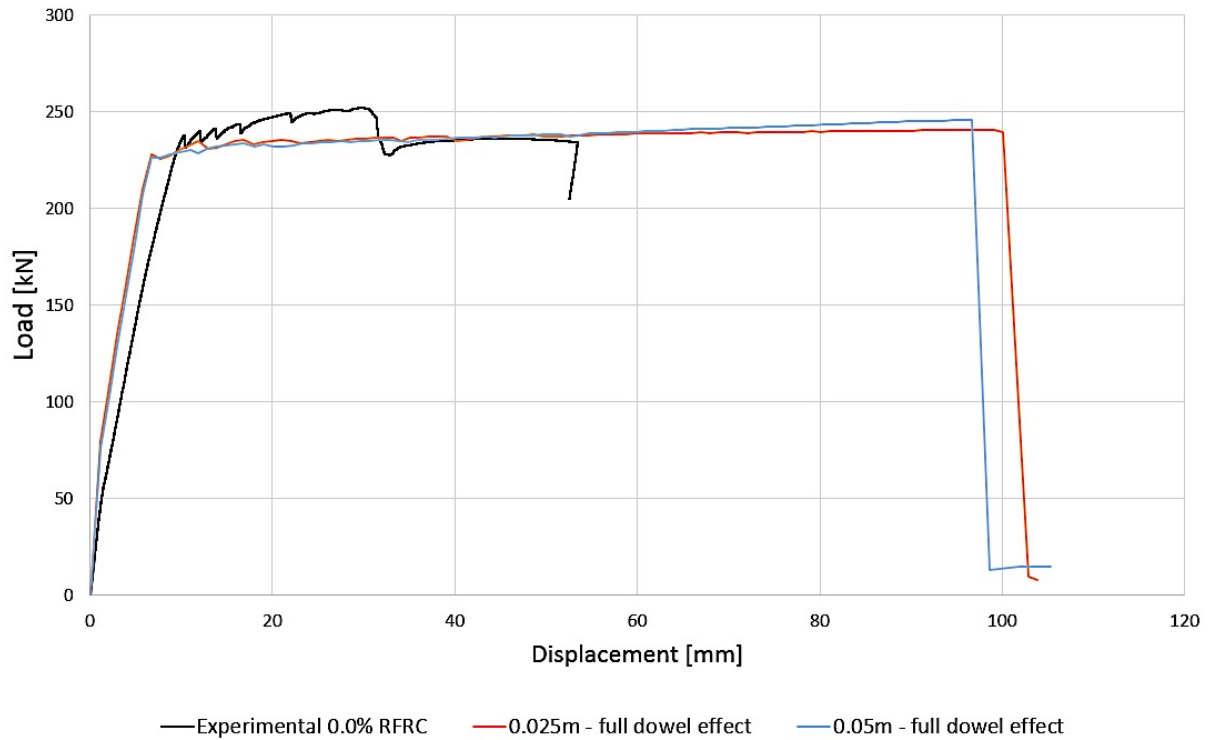
Figure 7-4: Accounting for dowel effect of longitudinal bars with different FE size

The above diagram shows that when taking the dowel effect into account, a full effect is not likely in real practise. The diagrams appear to smoothen out as they increase, and failure does not occur before reaching displacement of approximately 100mm.

7.3.5 Combinations resulting in best fit to experimental L-D diagram

By looking at the influences of the parameters in the L-D diagrams presented above, a combination of them is used to obtain the best fit to the experimental load-displacement curve. The corresponding crack pattern and crack widths for the specific diagrams are also taken into consideration when determining which curve to use. The aim is to construct a model based on the experimental data, and compare the result to the experimental results. Based on this, the models are not modified on too great extent even though it can be possible. The reinforcement is monitored to make sure no rupture occurs in the bars before failure is reached. The dowel effect of lower longitudinal reinforcement is taken into account, as well as shrinkage, which is applied as initial strain to the concrete volume by recommended value of $-5.5 \cdot 10^{-5}$. Default values calculated from the Model Code is used as input values, which are automatically calculated within material model. Table 7-5 gives the input data. Figure 7-5 displays the load-displacement curve for the ATENA model representing the reference beam.

Material type		Reinforced concrete		
Direct tensile strength	f_{ct}	0.9·2.18	1.962	MPa
Reinforcement ratio z-dir.	ρ	0.5·3ø16	0.004021	

Table 7-5: Input data other than those calculated with Model Code
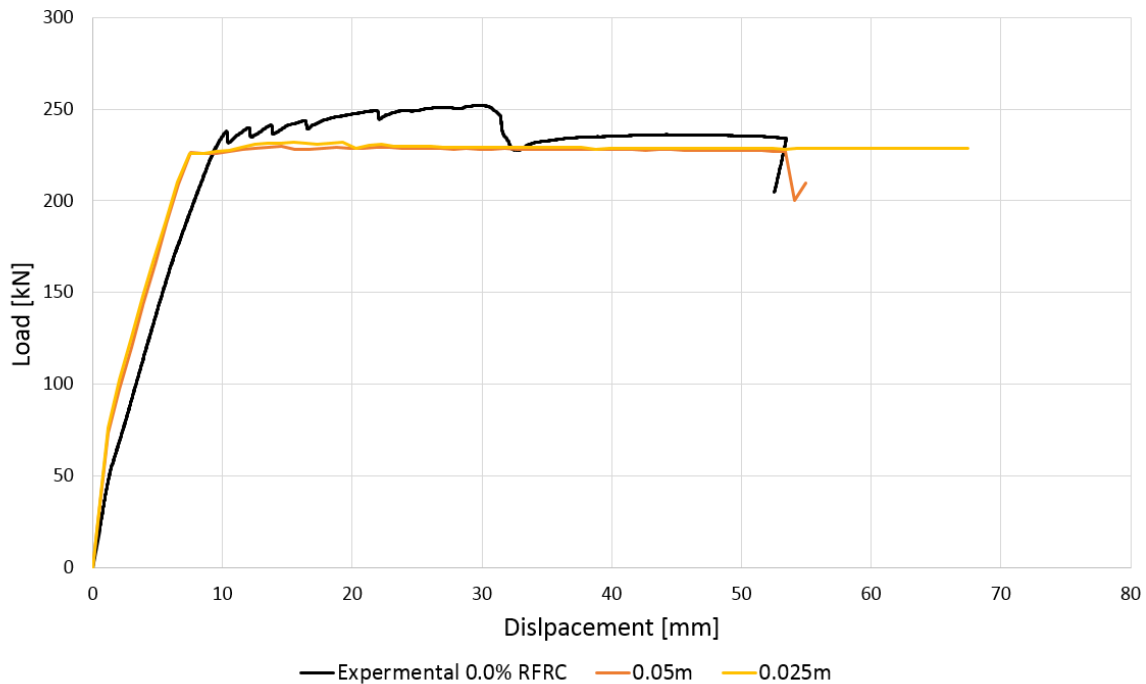
Figure 7-5: Constructed load-displacement diagrams for reference beam

All the constructed curves appear to be overestimated in comparison to the experimental one. The first peak for the ATENA-models is reached earlier than that of the experimental. On the other hand, the diagram never reaches beyond the experimental result i.e. difference in maximum loads of about 8% (232kN/252kN). In other words, the ATENA model is underestimated in comparison to the experimental reference beam. The curve representing the ATENA model with element size 0.05m reaches failure at a similar displacement as the experimental diagram. It should be noted that for the model with element size of 0.025m, unrealistic deformation occurs in some elements after reaching displacement of 40mm. The crack pattern is therefore assumed to be realistic until this point.

7.3.5.1 Crack pattern and crack widths

The beam model with element size of 0.025m is further investigated for crack widths at certain point on the load-displacement diagram. Monitored cracks are given in Table 7-6.

Cracks		Max. crack width [mm]	Load [kN]	Displacement [mm]
First crack		0.085	189.6	5.65
Cracks at softening region	0.116	226	7.47	
Cracks at max. load	0.830	231.8	19.25	
Cracks at ≈ 40mm	1.76	228.8	39.77	

Table 7-6: Crack widths for reference beam

The corresponding crack pattern and crack widths (x-direction) are displayed below. A crack width limit filter with limit width 0.1mm is used.
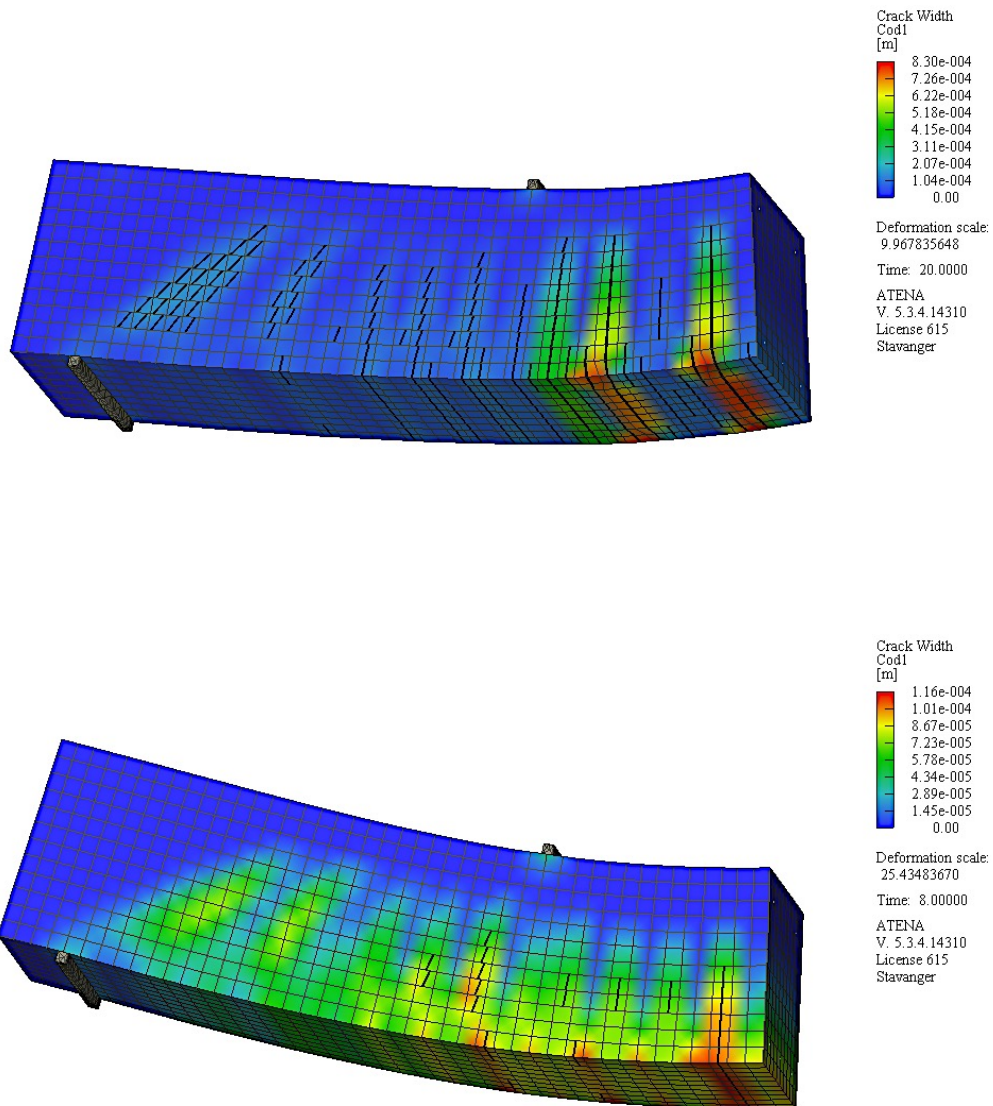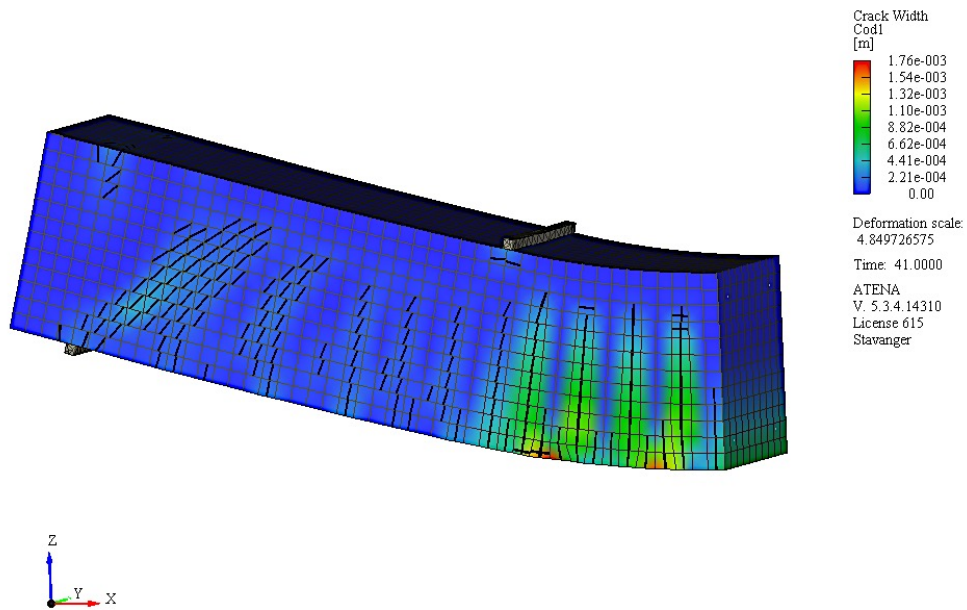
Figure 7-6: Crack pattern at different displacement, ref. Table 7-6

Similar crack pattern can be seen the two beams at a displacement of 53mm, see Figure 7-7 and Figure 7-8. However, the concrete crushing occurring on top of the beam does not appear in the ATENA model. The crack widths for the experimental beam are probably greater than the estimated crack widths in ATENA.
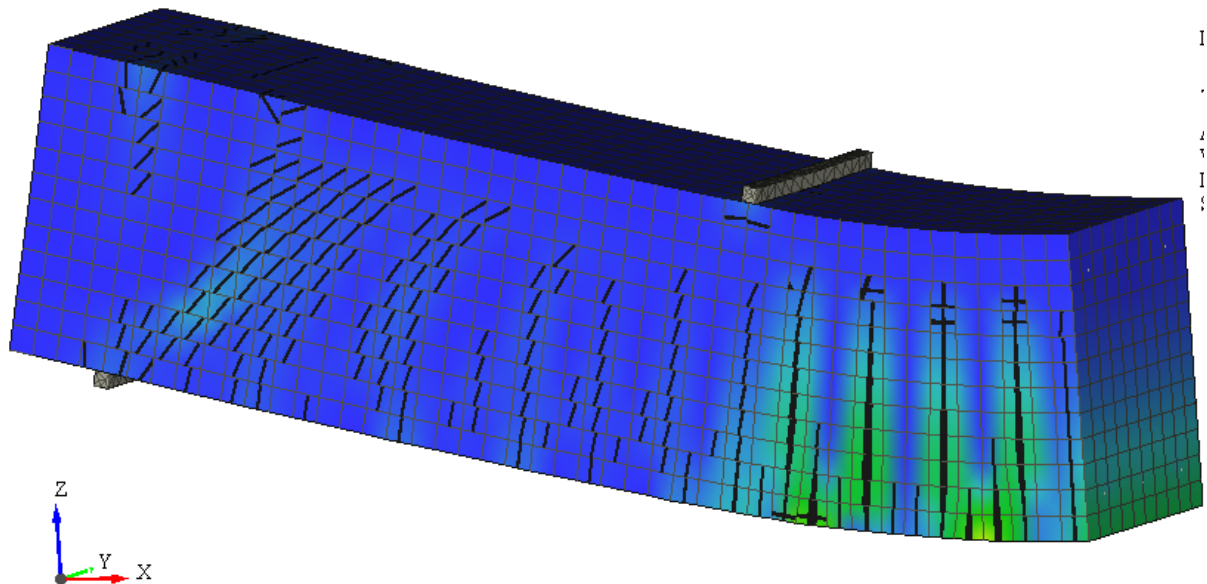
Figure 7-7: Crack pattern for reference beam in ATENA at displacement of 53mm

85

Figure 7-8: Crack pattern for reference beam at laboratory at a displacement of 53mm

7.4   Beam 2, 0.5% RFRC

The second test beam is reinforced with 0.5% recycled steel fibres in addition to conventional reinforcement bars. The material properties of the composite beam are generated in ATENA with the material model **Cementitious2**. Input values for 0.5% RFRC is given in Table 7-7.

Material type		CC3DNonLinCementitious2	
Elastic modulus	E_{ci}	31213.7	MPa
Poisson's ratio	ν	0.2	
Compressive strength	f_{cm}	30.2	MPa
Tensile strength	f_{ct}	2.322	MPa
Crack model		Fixed	

Table 7-7: Material parameters for concrete

7.4.1   Increasing the fracture energy

The fibres can be represented in the material model by simply increasing the fracture energy G_F for the concrete. To this end, the results from the wedge splitting test is used, see Table 7-8. Full dowel effect is assumed. To avoid rupture of stirrups, they are modelled as smeared.

Material prototype		CCSmearedReinf	
Fracture energy	G_F	592	N/m
Dowel effect	ρ_z	0.0008042	
Smeared stirrups	ρ_y	0.002234	
Smeared stirrups	ρ_z	0.002681	

Table 7-8: Material properties for material model with increased fracture enegry

7.4.2 Representing the fibres with smeared reinforcement

Alternative way to represent the fibres is to define them as smeared reinforcement, pointing in 6 different directions i.e. 3 in principal axes and 3 pointing in the middle of the octants (Pryl & Cervenka, 2017). The material properties for the fibres are given in Table 7-9, where the reinforcement ratio for fibres in each of the several directions is calculated as:

$$\frac{V_f}{6} \tag{7.1}$$

Material prototype		CCSmearedReinf	
Young's modulus	E_s	200	Gpa
Mean yield strength	σ_s	870	MPa
Ultimate strain	ε_2	2.8	%
Volume fraction	V_f	0.5	%
Reinforcement ratio	ρ	0.000833	
Fracture energy	G_F	134	N/m

Table 7-9: Material parameters for recycled steel fibres

The dowel effect of the fibres can be important to consider, and in such cases the reinforcement ratio may be up to 0.005 in all directions. However, the fibre contribution can be limited by fibre bond, and the reinforcement ratio must consequently be reduced in such cases. Both methods are tried, and the load-displacement diagrams are displayed in Figure 7-9.
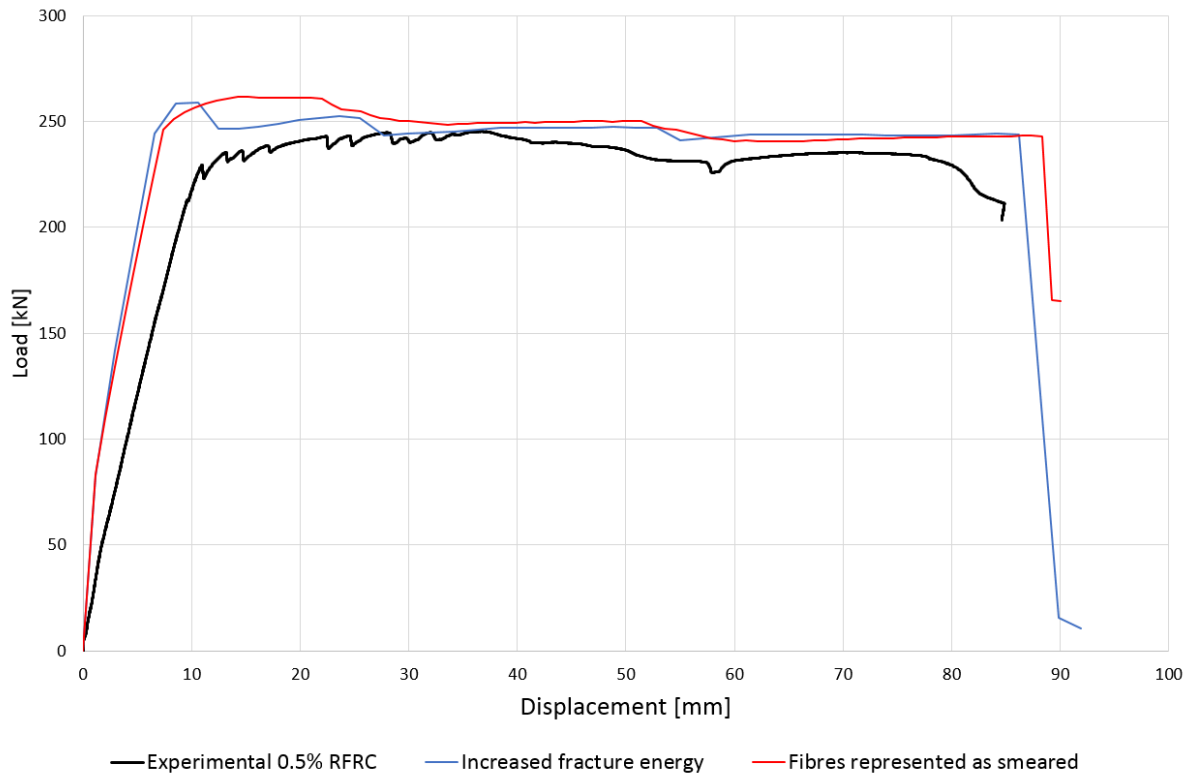
Figure 7-9: Load-displacement diagram for beam containing 0.5% recycled steel fibres

By simply increasing the fracture energy within the material model for concrete, the beam seems to be able to develop cracks with greater widths than to that of the reference beam. Two major cracks are computed in ATENA, as shown in Figure 7-9. Also, a higher peak-load is predicted for the ATENA model, with relative difference of peak loads 7.6%. The initial stiffness for the ATENA models are predicted steeper than to reality. This can be adjusted by decreasing the tensile strength. This might result in unrealistic crack pattern and deformation of beam, and is not reduced further than recommended in EC2. The aim of the thesis is to show the differences between theory and practice.

When representing the fibres with smeared reinforcement, the ATENA model predicts a greater bearing capacity of the beam i.e. difference in maximum loads 9.6%. It should be noted that it was not possible to change the value for modulus of elasticity within the chosen material model, and the default value of 200GPa was therefore used for the recycled steel fibres, even though this might not be the true value.

7.4.3 Crack pattern and crack widths

The ATENA model with increased fracture energy for beam containing 0.5% recycled steel fibre displays the most realistic crack pattern, and is the beam chosen to compare to the experimental beam. The transverse strains, ε_{xx}, are estimated in Strainmaster, by placing a virtual extensometer in the area where a crack is expected. It should be noted that the strains obtained are very sensitive to the placement of the extensometer, and are just approximate values. Linear relationship for strains are assumed, and the crack width ΔL can be calculated as:

$$\Delta L = \varepsilon_{xx} \cdot L_{extensometer} \qquad (7.2)$$

Where $L_{extensometer}$ represents the horizontal length of the virtual strain gauge in mm, see Appendix D for further details.

In ATENA	Displ. [mm]	Crack width for first generated crack [mm]	
		ATENA	Experiment
First crack	8.6	0.124	0.51
At maximum load	10.6	0.208	0.57
At displacement	40	3.10	3.87
Cracks before failure	86	4.20	4.48

Table 7-10: Crack widths obtained for ATENA model with smeared fibres for beam containing 0.5% commercial steel fibres

From the table above, it can be seen that the crack develops at a later stage for the ATENA model those of the experimental beam. The maximum crack widths are about the same right before failure of the beam. Crack development for the chosen ATENA model are displayed in the following with a crack limit filter of 0.0001m.
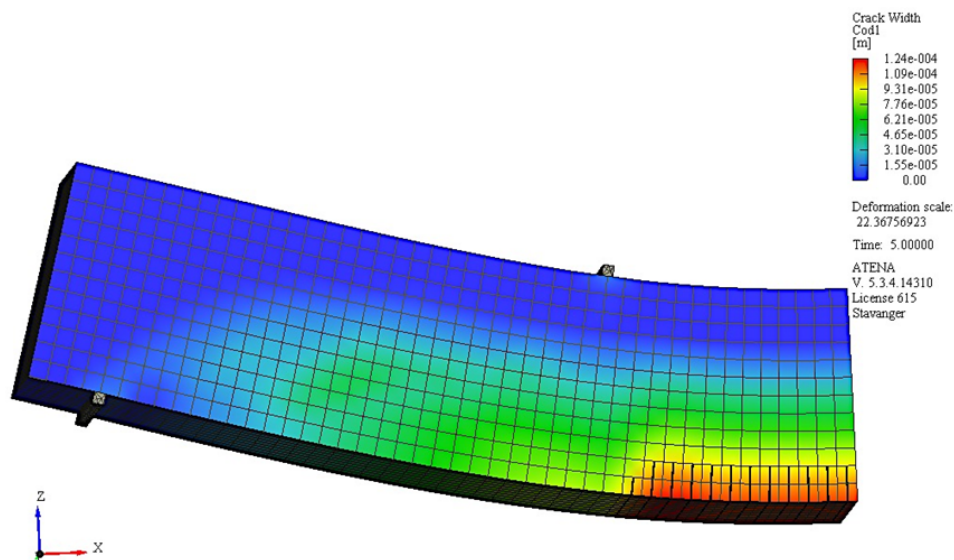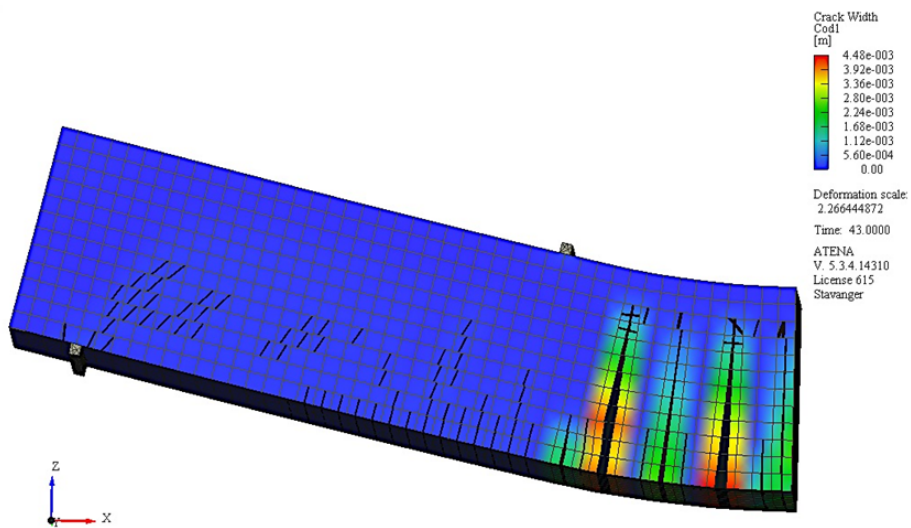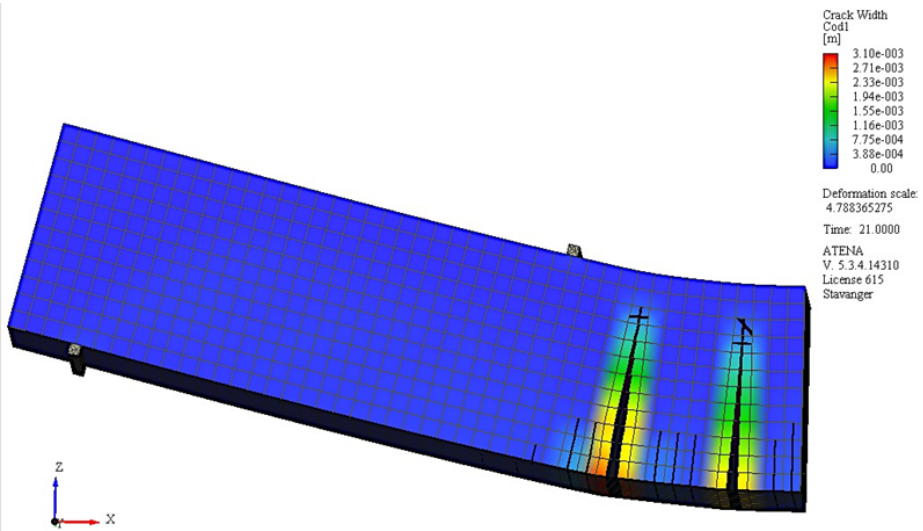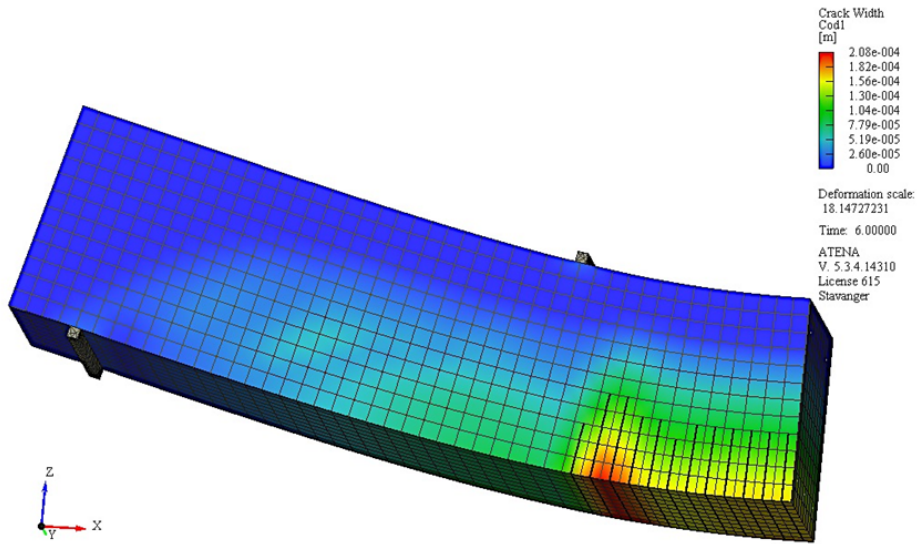
Similar crack pattern can be seen to when comparing to the experimental in the same order as presented above. Red lines are drawn to the right side of the major cracks to make them more visible.
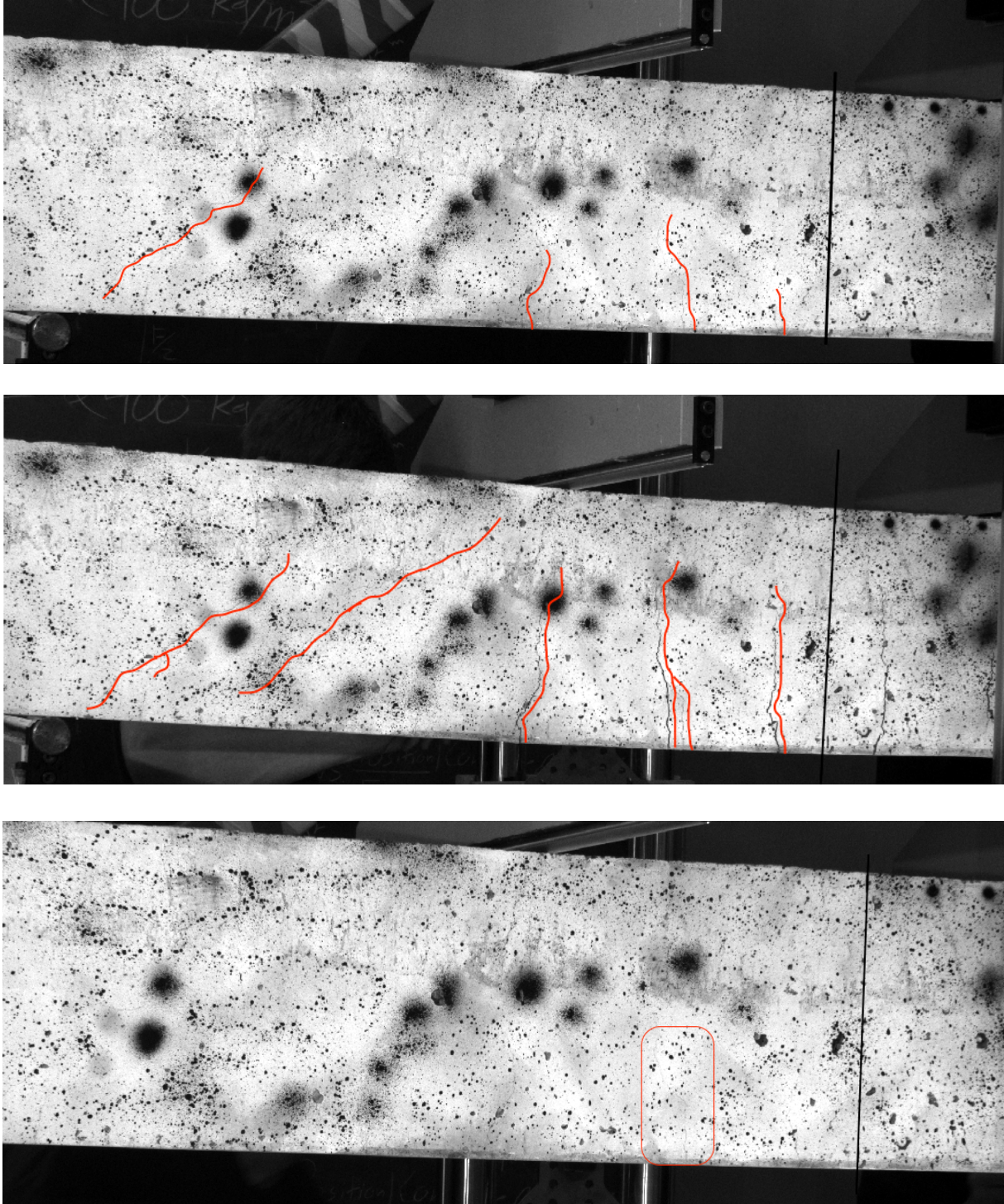
Figure 7-10: Crack pattern for experimental concrete beam containing 0.5% recycled steel fibres

7.5 1.0% RFRC

The third beam to be analysed in ATENA contains 1.0% recycled steel fibres. shows the material parameters for the concrete beam.

Material type		CC3DNonLinCementitious2	
Elastic modulus	E_{ci}	31970.6	MPa
Poisson's ratio	ν	0.2	
Compressive strength	f_{cm}	32.88	MPa
Tensile strength	f_{ct}	0.9·2.49	MPa
Fracture energy	G_F	137	N/m
Crack model		Fixed	

Table 7-11: Material parameters for concrete containing 1.0% recycled steel fibres

7.5.1 Representing fibres by increasing the fracture energy

From the WST, the fracture energy was roughly estimated to 1096N/m. Stirrups are modelled as smeared, and a full contribution of the dowel effect is assumed.

7.5.2 Representing fibres as smeared

The beam is also modelled with smeared fibres. It is assumed that the fibre bond is not optimal and an efficiency factor of 20% is chosen i.e. reinforcement ratio for fibres reduced with 80% of the original, see Table 7-12. The dowel effect is taken into account, and to avoid rupture of stirrups, they are modelled as smeared.

Material type		CCCombinedReinf	
Reinforcement ratio	ρ_y	0.002234+0.000334	0.002567
Yield strength, bars	σ_s	500	MPa
Ultimate strain, bars	ε_2	0.075	
Reinforcement ratio	ρ_z	0.008042+0.002681+0.000334	0.011056
Yield strength, bars	σ_s	500	MPa
Ultimate strain, bars	ε_2	0.075	
Reinforcement ratio other directions	ρ	(0.01/6)·0.2	0.000334
Yield strength, fibres	σ_s	870	MPa
Ultimate strain, fibres	ε_2	0.028	

Table 7-12: Material properties for smeared fibres and ordinary reinforcement

Figure 7-11 displays the computed-load diagrams for the ATENA models and the experimental.
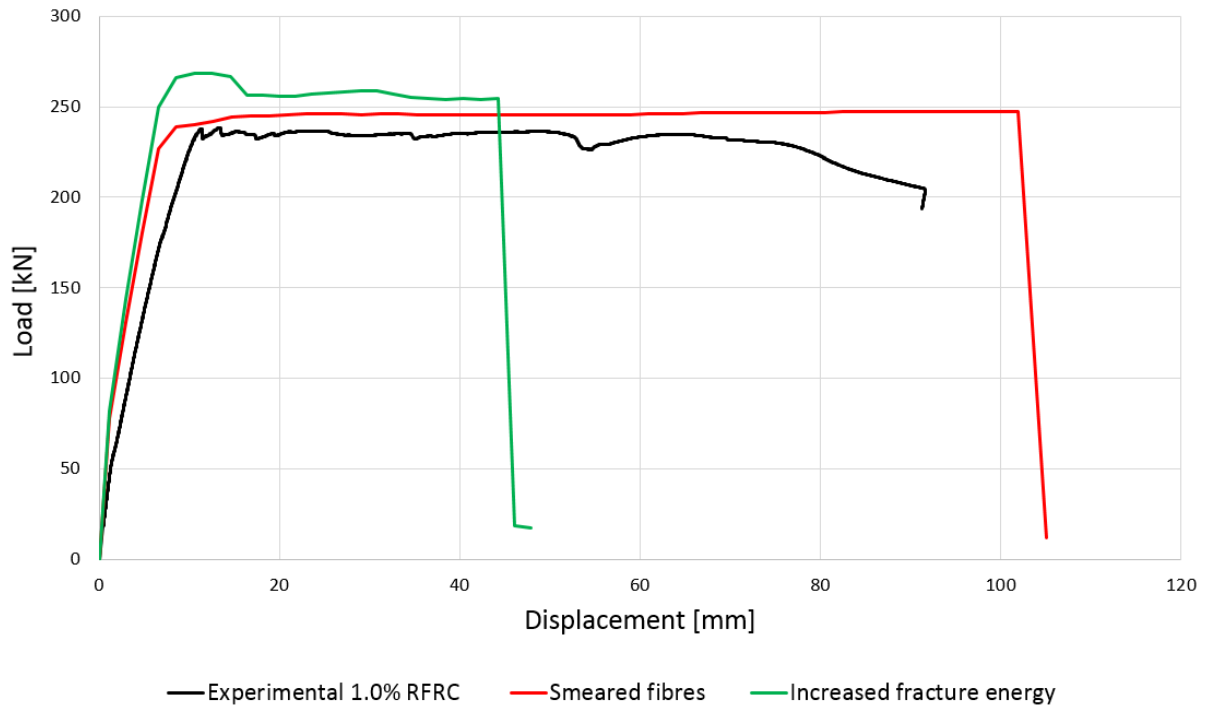
Figure 7-11: Load-Displacement diagram for beam containing 1.0% recycled steel fibres

Both diagrams are overestimated in comparison to the experimental result. Difference in maximum load is about 4%. When representing fibres as smeared, the crack pattern appears to be the most realistic. The crack pattern and crack widths for the beam with smeared fibres is therefore examined in the following.

7.5.3 Crack pattern and crack widths

Crack widths at different stadiums are shown in Table 7-13.

Cracks	Max. crack width [mm]	Load [kN]	Displacement [mm]
First crack	0.148	238.4	8.5
Cracks at softening region	0.257	240.2	10.56
Cracks at ≈ 40mm	1.73	231.8	39.4
Cracks at ≈ 90mm	4.24	247	90.2

Table 7-13: Maximum crack widths at different stadiums

93
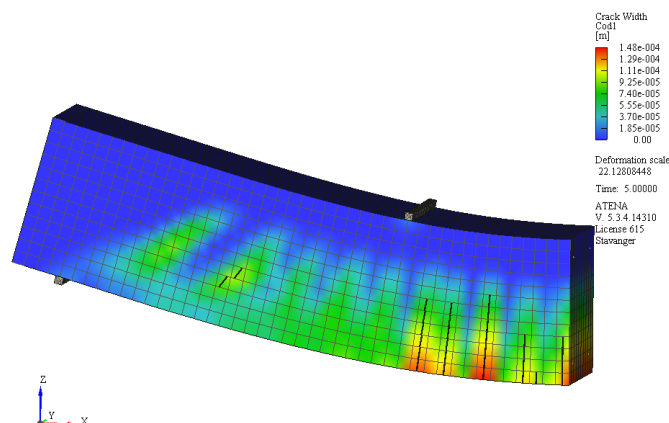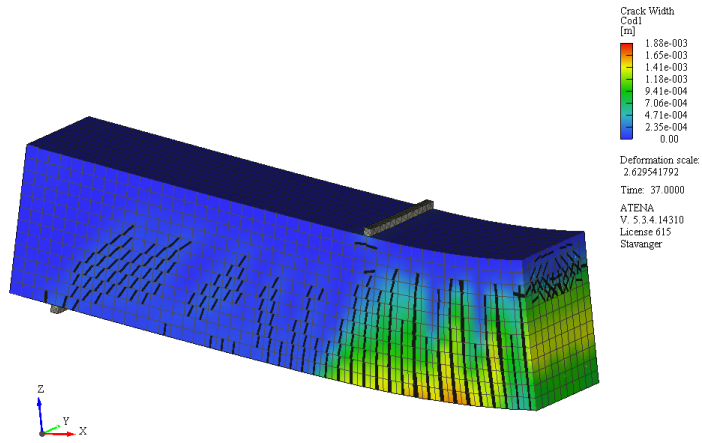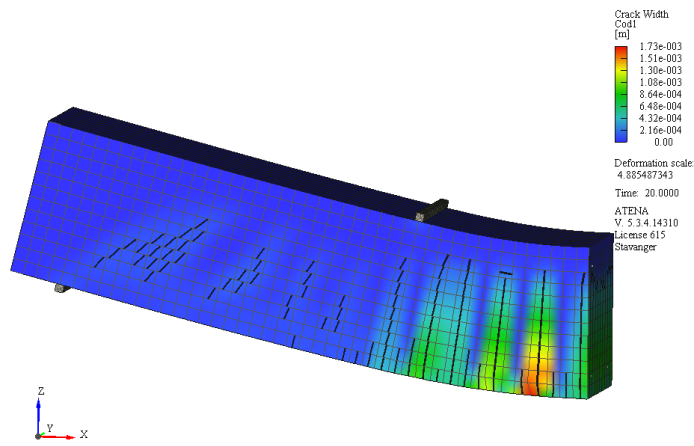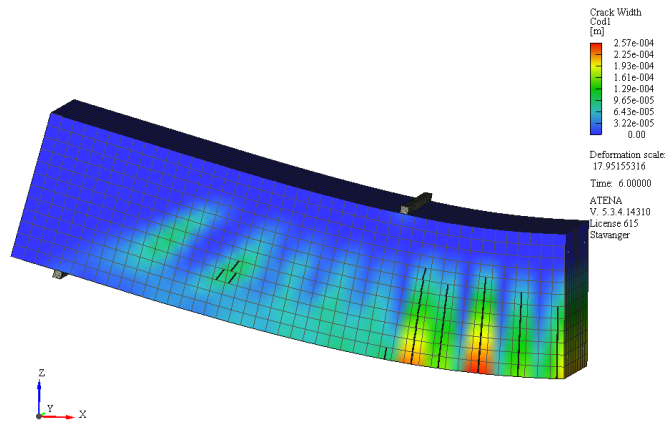
Due to lost data, some "random" pictures from the DIC recording are displayed below. It should be noted that this is just to show the crack development as the loading is applied to the experimental beam.
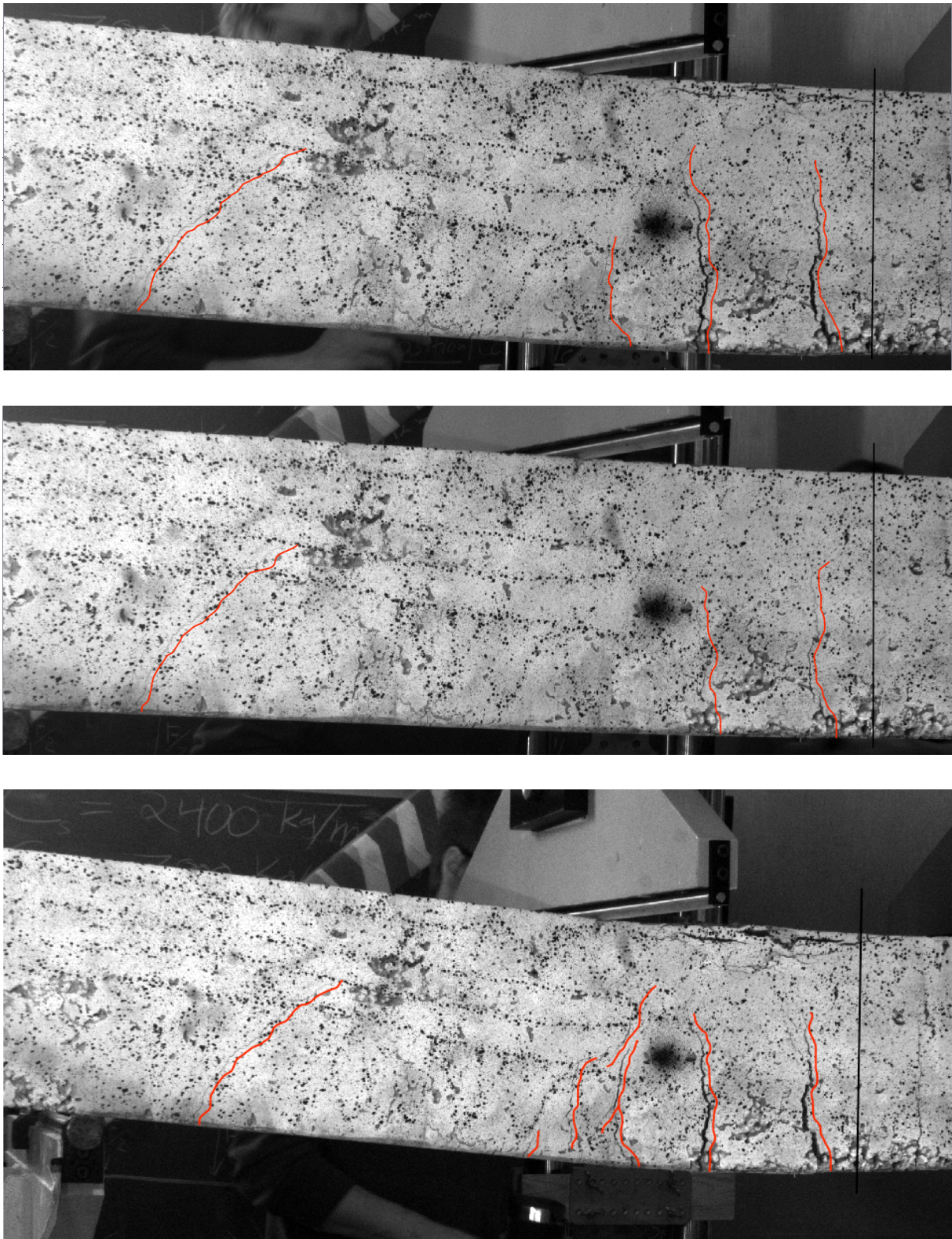
Figure 7-12: Crack pattern for experimental concrete beam containing 1.0% recycled steel fibres

As in the numerical model, the three cracks with greatest crack widths are located at the middle of the beam. From the images above, it is likely to think the experimental crack widths are somewhat greater than those in the numerical model.

7.6 0.5% SFRC

The fourth beam to be analysed contains 0.5% commercial steel fibres. Material parameters for the fibre reinforced concrete beam are given in Table 7-14.

Material type		CC3DNonLinCementitious2	
Elastic modulus	E_{ci}	32411.63	MPa
Poisson's ratio	ν	0.2	
Compressive strength	f_{cm}	34.26	MPa
Tensile strength	f_{ct}	0.9·2.86	MPa
Fracture energy	G_F	138	N/m
Crack model		Fixed	

Table 7-14: Material properties for concrete containing 0.5% commercial steel

7.6.1 Representing fibres by increasing the fracture energy

The beam is modelled with commercial steel fibres by simply increasing the fracture energy of the concrete composite i.e. 2616 N/m. The dowel effect is taken into full account for longitudinal bars, and stirrups are modelled as smeared.

7.6.2 Representing fibres with smeared reinforcement

Fibres are also modelled as smeared, where the fibre bond is assumed reduced with 50% i.e. reinforcement ratio of fibres reduced to the half. The dowel effect is accounted for and stirrups are designed as smeared. Input material values are given in Table 7-15. Fibres are assumed to be of reduced efficiency, due to reduced bonding of fibres and matrix. The reinforcement ratio of fibre is decreased with 50%.

Material type		CCCombinedReinf	
Reinforcement ratio	ρ_y	0.002234+0.000417	0.002651
Yield strength, z-dir.	σ_s	500	MPa
Ultimate strain, z-dir.	ε_2	0.075	
Reinforcement ratio	ρ_z	0.008042+0.002681+0.000417	0.01114
Yield strength, y-dir.	σ_s	500	MPa
Ultimate strain bars	ε_2	0.075	
Reinforcement ratio other directions	ρ	(0.005/6)·0.5	0.000417
Yield strength	σ_s	870	MPa
Ultimate strain fibres	ε_2	0.028	

Table 7-15: Material parameters for reinforcement

Figure 7-13 displays the load-displacement diagrams. The difference between the maximum loads for the ATENA model and the experimental beam is about 1%.
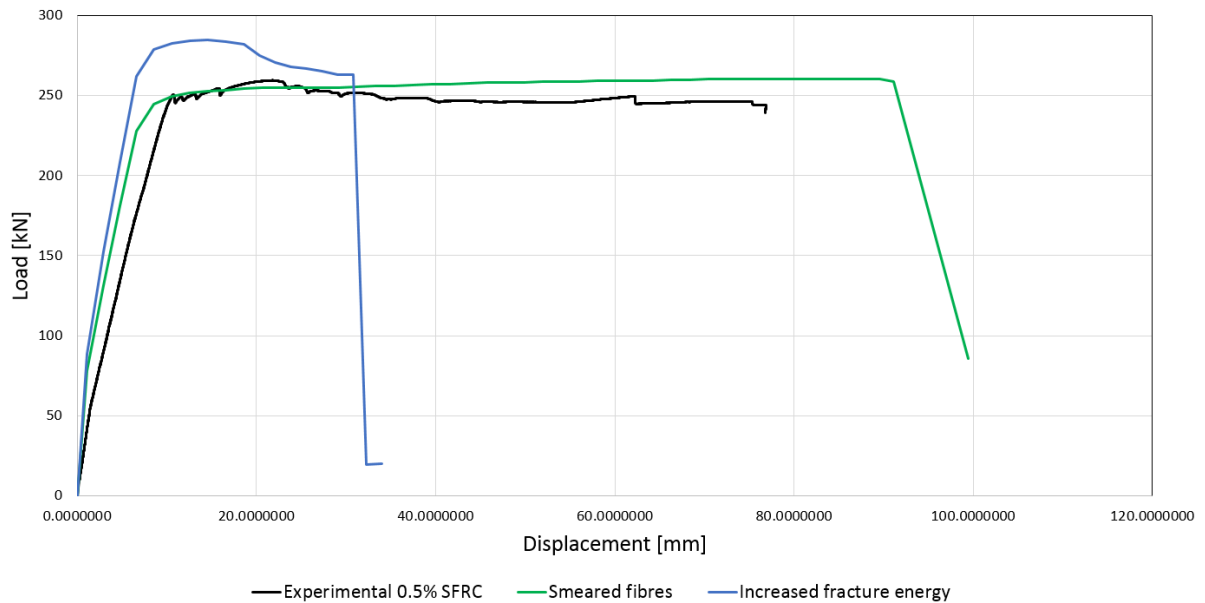
Figure 7-13: Load-displacement diagram for 0.5% SFRC

7.6.3 Crack pattern and crack widths ← heeeeeeeer
Crack widths at different stages of loading are given in Table 7-16.

Cracks	Max. crack width [mm]	Load [kN]	Displacement [mm]
First crack	0.124	244.8	8.5
Cracks at softening region	0.171	249.4	10.5
Cracks at ≈ 40mm	1.09	257.0	39.5
Cracks at ≈ 75mm	1.88	260.2	74.6

Table 7-16: Crack widths obtained for ATENA model with smeared fibres for 0.5% SFRC

As can be seen from the cracks developed in ATENA, a greater amount of cracks are generated. In contrary to the beam containing 0.5% recycled steel fibres, the cracks appears to be more evenly distributed over the beam containing 0.5% commercial steel fibres, see APPENDIX F.

7.7 1.0% SFRC
The material parameters for the beam containing 1.0% commercial steel fibres are given in Table 7-17.

Material type		CC3DNonLinCementitious2	
Elastic modulus	E_{ci}	32674.4	MPa
Poisson's ratio	ν	0.2	
Compressive strength	f_{cm}	35.1	MPa
Tensile strength	f_{ct}	0.9·2.97	MPa
Fracture energy	G_F	138	N/m
Crack model		Fixed	

Table 7-17: Material properties for concrete containing 1.0% steel fibres

7.7.1 Fibres represented by increasing the fracture energy

For the model with increased fracture energy the value 1726 N/m is inserted within the material model for the concrete composite.

7.7.2 Smeared fibres

The material parameters for beam with fibres defined as smeared can be found in Table 7-18. Efficiency of commercial steel fibre with content of 1% is assumed to be 30% i.e. reinforcement ratio for fibre is reduced with 70%.

Material type		CCCombinedReinf	
Reinforcement ratio	ρ_y	0.002234+0.0005	0.002734
Yield strength, z-dir.	σ_s	500	MPa
Ultimate strain, z-dir.	ε_2	0.075	
Reinforcement ratio	ρ_z	0.008042+0.002681+0.0005	0.011223
Yield strength, y-dir.	σ_s	500	MPa
Ultimate strain bars	ε_2	0.075	
Reinforcement ratio other directions	ρ	(0.01/6)·0.3	0.0005
Yield strength	σ_s	870	MPa
Ultimate strain fibres	ε_2	0.028	

Table 7-18: Material properties for reinforcement
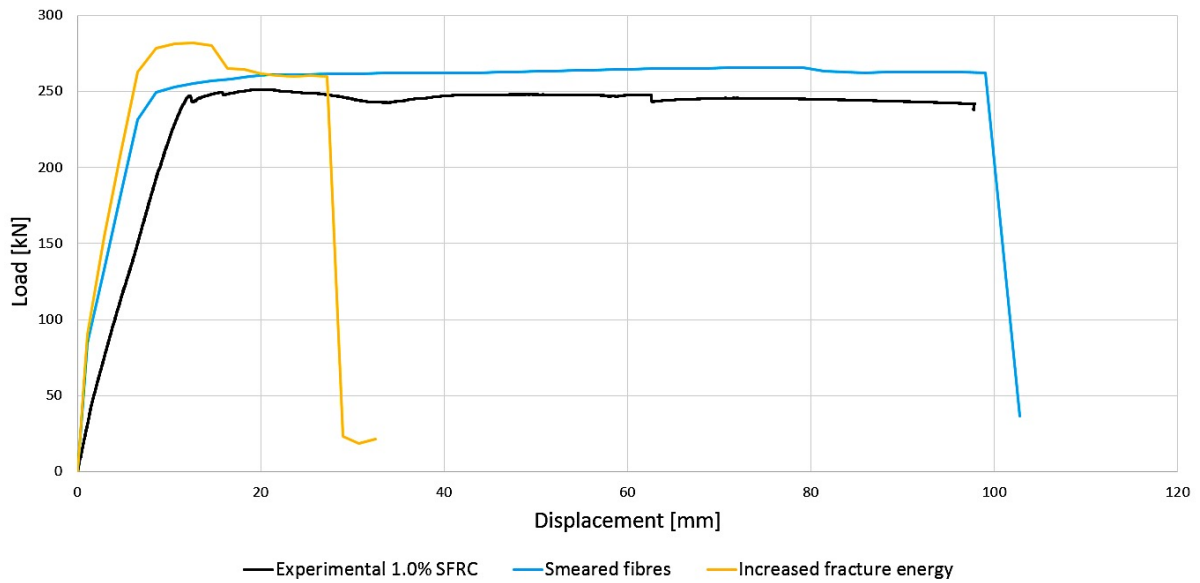
Figure 7-14: Load-displacement diagram for beam containing 1.0% commercial steel fibres

From the load-displacement diagram, the model with representing fibres as smeared in 6 different directions appears to be similar to the experimental. As for all the other ATENA models, the initial stiffness of the beam (slope of pre-peak) is much greater than the experimental stiffness. The ATENA model with smeared fibres is somewhat overestimated, in which the difference in maximum loads between the experimental results and the model with smeared fibres is about 5%.

7.7.3 Crack widths and crack pattern

Crack widths obtained in ATENA with the model representing fibres as smeared are given in Table 7-19.

Cracks	Max. crack width [mm]	Load [kN]	Displacement [mm]
First crack	0.110	182.6	4.7
Cracks at softening region	0.228	253.2	10.6
Cracks at ≈ 40mm	1.03	262.2	39.57
Cracks at ≈ 90mm	3.32	260.4	90.3

Table 7-19: Crack widths for ATENA model with smeared fibres for 1.0% SFRC

Similar crack pattern to the beam containing 0.5% commercial steel fibres can be seen for the ATENA model with 1.0% commercial steel fibres, see APPENDIX F.

8 Discussion and conclusions

The object of this thesis was to study by nonlinear analysis the behaviour of recycled fibre reinforced concrete, and compare the performance with commercial steel fibre reinforced concrete. Several tests were performed at the laboratory, in which served as input values for the ATENA-models. The load-displacement diagrams computed in ATENA were compared to the experimental load-displacement diagrams.

Mostly, the load-displacement diagrams computed with nonlinear FEA were overestimated in comparison to the experimental results by 1-9%. In addition, all L-D diagrams computed in ATENA were steeper than to that of the experimental. In order to reduce the slope of the diagrams, additional shrinkage could be applied i.e. reducing tensile strength. On the other hand, applying additional shrinkage caused too early failure of the beam due to rupture of reinforcement bars at relatively small displacements. Unrealistic deformations and cracking appeared in such cases. With respect to this, a more sophisticated and advanced material model should be employed.

The analysis showed somewhat similar behaviour to the experimental, including crack pattern and crack widths. However, the results were very depending on the parameters adjusted to create load-displacement diagrams e.g. representing the fibres as smeared or by simply increase the specific fracture energy. It should also be noted that several simplifications and assumptions were made along the way, which also may have influenced the results.

From the results obtained in this thesis, it can be concluded that recycled steel fibre reinforced concrete behaves similar to commercial steel fibre reinforced concrete containing the equal amount of fibres. Promising load bearing capacity can bee seen for concrete containing recycled steel fibres, and can therefore function as replacement to the commercial steel fibres.

8.1 Suggestions for further work

Only one beam is analysed for crack widths and compared to the actual experimental crack widths result. The other beams were only compared visually, as data went missing along the way. However, analysis should be conducted for all beams to be able to obtain a more throughout analysis and to be able to make further conclusions.

Also, the wedge splitting tests were not executed in satisfactory manner, as none of the specimens were loaded until failure. To obtain more accurately results for the fracture energy, additional wedge splitting tests should be performed.

To get a better understanding of how the fibres performs in arresting cracks and alters the fracture energy, numerical analysis of WST specimens should be conducted in ATENA e.g. behaviour of recycled fibres versus commercial fibres, and the influence of volume fractions.

Another suggestion is to use the more sophisticated material model **CC3Dcementitious2User** to make a better fit to the experimental results. In this way the tension function can be modified with respect to the load-displacement diagram, and be obtained for the specific experimental beam result.

9 References

Ahmadyar, M. (2011). *Ductility in lightweight concrete with fiber.* (Master thesis, University of Stavanger). Retrieved from https://brage.bibsys.no/xmlui//handle/11250/182794

Belytschko, T., Liu, W. K., & Moran, B. (2000). *Nonlinear Finite Elements for Continua and Structures*. Chichester, New York: John Wiley & Sons Ltd.

Cervenka Consulting. (2017, 12.02). Software products. Retrieved from http://www.cervenka.cz/products/

Červenka, V., Jendele, L., & Červenka, J. (2016). *ATENA Program Documentation Part 1: Theory* (pp. Chapter 4). Retrieved from http://www.cervenka.cz/assets/files/atena-pdf/ATENA_Theory.pdf

Červenka, V. r., Červenka, J., Janda, Z. k., & Pryl, D. (Eds.). (2017). *ATENA Program Documentation Part 8 - User's Manual for ATENA-GiD Interface.* Prague: Cervenka Consulting.

Concrete Cylinder Splitting Tensile Strength Test [2] [Picture]. (2015). Retrieved from https://www.researchgate.net/figure/281826801_fig3_Concrete-Cylinder-Splitting-Tensile-Strength-Test-2

Cook, R. D., Malkus, D. S., Plesha, M. E., & Witt, R. J. (2002). *Concepts and applications of finite element analysis* (4th ed.). New York: John Wiley & Sons, Inc.

Delphin, I. L. A. (2009). Betong: historie. *Store norske leksikon.* Retrieved from https://snl.no/betong%2Fhistorie.

Di Prisco, M., Colombo, M., & Dozio, D. (2013). *Fibre ‐ reinforced concrete in fib Model Code 2010: principles, models and test validation* Vol. 14. *Structural Concrete* (pp. 342-361). Retrieved from http://onlinelibrary.wiley.com/doi/10.1002/suco.201300021/epdf doi:10.1002/suco.201300021

Døssland, Å. L. (2008). *Fibre Reinforcement in Load Carrying Concrete Structures: Laboratory and Field Investigations compared with Theory and Finite Element Analysis.* (PhD. Thesis, Department of Structural Engineering), Norwegian University of Science and Technology, Trondheim. Retrieved from https://brage.bibsys.no/xmlui/bitstream/handle/11250/236403/124658_FULLTEXT02.pdf?sequence=1&isAllowed=y

Espedal, J. E. (2015). *Fiberarmert betong.* (Master thesis, University of Stavanger). Retrieved from https://brage.bibsys.no/xmlui/handle/11250/297502

Güner, S. (2008). *Performance assessment of shear-critical reinforced concrete plane frames.* (PhD, University of Toronto). Retrieved from https://tspace.library.utoronto.ca/handle/1807/16730

Ilankeeran, P. K., Mohite, P. M., & Kamle, S. (2012). Axial Tensile Testing of Single Fibres. *Modern Mechanical Engineering, Vol.02No.04*, 6. doi:10.4236/mme.2012.24020

Jahren, P. (2011). *Betong: historie og historier*. Trondheim: Tapir akademisk forl.

Kabele, P., & Cervenka, V. (2010). *ATENA Program Documentation Part 1-3 - Example Manual ATENA Engineering* Retrieved from http://www.cervenka.cz/assets/files/atena-pdf/ATENA-Engineering_Example_Manual.pdf

Kanstad, T., Juvik, D. A., Vatnar, A., Mathisen, A. E., Sandbakk, S., Vikan, H., . . . Overrein, G. O. (2011). *Forslag til retningslinjer for dimensjonering, utførelse og kontroll av fiberarmerte betongkonstruksjoner.* COIN Project report, Vol. 29. Retrieved from

https://www.sintefbok.no/Product.aspx?sectionId=0&productId=1010&categoryId=27

Klausen, A. B. E. (2009). *Steel fibres in load carrying concrete structures. Guideline survey and practical examples* COIN Project report, Vol. 17. Retrieved from http://www.sintef.no/publikasjoner/Publikasjon/?pubid=SINTEF+A20094

Knudsen, O. Ø., Nolte, D., Gaarder, R., & Hammer, T. A. (2016). *New materials in tunnels and bridges* Vol. 557. *Durable structures 2012-2015 (SINTEF A27441)* Retrieved from http://www.vegvesen.no/fag/teknologi/Tunneler/Publikasjoner/_attachment/1596178?_ts=158251f2948&fast_title=Nye+materialer+for+bruk+i+tunnel+og+bru

Lu, Y. (2015). *Infrastructure Corrosion and Durability - A sustainability study Go Green: Using waste and recycling materials* Retrieved from https://www.esciencecentral.org/ebooks/infrastructure-corrosion-durability/go-green-using-waste-and-recycling-materials.php

Löfgren, I. (2005). *Fibre-reinforced Concrete for Industrial Construction - a fracture mechanics approach to material testing and structural analysis.* (PhD. Thesis, Department of Civil and Environmental Engineering, Structural Engineering), Chalmers University of Technology, Göteborg. Retrieved from http://publications.lib.chalmers.se/records/fulltext/8627/8627.pdf

Mehta, P. K., & Monteiro, P. J. M. (2006). *Concrete : microstructure, properties, and materials* (3rd ed. ed.). New York: McGraw-Hill.

Model Code 2010 - First complete draft. (2010). Vol. 1. Retrieved from http://210.42.35.80/G2S/eWebEditor/uploadfile/20161006233323944.pdf

Maage, P. M. (2008). *TKT 4215 Concrete Technology 1* (2011 ed.). Norway: Norwegian University of Science and Technology.

Nawy, E. G. (2001). *Fundamentals of high-performance concrete* (2nd ed. ed.). New York: Wiley.

NT-METHOD - Wedge splitting test method (WST): Fracture testing of fibre.reinfroced concrete (Mode I). (2005). Retrieved from

Park, K., Paulino, G. H., & Roesler, J. R. (2008). Determination of the kink point in the bilinear softening model for concrete. *Engineering Fracture Mechanics, 75*(13), 3806-3818. doi:10.1016/j.engfracmech.2008.02.002

Pryl, D., & Cervenka, J. (2017). *ATENA Program Documentation Part 11 - Troubleshooting Manual* Retrieved from http://www.cervenka.cz/assets/files/atena-pdf/ATENA-Troubleshooting.pdf

Sajdlová, T. (2016a). *ATENA Program Documentation Part4-7 ATENA Science - GID FRC Tutorial* (pp. p. 12). Retrieved from http://www.cervenka.cz/assets/files/atena-pdf/ATENA-Science-GiD_Tutorial_FRC.pdf

Sajdlová, T. (2016b). *ATENA Program Documentation Part 4-7, ATENA Science - GiD FRC Tutorial Step by step guide for nonlinear analysis of fiber reniforced concrete structures with ATENA and GiD* Retrieved from http://www.cervenka.cz/assets/files/atena-pdf/ATENA-Science-GiD_Tutorial_FRC.pdf

Shi, C., & Mo, Y.-L. (2008). *High-Performance Construction Materials : Science and Applications* (Vol. 1). Singapore: World Scientific Publishing Company.

Standard Norge. (2009a). *NS-EN 12350-2: Testing fresh concrete, Part 2: Slump-test* Retrieved from http://www.standard.no/nettbutikk/sokeresultater/?search=betong&subscr=1

Standard Norge. (2009b). *NS-EN 12350-6:Testing fresh concrete - Part 6: Density* Retrieved from http://www.standard.no/no/Abonnement/Standarder/

Standard Norge. (2009c). *NS-EN 12350-7: 2009: Testing fresh concrete, Part 7: Air content Presure methods* Retrieved from http://www.standard.no/nettbutikk/sokeresultater/?search=betong&subscr=1

Standard Norge. (2009d). *NS-EN 12390-3:2009 Testing hardened concrete - Part 3: Compressive strength of test specimens* Retrieved from http://www.standard.no/nettbutikk/sokeresultater/?search=betong&subscr=1

Standard Norge. (2009e). *NS-EN 12390-6:2009 Testing hardened concrete – Part 6: Tensile splitting strength of test specimens.* Retrieved from http://www.standard.no/nettbutikk/sokeresultater/?search=betong&subscr=1

Standard Norge (Ed.) (2013). *NS-EN 12390-13:2013 - Testing hardened concrete, Part 13: Determination of secant modulus of elasticity in compression.*

Vikan, H. (2007). *Concrete workability and fibre content* SINTEF report; SBF BK A07029, Retrieved from https://brage.bibsys.no/xmlui/handle/11250/2424151

APPENDIX A

Tensile strength of recycle steel fibres obtained though tests.

10

Specimen	Tenile strength [N/mm^2]
1	214
2	220
3	1597
4	1248
5	1162
6	1185
7	425
8	1668
9	1539
10	570
11	434
12	174
Average	**869.6666667**
Variance	341421.697
Standard derviation	584.3130128

APPENDIX B

Output from ATENA for maximum crack widths.

Reference beam 0.025m

1. First crack

Output data for request: CRACK_WIDTH
Description: Crack width
  Step: 6 Iteration: 6 at Time: 6

Node	COD1	COD2	COD3
Units	m	m	m
5541	8.55e-005	0.0	0.0

2. Cracks at softening region

Output data for request: CRACK_WIDTH
Description: Crack width
  Step: 8 Iteration: 7 at Time: 8

Node	COD1	COD2	COD3
Units	m	m	m
5982	0.0001157	0.0	0.0

3. Cracks at maximum load

Output data for request: CRACK_WIDTH
Description: Crack width
  Step: 20 Iteration: 4 at Time: 20

Node	COD1	COD2	COD3
Units	m	m	m
5655	0.0008296	1.59e-005	0.0

4. Cracks at displacement of 40mm

Output data for request: CRACK_WIDTH
Description: Crack width
  Step: 41 Iteration: 5 at Time: 41

Node	COD1	COD2	COD3
Units	m	m	m
5503	0.0017649	2.26e-005	1.10e-005

0.5% RFRC 0.025m

   1. First crack

Output data for request: CRACK_WIDTH
Description: Crack width
 Step: 5 Iteration: 8 at Time: 5

Node	COD1	COD2	COD3
Units	m	m	m
4992	0.0001241	0.0	0.0

   2. Crack width at maximum load

Output data for request: CRACK_WIDTH
Description: Crack width
 Step: 6 Iteration: 4 at Time: 6

Node	COD1	COD2	COD3
Units	m	m	m
4931	0.0002078	0.0	0.0

   3. Crack width at displacement of 40mm

Output data for request: CRACK_WIDTH
Description: Crack width
 Step: 21 Iteration: 7 at Time: 21

Node	COD1	COD2	COD3
Units	m	m	m
5032	0.0031002	2.46e-007	0.0

   4. Crack width at displacement of 86mm

Output data for request: CRACK_WIDTH
Description: Crack width
 Step: 43 Iteration: 8 at Time: 43

Node	COD1	COD2	COD3
Units	m	m	m
6354	0.0044796	1.44e-005	1.29e-007

1.0% RFRC 0.025m
   1. First crack

Output data for request: CRACK_WIDTH
Description: Crack width
  Step: 5 Iteration: 8 at Time: 5

  Node   COD1   COD2   COD3
  Units   m   m   m
  5031   0.0001479   0.0   0.0

   2. At softening region

Output data for request: CRACK_WIDTH
Description: Crack width
  Step: 6 Iteration: 5 at Time: 6

  Node   COD1   COD2   COD3
  Units   m   m   m
  5393   0.0002573   0.0   0.0

   3. At displacement of 40mm

Output data for request: CRACK_WIDTH
Description: Crack width
  Step: 20 Iteration: 4 at Time: 20

  Node   COD1   COD2   COD3
  Units   m   m   m
  5503   0.0017274   3.09e-005   0.0

   4. At displacement of 40mm

Output data for request: CRACK_WIDTH
Description: Crack width
  Step: 46 Iteration: 4 at Time: 46

  Node   COD1   COD2   COD3
  Units   m   m   m
  5218   0.0042404 2.03e-005 7.65e-006

0.5% SFRC 0.025m

1. First crack

2. Cracks at softening region

Output data for request: CRACK_WIDTH
Description: Crack width
 Step: 6 Iteration: 4 at Time: 6

 Node   COD1   COD2   COD3
 Units   m   m   m
 5405   0.0001709   0.0   0.0

3. Cracks at displacement of 40mm
4.

Output data for request: CRACK_WIDTH
Description: Crack width
 Step: 20 Iteration: 4 at Time: 20

 Node   COD1   COD2   COD3
 Units   m   m   m
 4898   0.0010882 1.60e-005   0.0

5. Cracks at displacement of 75mm (about before failure)

Output data for request: CRACK_WIDTH
Description: Crack width
 Step: 37 Iteration: 5 at Time: 37

 Node   COD1   COD2   COD3
 Units   m   m   m
 5192   0.0018829   2.90e-005   0.0

1.0% SFRC 0.025m

1. First crack

Output data for request: CRACK_WIDTH
Description: Crack width
 Step: 3 Iteration: 10 at Time: 3

Node	COD1	COD2	COD3
Units	m	m	m
3457	0.0001101	0.0	0.0

2. Cracks at softening region

Output data for request: CRACK_WIDTH
Description: Crack width
 Step: 6 Iteration: 6 at Time: 6

Node	COD1	COD2	COD3
Units	m	m	m
4542	0.0002283	0.0	0.0

3. Cracks at displacement of 40mm

Output data for request: CRACK_WIDTH
Description: Crack width
 Step: 20 Iteration: 5 at Time: 20

Node	COD1	COD2	COD3
Units	m	m	m
5192	0.0010285	1.66e-005	0.0

4. Cracks at about 90mm

Output data for request: CRACK_WIDTH
Description: Crack width
 Step: 44 Iteration: 6 at Time: 44

Node	COD1	COD2	COD3
Units	m	m	m
5663	0.0033164	4.87e-005	0.0

APPENDIX C

Simple calculations to estimate maximal load capacity of designed beam.

Concrete geometry:

$$h = 300mm$$

$$b = 250mm$$

$$L_{span} = 2.0m$$

Concrete cover:
$$C_{nom} = 25mm$$

Diameter of a stirrup Øs: $\quad\quad Ø_s = 8mm$
Diameter of a longitudinal bar: $\quad Ø_l = 16mm$

$$d = h - C_{nom} - Ø_s - \frac{Ø_l}{2} = 0.259mm$$

Steel quality B500NC: $\quad\quad f_{yd} = f_{yk} = 500MPa$

Concrete quality: $\quad\quad f_{ck} = 25MPa$
$$f_{cd} = f_{ck} = 25MPa$$

$$A_s = 3\pi \cdot \frac{0.016^2}{4} \ [mm^2]$$

Beam is singly reinforced and Ø12 bars are used to stabilize the stirrups in vertical position.

$$x = \frac{f_{yd} \cdot A_s}{0.8 \cdot b \cdot f_{cd}} = 60.3mm$$

To ensure yielding of tensile steel:
$$0.617 \cdot d = 159.803mm$$
$$x < 0.617 \cdot d$$

Moment capacity of the cross section:
$$M_{Rd} = 0.8 \cdot x \cdot b \cdot f_{cd} \cdot (d - 0.4 \cdot) = 70.816kN$$

Span between point loads: $\quad\quad a = 0.7m$
Maximum load capacity:

$$P = 2 \cdot \frac{M_{Rd}}{a} = \underline{202.322kN}$$
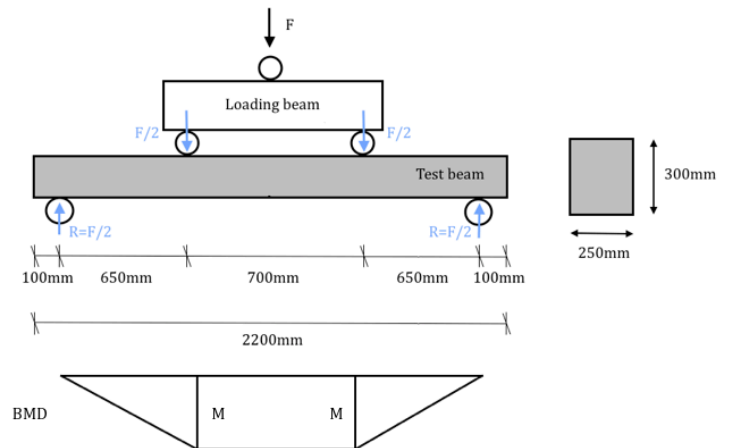
APPENDIX D

Calculations to determine crack widths from the DIC system for 0.5% RFRC.

|	Time [s]		Image	ε_{xx}	L_{ext}	ΔL (crack width)
Displacement [mm]	Directly measured	DIC system	Number	%	[mm]	[mm]
8.6	381	381	636	0.006404	79.9	0.511
10.6	442	442	722	0.007218	79.9	0.577
40	1328	1328	2215	0.048476	79.9	3.873
84	2648	2648	4693	0.056075	79.9	4.480

Placement of virtual strain gauge in Strainmaster, located where the first crack is expected.
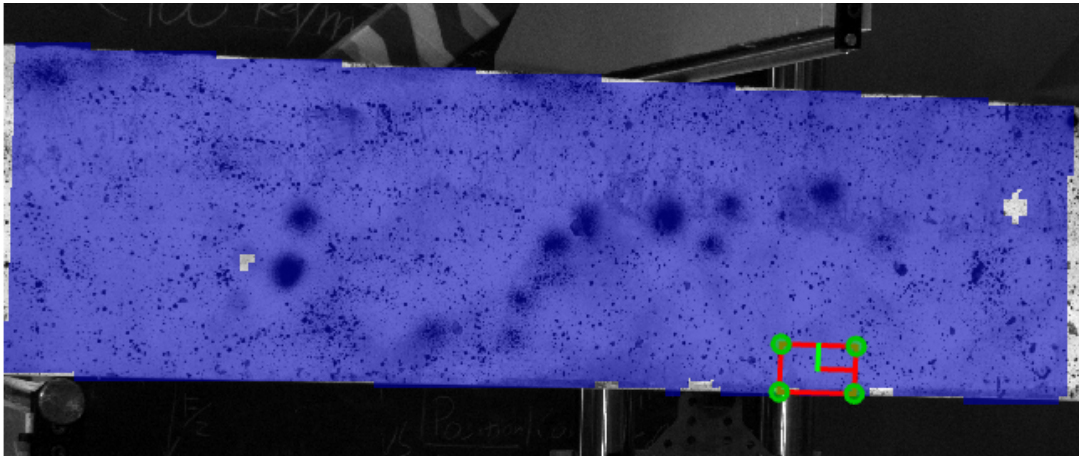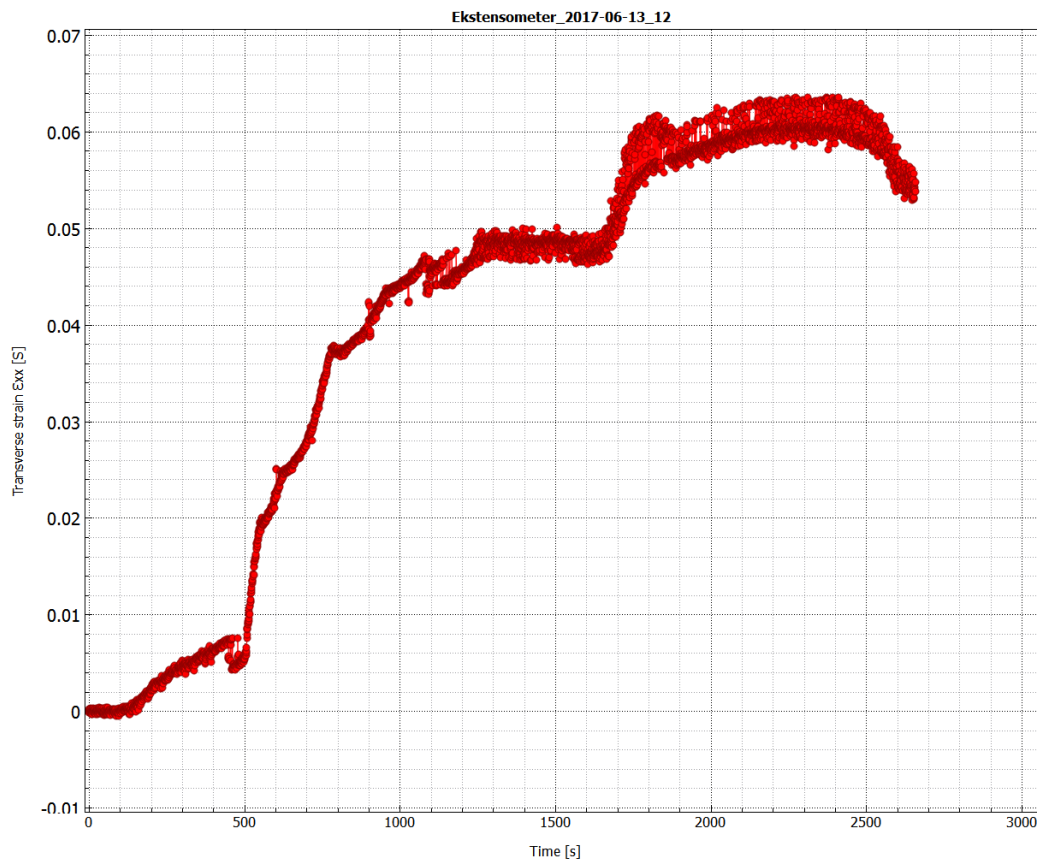
Output from Strainmster: transverse strain – time diagram.
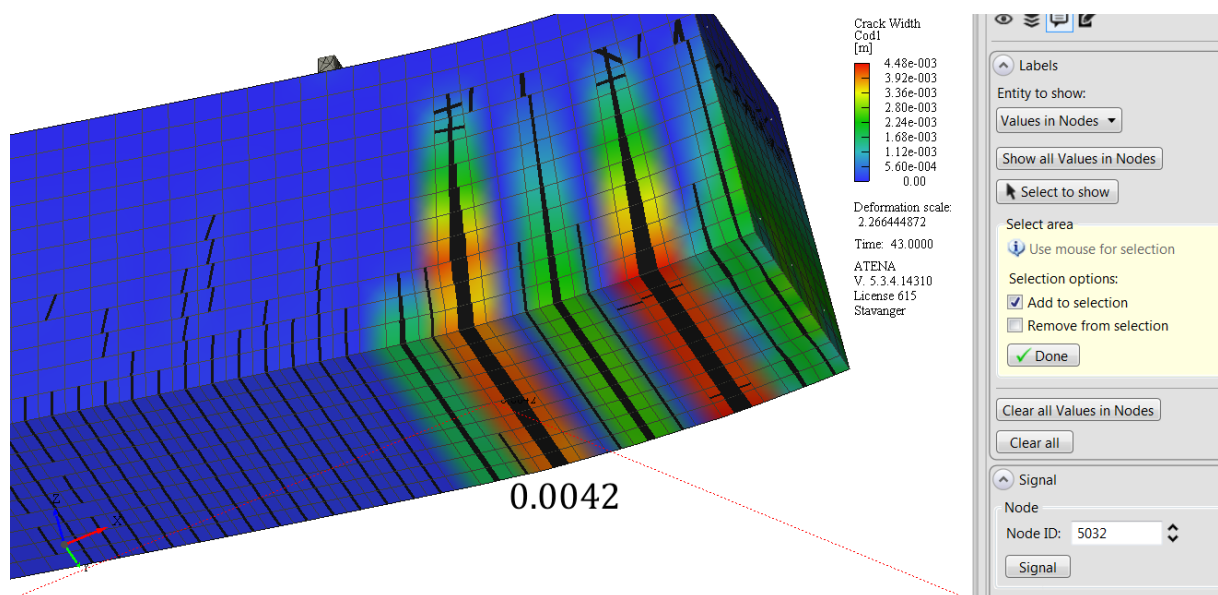
Location of first generated crack computed in ATENA.

APPENDIX E

Figures – determination of E-modulus.

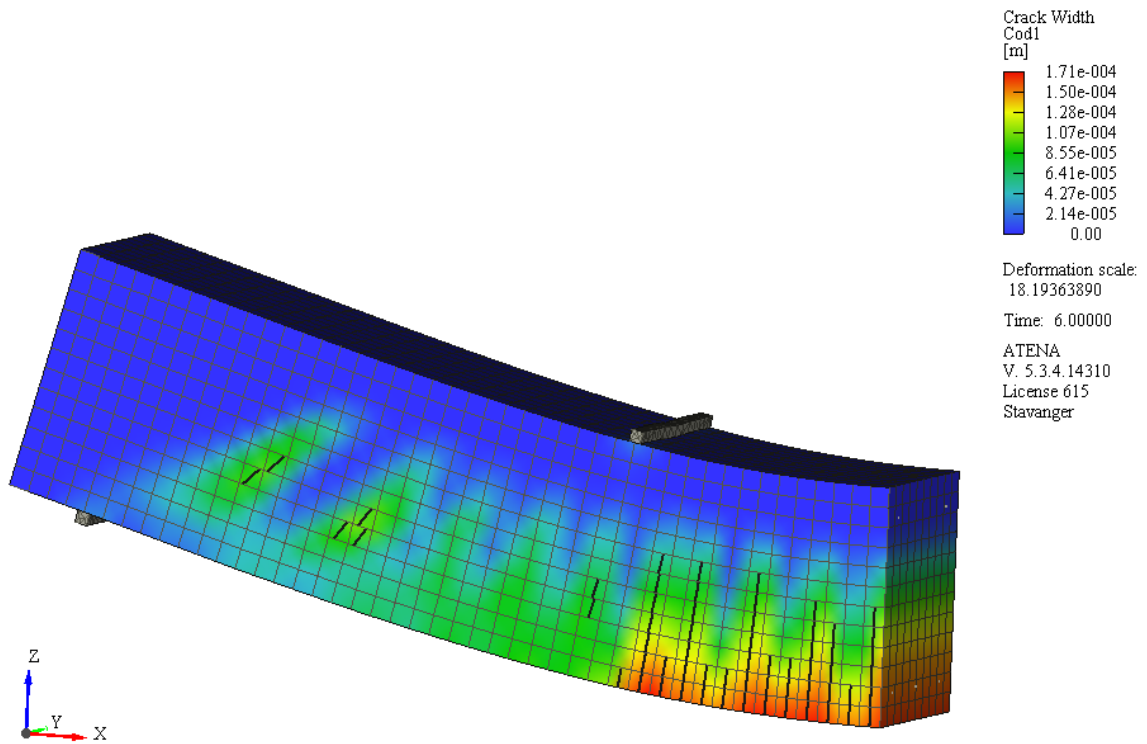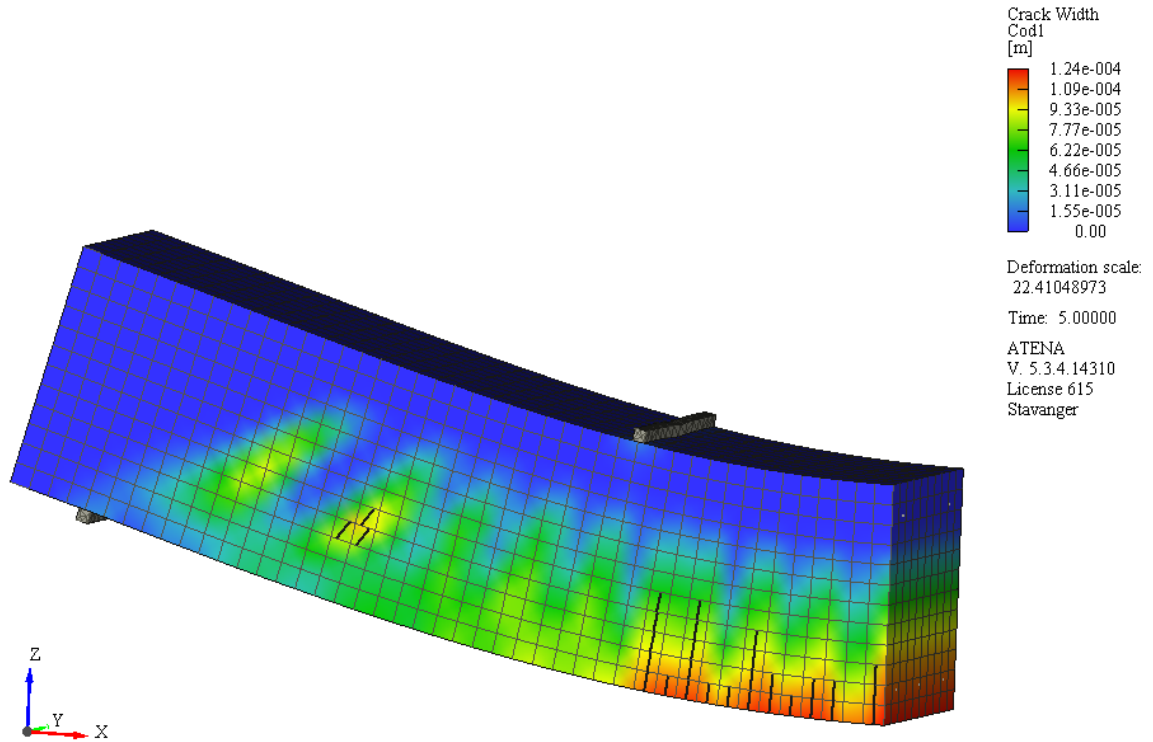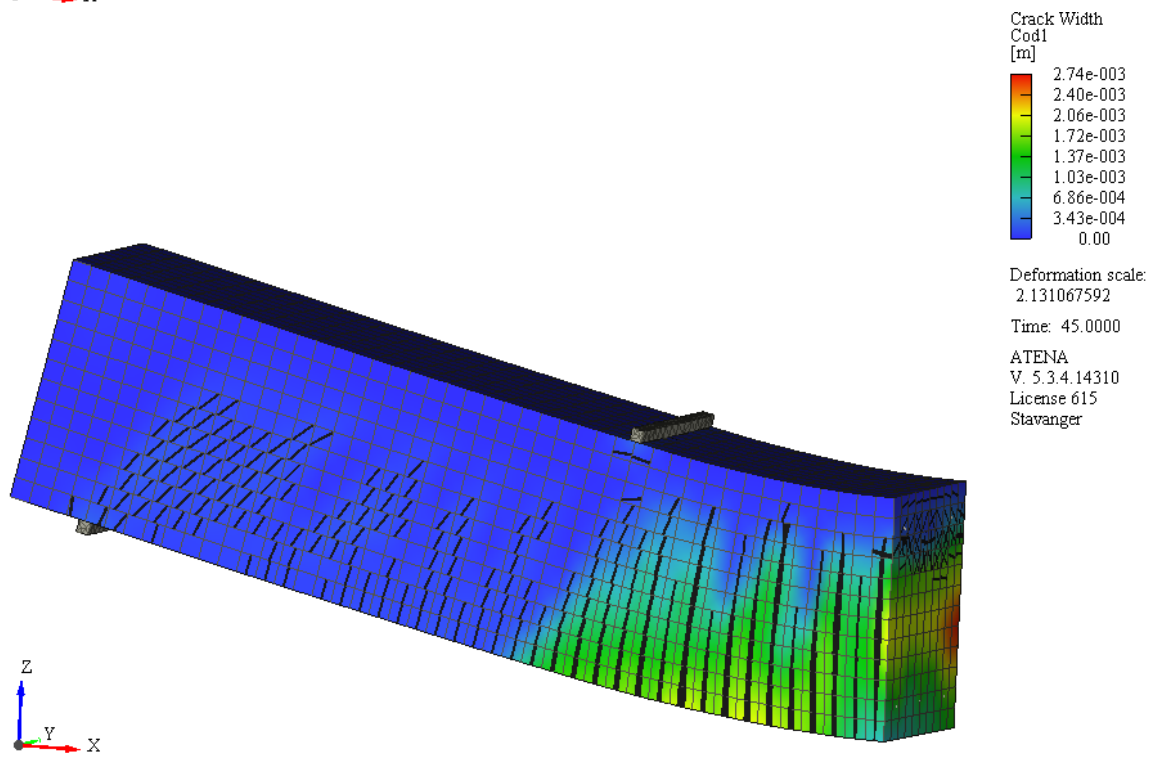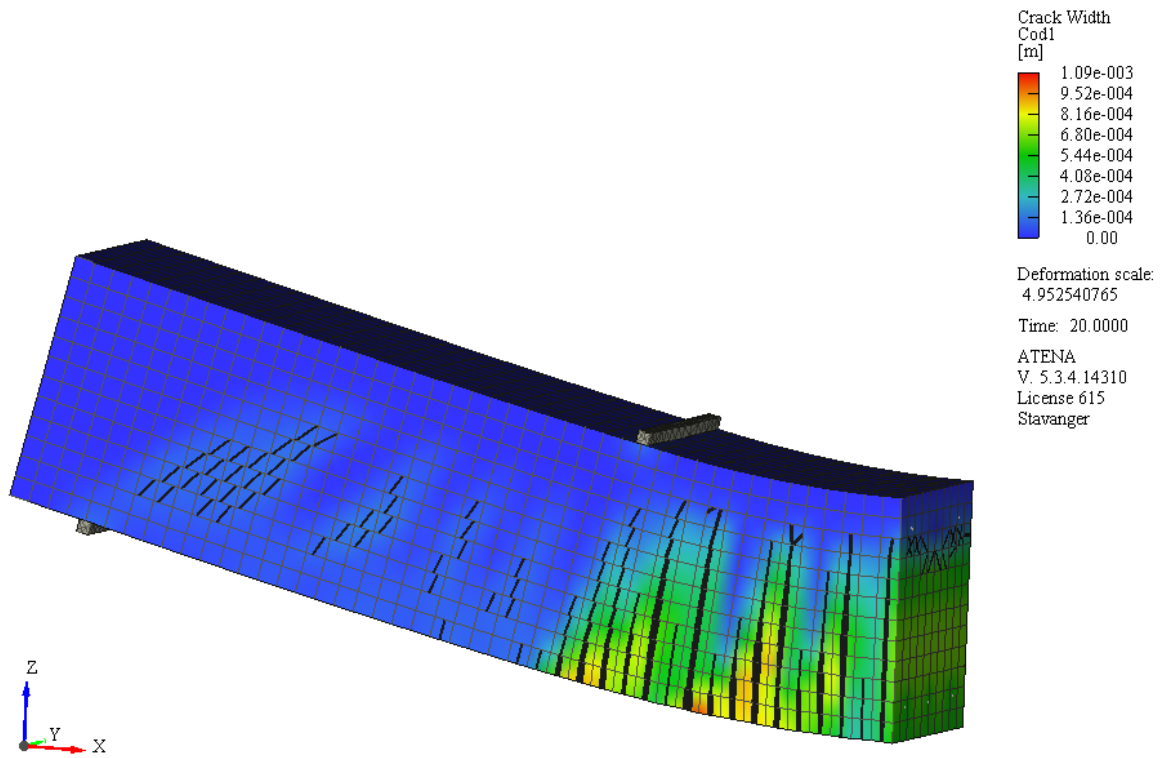Estimations of modulus of elasticity in Excel.
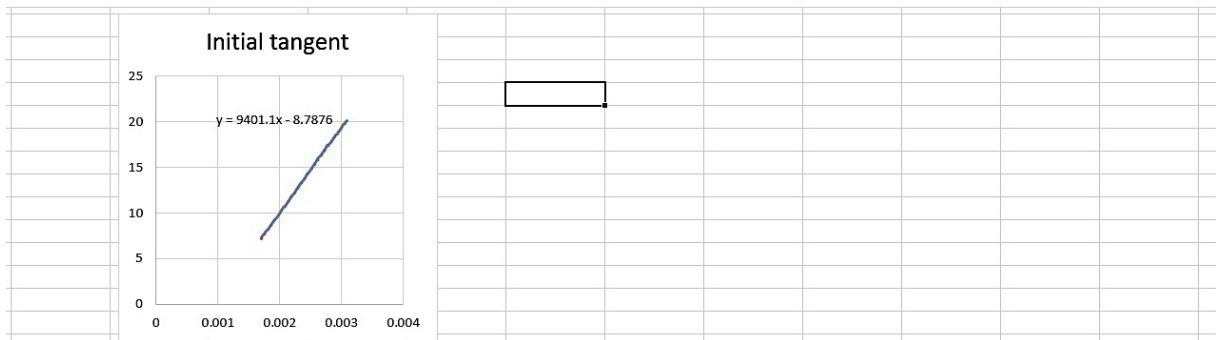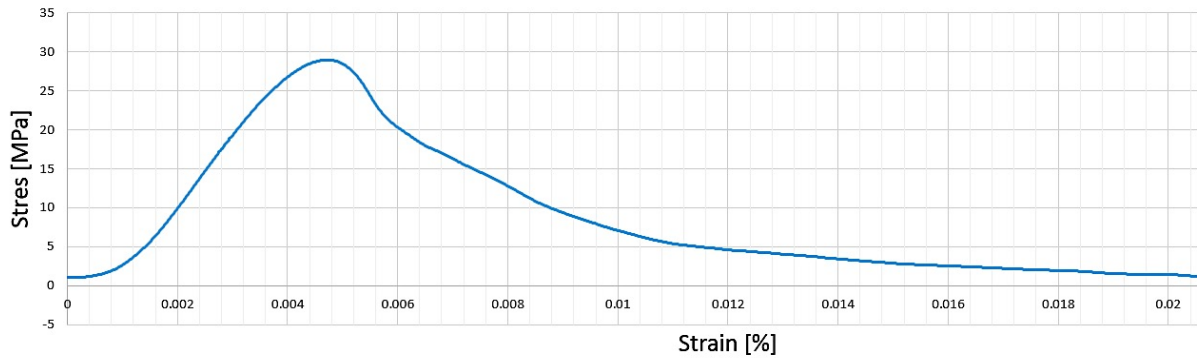
Estimation of tangent modulus of elasticity with results from DIC system.

APPENDIX F

Cracks generated in ATENA for 0.5% SFRC

Cracks computed in ATENA for 1.0% SFRC.